

PHYSIOLOGICAL RESPONSES OF GRAPEVINE SHOOTS TO WATER STRESS AND  
THE DEVELOPMENT OF A MICROTENSIOMETER TO CONTINUOUSLY MEASURE  
WATER POTENTIAL

A Dissertation presented to the Faculty of the Graduate School  
of Cornell University

In Partial Fulfillment of the Requirements for the Degree of  
Doctor of Philosophy

by

Vinay Vijay Pagay

May 2014

© 2014 Vinay Vijay Pagay

PHYSIOLOGICAL RESPONSES OF GRAPEVINE SHOOTS TO WATER STRESS AND  
THE DEVELOPMENT OF A MICROTENSIOMETER TO CONTINUOUSLY MEASURE  
WATER POTENTIAL

Vinay V. Pagay, Ph.D.

Cornell University 2014

ABSTRACT

Water availability plays a key role in growth processes in grapevines (*Vitis vinifera* L.), moderating the balance between vegetative and reproductive growth. It was hypothesized that differences in vegetative growth of individual shoots within a grapevine on a single cane were due to differences in the water status of those shoots as indicated by their midday stem water potentials,  $\Psi_{md}$ . A combination of leaf pressure chamber, leaf gas exchange, ultrasonic acoustic emissions, stem hydraulic measurements, and histology techniques were used on field-grown ‘Riesling’ grapevines that were subjected to progressive soil moisture deficits during the 2011 and 2012 growing seasons. Differences in  $\Psi_{md}$  were not large enough to explain the large differences in shoot length within a single vine. Longer shoots had greater hydraulic conductivities, but shorter shoots were found to have higher rates of xylem acoustic emissions occurring under less water stress (higher  $\Psi_{md}$ ) than longer shoots. Longer shoots had larger cross-sectional xylem vessel area and somewhat less inter-vessel pitting compared to shorter shoots. These differences could contribute to the higher hydraulic efficiency of long shoots, and with fewer pits per vessel, there may be fewer embolisms. Stomatal conductance and photosynthetic responses to increasing water stress were not different in relation to shoot length. In summary, although there were differences in water status between long and short shoots on the same vine, the differences were not great enough to explain the differences in growth rate of the shoots.

Tensiometry is a technique to measure the chemical potential of stretched liquid water based on a thermodynamic equilibrium between liquid water and its vapor. It provides the most sensitivity in the range of (high) water potentials relevant to plants and soils, and is compatible with miniaturization for embedding in plants. Based on this technique, we developed a

microelectromechanical system (MEMS)-based microtensiometer in which a piezoresistive pressure sensor coupled to a nanoporous silicon membrane was able to measure large internal negative pressures of liquid when exposed to sub-saturated vapors. We demonstrated its function in sub-saturated vapors across a range of activities ( $a_w$ ) or relative humidities (RH), measuring internal hydrostatic pressures approaching -33 MPa ( $a_w=0.78$  or 78% RH), the largest negative liquid pressure directly measured by any method. The extended range of measurement combined with a small form factor make the microtensiometer an attractive instrument for the measurement of water activity in a variety of materials (e.g. concrete), physical, biological, and environmental systems. The microtensiometer can also be embedded in the stems of woody plants and in soils for the continuous measurement of water potential. Scalable microtensiometer arrays in conjunction with wireless networks offer the potential to provide continuous, high-resolution data to geographic information system (GIS) centers to aid in irrigation decisions and optimize water resource management for sustainable crop production.

## BIOGRAPHICAL SKETCH

Vinay Pagay began his undergraduate education in electrical and computer engineering (B.Eng.) at McGill University, Montreal, Quebec (Canada), followed by a second degree (B. Sc. Hons.) in enology and viticulture from Brock University, St. Catharines, Ontario (Canada). At Brock, Vinay studied under Drs. Andrew Reynolds and Helen Fisher for his honors project in which he investigated the effect of long-term bird netting on grapevine physiology, grape yield, and wine composition. After receiving his degree at Brock in 2005, Vinay pursued a M.S. degree in viticulture at Cornell, studying under Drs. Lailiang Cheng and Alan Lakso; his research focused on understanding the variability in grape ripening of commercially important red grape varieties in New York State – Concord and Cabernet franc. He also investigated the effects of several exogenous plant growth regulators on the advancement of grape ripening and ripening synchronization.

After receiving his M.S. degree at Cornell in 2008, Vinay received the William Frederick Dreer Award for international horticulture research awarded by the Department of Horticulture (Cornell) through which he got to travel to China, India, and Australia to study the effects of regional climate change on viticultural practices and water availability in vineyards. During this period, Vinay worked at The Northwest Agricultural and Forestry University (Yangling, China), and The University of Adelaide (Australia) in their viticulture research groups. During his studies at Brock and Cornell, Vinay had the opportunity to work at several commercial vineyards, wineries, and viticulture research institutes across North America, Europe, Asia, and Australia.

After returning to the U.S. from Australia in mid-2009, Vinay commenced a doctoral degree in viticulture at Cornell University under the supervision of Drs. Alan Lakso

(Horticulture, NYSAES, Geneva), Taryn Bauerle (Horticulture, Ithaca), and Abraham Stroock (Chemical Engineering, Ithaca), the work which is described in this dissertation.

## ACKNOWLEDGMENTS

I would like to thank the following departments, funding agencies, and individuals for their financial, technical and other support without which or whom the work undertaken during my doctorate at Cornell would have been impossible.

- Department of Horticulture, Cornell University, for financial support through teaching and research assistantships.
- Funding agencies: USDA-NIFA, NSF
- Scholarships: ASEV-ES, ASEV-National
- Ph.D. special committee: Dr. Alan Lakso, Dr. Taryn Bauerle, Dr. Abraham Stroock
- NYSAES, Geneva: Dr. Martin Goffinet, Dr. Bruce Reisch, Rick Piccioni, Mike Fordon
- Department of Chemical Engineering (Ithaca): Dr. David Sessoms, Dr. Olivier Vincent, Michael Santiago, Erik Huber, Eugene Choi, I-Tzu Chen
- Staff of the Cornell Nanoscale Science & Technology Facility (CNF), especially Meredith Metzler and Rob Ilic, for their help with the cleanroom fabrication process of the microtensiometer.
- Staff of the Materials Research Institute at The Pennsylvania State University (State College, PA), especially Guy Lavalee and Shane Miller for their help with DRIE.
- Ms. Franziska Doerflinger, for her love, help, support, and immense patience as I went through this degree.

## TABLE OF CONTENTS

CHAPTER 1: General Introduction .....	1
1.1 Importance of Water to Plants – Ecological and Physiological Perspectives .....	2
1.2 The Concept of Water Potential .....	3
1.3 Soil Water Relations.....	10
1.4 Plant Water Relations .....	12
1.5 Grapevine Physiological Responses to Water Stress .....	14
1.5.1 Vegetative and reproductive responses .....	14
1.5.2 Xylem hydraulic conductance and its measurement .....	18
1.5.3 Ultrasonic acoustic emissions to quantify xylem cavitation .....	19
1.6 The need to measure water potential in plants and soils .....	21
1.6.1 Rationale of measuring stem water potential in plants.....	22
1.7 Techniques to measure water potential in plants and soils, and their limitations.	24
1.7.1 Current instruments .....	24
1.7.2 MEMS-based sensors to measure water potential.....	35
1.7.3 The ideal water potential sensor .....	37
1.8 Summary .....	38
1.9 References .....	40
CHAPTER 2: A microtensiometer for the continuous measurement of very negative pressures of liquid water.....	55
Abstract.....	55
2.1 Introduction .....	55
2.2 Background and theory .....	61
2.2.1 Working principle of tensiometry .....	61
2.2.2 Stability limit of tensiometers .....	63
2.2.3 Piezoresistive pressure sensor .....	64
2.2.4 Porous silicon membrane .....	65
2.3 Material and Methods.....	67

2.3.1	Materials.....	67
2.3.2	Mask designs.....	67
2.3.3	Fabrication.....	68
2.3.4	External electrical connections and measurements.....	71
2.3.5	Filling.....	73
2.3.6	Operation.....	73
2.4	Results and discussion.....	74
2.4.1	Pressure sensor calibration.....	74
2.4.2	Membrane stability limit.....	77
2.4.3	Transient responses to sub-saturated vapor.....	79
2.4.4	Response to sub-saturated salts and vapors.....	80
2.5	Applications.....	81
2.6	Conclusions.....	83
2.7	References.....	84
CHAPTER 3: Vegetative growth, gas exchange, water relations, hydraulic performance, and xylem morphology of varying vigor shoots of <i>Vitis vinifera</i> L. ....		
	Abstract.....	89
3.1	Introduction.....	91
3.2	Material and Methods.....	96
3.2.1	Plant material and site.....	96
3.2.2	Water restriction treatments.....	96
3.2.3	Shoot growth measurements.....	97
3.2.4	Water status measurements.....	98
3.2.5	Gas exchange measurements.....	98
3.2.6	Leaf size and stomatal density.....	99
3.2.7	Shoot hydraulics measurements.....	99
3.2.8	Xylem air-seeding estimation by acoustic emissions.....	101
3.2.9	Xylem anatomical measurements.....	103
3.2.10	Fruit measurements.....	104
3.2.11	Statistical analysis.....	104
3.3	Results.....	105

3.3.1	Water status measurements .....	105
3.3.2	Shoot growth and leaf measurements .....	107
3.3.3	Gas exchange measurements .....	109
3.3.4	Shoot hydraulics measurements .....	110
3.3.5	Acoustic emissions estimation of xylem air-seeding .....	113
3.3.6	Xylem anatomical measurements .....	114
3.3.7	Fruit measurements .....	115
3.4	Discussion .....	116
3.4.1	Shoot Water Status and Physiological Performance .....	116
3.4.2	Shoot Gas Exchange .....	118
3.4.3	Shoot hydraulic characteristics .....	119
3.4.4	Xylem morphology and air-seeding rates .....	122
3.4.5	Fruit growth and composition .....	124
3.5	Conclusion .....	125
3.6	References .....	126
Appendix A: Water-stress induced xylem cavitations in oaks ( <i>Quercus</i> sp.) and possible links to stomatal behavior .....		I
Appendix B: Microtensiometer fabrication process flow .....		XX
Appendix C: Photolithographic masks for microtensiometer fabrication .....		XXI
Appendix D: Calculation of Vapor Pressure Deficit (VPD) .....		XXII

## CHAPTER 1: General Introduction

Water is a primary component of plants, accounting for up to 95% of the fresh weight of certain plant cells (Jones 1992). It determines the physiological, morphological, and reproductive traits associated with an individual plant and is, therefore, considered essential to its growth and survival. In the agronomic context, water is one of the main factors setting the upper limit on productivity and yield of crops that are of chief economic concern to growers worldwide.

Grapevines (*Vitis* sp.) are extensively cultivated around the world between 30-50° N-S latitudes. Grapevines have been historically cultivated in semi-arid to arid regions such as the Mediterranean, although increasingly their cultivation has been spreading to temperate and tropical regions around the world. Grapes are consumed fresh (table grapes), used for juice and jelly production, or for wine production. The yield and quality of grapes depends strongly on the water availability to the vine (Lovisolo *et al.* 2010).

My research was motivated by two main contexts: (i) the effects of predicted regional and global climate change (IPCC 2007) include increased severity of water stress in major viticultural regions worldwide, particularly in arid and semi-arid regions that are already experiencing seasonal droughts (Chaves *et al.* 2010); and, (ii) a moderate amount of water stress in grapevines can be beneficial in order to balance vegetative and reproductive growth, and to enhance grape and wine quality (Chaves *et al.* 2007). I studied the effects of water stress on the physiological and reproductive performance of grapevines, and also developed a new technique to measure vine water stress *in situ* that could be valuable in precision irrigation programs in vineyards and other irrigated agriculture farms.

## **1.1 Importance of Water to Plants – Ecological and Physiological Perspectives**

Water constitutes the basis of life on Earth. The unique molecular properties of water, e.g. higher density as a liquid than as a solid, make it an indispensable natural resource, one that is vital to Earth's geological and biological processes (Solomon 2010). Freshwater is an essential resource for agriculture and crop production worldwide; nearly 70% of the world consumption of freshwater is utilized by agriculture and irrigated agriculture (FAO Aquastat 2013). In addition to the increased demand for renewable water resources resulting from rapid population growth, economic development, and urbanization, declining and more erratic precipitation patterns worldwide have placed an increased demand for water for agriculture in order to increase or even maintain yields.

The distribution of vegetation around the world is in large part dictated by climatic conditions (i.e. temperature, precipitation), irradiance, and nutrient availability in the soils (Kramer and Boyer 1995). Precipitation patterns (quantity, frequency, distribution or timing) determine the availability of water to plants, as does the composition and structure of the soil that forms the reservoir of water for plants. In regions of abundant rainfall and cool temperatures (e.g. equatorial rainforests of Amazon, Indonesia, and Central Africa), tree growth is uninhibited by water availability. However, in regions with higher temperatures and consequently higher evapotranspiration (ET) levels, the same amount of rainfall may not be adequate to support a dense forest, and may only have shrubs or grassland as their native vegetation (e.g. steppes of Eurasia, prairies of North America). So, although water plays a key role in plant survival and growth, the availability of water alone is inadequate to predict the type of vegetation that exists in a given region.

In plants, water plays a key role in influencing many physiological processes at the cellular and whole-plant levels. At the whole-plant level, water is the medium for the transport of carbohydrates, nutrients, and growth regulators between organs, or from the soil to a specific organ. Within cells, water is the main medium of biochemical reactions and used for the transport of metabolites such as sugars, amino acids, proteins (Lambers et al. 1998). Cell division and enlargement, both which contribute to growth, depend on water availability. Water also aids in the structural support of plants via turgor (positive hydrostatic pressure) on their cell walls (Lambers et al. 1998). Also, water's thermal properties (high latent heat of vaporization,  $\lambda=2.45 \text{ MJ kg}^{-1}$  at  $20^\circ\text{C}$ ) help in the regulation of leaf temperature via evaporative cooling (Jones 1992). Water is, therefore, of vital importance to proper plant functioning. While mild water deficits may elicit little physiological response in plants such that leaf relative water content (RWC) and turgor are maintained at adequate levels for processes such as photosynthesis, severe water deficits may result in loss of turgor in leaves, decrease in photosynthetic capacity and quantum yield, and, in extreme cases, result in leaf desiccation and plant mortality (Barigah et al. 2013). However, in some contexts such as viticulture, water deficits may be desirable for the production of high quality red winegrapes (van Leeuwen et al. 2009).

## **1.2 The Concept of Water Potential**

The passive movement of water follows a gradient from high energy state to low energy state. The energy state of water is described in thermodynamic terms as the chemical potential of water,  $\mu_w$  ( $\text{J mol}^{-1}$ ). Chemical potential, in turn, is defined by the change in Gibb's free energy ( $G$ ) when the amount of water in a given system is changed keeping temperature ( $T$ ), pressure ( $P$ ), and composition with respect to other species constant (Eq. 1.1; Jones 1992).

$$\mu_w = \left( \frac{\partial G}{\partial n_w} \right)_{T,P,n_i} \quad (1.1)$$

where  $n_w$  is the moles of water added or removed from the system, and  $n_i$  is the number of particles (of  $i$ ) in the system. Water potential ( $\Psi_w$ ) of a system is defined in terms of its chemical potential ( $\mu_w$ ) compared to pure water at a reference state ( $\mu_w^0$ ). Dividing this difference by the molar volume of water ( $\tilde{V}$ ) allows  $\Psi_w$  to be defined in pressure units (J m<sup>-3</sup> or Pa) (Jones 1992):

$$\Psi_w = \frac{\mu_w - \mu_w^0}{\tilde{V}} \quad (1.2)$$

where  $\tilde{V}$  is the molar volume of pure water (18.05 x 10<sup>-6</sup> m<sup>3</sup> mol<sup>-1</sup> at 20°C). From Eq. 1.2, water potential in the vapor phase can be expressed as (Lambers et al. 1998, Slatyer and Taylor 1960):

$$\Psi_w^{vap} = \frac{\mu_w - \mu_w^0}{\tilde{V}} = \frac{RT}{\tilde{V}} \ln \left( \frac{p}{p_{sat}(T)} \right) \quad (1.3)$$

where  $p$  (Pa) is the partial pressure of vapor, and  $p_{sat}$  (Pa) is the saturated vapor pressure at a given temperature,  $T$  (K). The term  $(p/p_{sat})$  is simply the water activity ( $a_w$ ) or relative humidity (RH). Table 1 shows the values of water potential (in MPa) for a range of activities ( $a_w$ ) at different temperatures, calculated using Eq. 1.3. Most agricultural soils have  $\Psi_w > -0.6$  MPa ( $a_w > 0.995$ ) while cultivated plants have  $\Psi_w > -2$  MPa ( $a_w > 0.985$ ). Some desert shrubs have been reported to have  $\Psi_w$  values as low as -10 MPa ( $a_w \approx 0.926$ ).

**Table 1:** Calculated values of water potential ( $\Psi_w$ , MPa) of vapors or liquids at various activities ( $a_w$ ) and temperatures based on Eq. 1.3.

$a_w$	Temperature (°C)					
	5	10	15	20	25	30
<b>1</b>	0.00	0.00	0.00	0.00	0.00	0.00
<b>0.995</b>	-0.64	-0.65	-0.67	-0.68	-0.69	-0.70
<b>0.99</b>	-1.29	-1.31	-1.33	-1.36	-1.38	-1.40
<b>0.98</b>	-2.59	-2.63	-2.68	-2.73	-2.77	-2.82
<b>0.95</b>	-6.57	-6.69	-6.81	-6.92	-7.04	-7.16
<b>0.9</b>	-13.49	-13.74	-13.98	-14.22	-14.46	-14.71
<b>RT/V</b>	128.07	130.37	132.67	134.98	137.28	139.58

The activity ( $a_w$ ) and, hence, chemical potential ( $\mu_w$ ) of a system are influenced by the presence of solutes. For example, the addition of osmotic solutes to pure water results in a decrease of  $a_w$  and  $\mu_w$ , and an increase of osmotic potential ( $\Psi_w^s$ ) or pressure,  $\Pi$  (Pa). Osmotic potential can be expressed as:

$$\Pi = -\Psi_w^s = -\frac{RT}{\tilde{V}} \ln(\gamma_w x_w) = -\frac{RT}{\tilde{V}} \ln(a_w) \quad (1.4)$$

where  $\gamma_w$  is the activity coefficient of water (= 1 for ideal solutions;  $\approx 1$  for dilute solutions),  $x_w$  is the mole fraction of water, and  $a_w$  its activity. The expression for osmotic pressure for dilute solutions was originally put forth by van't Hoff (1885):

$$\Pi = \frac{\mu_w - \mu_w^0}{\tilde{V}} = -RTc_s \quad (1.5)$$

where  $c_s$  ( $\text{mol m}^{-3}$ ) is the concentration of solute in the solution. Eq. 1.5 defines the water potential of the solution ( $\Psi_w^s = -\Pi$ ); its derivation can be found in Nobel (1995). Osmotic pressure or potential refers to the energy required to move water from a region of low (or no) solute concentration (low  $\Psi_w^s$ ) to a region of high solute concentration (high  $\Psi_w^s$ ), where the two regions are separated by a semi-permeable membrane that allows water but not solutes to

pass through it. Assuming no hydrostatic or turgor pressure, water tends to flow down a gradient of total water potential caused by a gradient of osmotic potential since the entropy of the system increases, obeying the second law of thermodynamics. It should be noted that osmotic potential is a colligative property that depends on the molar concentration of the solute and not on the size of the solute molecule. This can be significant as plants can increase osmoticum more economically with ions (e.g. potassium ions in stomatal guard cells) or small molecules than with large molecules, and regulate osmolarity by polymerizing and depolymerizing sugars.

Another component of  $\Psi_w$  important in plants relates to the positive pressure (relative to atmospheric pressure,  $P_{atm}$ ) in cells and the reduced hydrostatic pressure of water in the xylem vessels of the plant,  $P_x$ . These pressures are referred to as the pressure potential ( $\Psi_w^p = P_{cell} - P_{atm}$ ), or turgor when positive and tension when negative. In the plant cell, turgor pressure counterbalances the osmotically-driven movement of water into the cell. Accumulation of osmoticum in a cell can maintain turgor as external water potential declines with reduced water availability.  $\Psi_w^p$  may also be negative in the xylem and is a function of the transpiration rate and the hydraulic resistances in the pathway between the leaf and root. The plant hydraulic system has been modeled by van den Honert (1948) using an Ohm's Law analogy where the water potential gradient,  $\Delta\Psi_w$ , generally from the soil to the top of the plant, is the product of hydraulic resistance,  $R$ , and transpiration or flux,  $E$  (Tyree and Ewers 1991):

$$\Delta\Psi_w = R \cdot E \quad (1.6)$$

These gradients of water potential determine the direction of water flow from high (less negative) water potential (e.g. the soil) to lower water potential (e.g. a transpiring leaf).

Although water flows are generally from the soil to the leaves, water may move in any direction dictated by  $\Delta\Psi_w$ . In some cases, water has been shown to move laterally across a plant or even from the leaves to the roots (Eller et al. 2013, Smart et al. 2005).

Another component of water potential applies to soils and other porous media and is known as matric potential,  $\Psi_w^m$ . Matric potential is comprised of the total energy of two interactions: capillarity and adsorption (Kramer and Boyer 1995, Campbell 1998; Fig. 1). Capillarity refers to the pressure difference generated between a bulk liquid and a gas (or other immiscible fluid) that are separated by a curved interface; for a negatively-curved interface (curved in toward the liquid), the pressure in the liquid is reduced and the capillary contribution to the matric potential is negative. This scenario occurs in the pores of sub-saturated soils and plant tissues, e.g. leaf mesophyll.

Adsorption refers to the local, molecular-scale interaction of the liquid with materials via van der Waals, electrostatic, and other molecular forces. For hydrophilic materials in the soil and plant tissues, these attractive interactions stabilize the condensed phase and, thus, lower the water potential. Matric potential can be expressed as the sum of two components:

$$\Psi_w^m = P_{capillary} + P_{adsorbed} \quad (1.7)$$

where  $P_{capillary}$  and  $P_{adsorbed}$  are the pressures associated with capillary and adsorbed water, respectively (Fig. 1). Smaller soil particles such as clays tend to produce higher matric potentials (more negative values) for the same

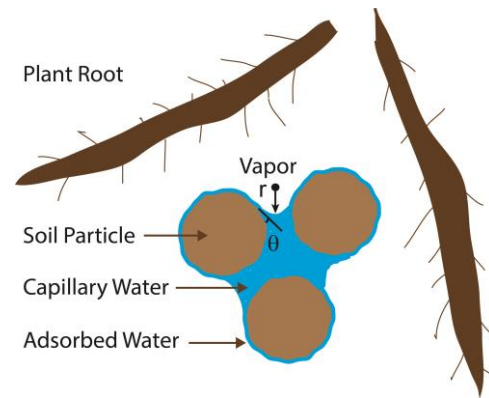


**Figure 1:** Matric potential as determined by capillary and adsorbed water in soil.

volumetric water content than do silts or sandy soils (Warrick 1990; Fig. 2). Small pores have larger radii of curvature on the air-liquid interfaces and greater surface area for adsorption of water, both of which result in a larger capillary contribution to matric potential. Matric potential is an important measure of the relative ability of plants to extract water from soils of different characteristics.

In a cylindrical pore, the force or pressure acting on the capillary,  $P$  (Pa), is given by the vertical force acting on the capillary per unit area (Jones 1992). The vertical component of the adhesive force is given by  $\sigma \cos\theta$  times the perimeter of the capillary,  $2\pi r$ . Therefore,

$$P_{liq} - P_{atm} = \frac{2\pi r \cdot \sigma \cos\theta}{\pi r^2} = \frac{2\sigma \cos\theta}{r} \quad (1.8)$$

Most plant organs (xylem, cell walls) and soils have hydrophilic (highly wettable) surfaces, where  $\theta \approx 0^\circ$ , so Eqn. 1.8 can be simplified to:

$$P_{liq} - P_{atm} = \frac{2\sigma}{r} \quad (1.9)$$

The last component of total water potential is gravitational potential,  $\Psi_w^g$  (Pa) is given by the potential energy of water of molar mass,  $m$  ( $18.02 \times 10^{-3}$  kg mol<sup>-1</sup>) at a given height,  $h$  [m], above the surface of earth:

$$\Psi_w^g = \frac{mgh}{\tilde{V}} = \rho_l gh \quad (1.10)$$

where  $g$  is the gravitational acceleration ( $9.8$  m s<sup>-2</sup> at sea level), and  $\rho_l$  is the density of water. This term contributes up to only 0.1 MPa in water potential for every 10 m in height, so for most land plants that are under 10 m in height, this term is considered negligible. For trees

such as Giant Redwood (*Sequoia sempervirens*) and Douglas Fir (*Pseudotsuga menziesii*) that routinely reach heights exceeding 100 m (Koch et al. 2004), the gravitational term can be significant and should be included in the  $\Psi_w$  calculation (Jones 1992).

Putting all the above components of water potential together, we reach an expression for the total water potential of a system as:

$$\Psi_w = \Psi_w^s + \Psi_w^p + \Psi_w^m + \Psi_w^g \quad (1.11)$$

Over the past century, water potential ( $\Psi_w$ ) has gained wide acceptance as a key measure of plant water status (Hsiao 1973, Shackel 2007). In my research, I specifically measure plant (stem) water potential as quantitative measure of the water status of the grapevine as water stress is imposed (Chp. 3).

### 1.3 Soil Water Relations

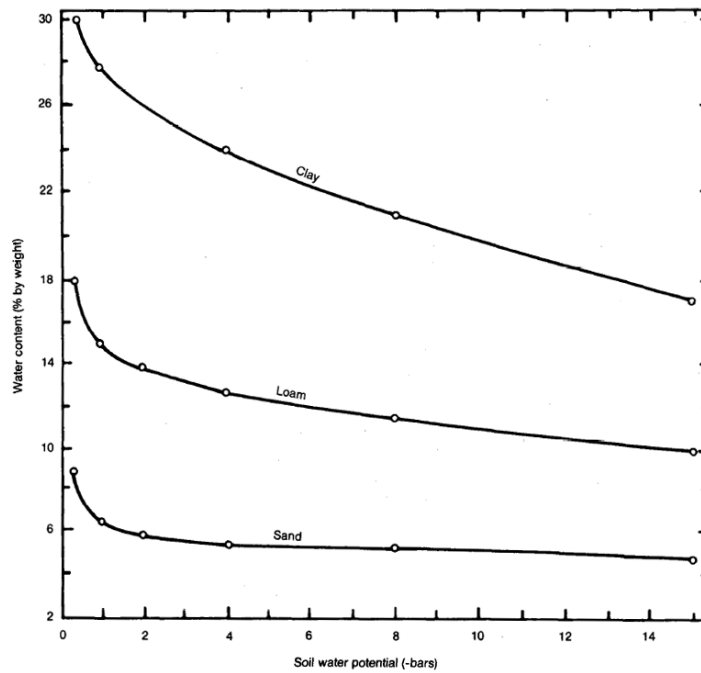


**Figure 2:** Moisture release curve for sand, loam, silt and clay soils. Source: USDA National Engineering Handbook. Section 15: Irrigation.

The availability of water for plants depends primarily on the quantity of water stored in the soil or provided by irrigation, as well as the ease with which roots are able to take up soil water. The latter is quantified by water potential, predominantly matric potential, and is a function of soil type (clay, silts, sand, etc.), structure (size of soil particles, distribution of rock), and the amount of water in the soil. Soils that are predominantly clay-based have the smallest particles and, therefore, have the smallest pores between the clay particles. The size of these pores is a critical factor in determining the soil's maximum water-holding capacity and the water potential required by roots to extract water from the soil. This concept is illustrated in the soil moisture release curve, Fig. 2. The smaller the particle and hence the pore (or capillary) size, e.g. in clay soils, the lower is the water potential for a particular volumetric moisture content,  $\theta_v$ . In order to extract water from the soil, plants have to lower

their root water potential to a value lower than that of the soil. For a given level of soil moisture, annuals such as beans and sunflowers may only reach  $\Psi_{\text{leaf}}$  of -1 MPa, which may be higher than the soil water (matric) potential,  $\Psi_w^m$ , say -1.2 MPa. In this case, the plant does not have the ability to extract water from the relatively dry soil and loses cell turgor. In contrast, other, more drought-tolerant species may be able to generate more negative water potentials, say,  $\Psi_{\text{leaf}} < -1.3$  MPa, in their leaves and, therefore, be able to extract water from the same soil. Therefore, when considering the availability of water to plants, it is important to consider both soil water availability as well as the ability of the plant to extract soil water. In Chapter 3, a soil moisture deficit in silt loam soil is used in order to impose water stress in field-grown grapevines. Silt loams being relatively dense with small pores, have a moderately high water holding capacity, thus making the imposition of drought challenging.

## 1.4 Plant Water Relations

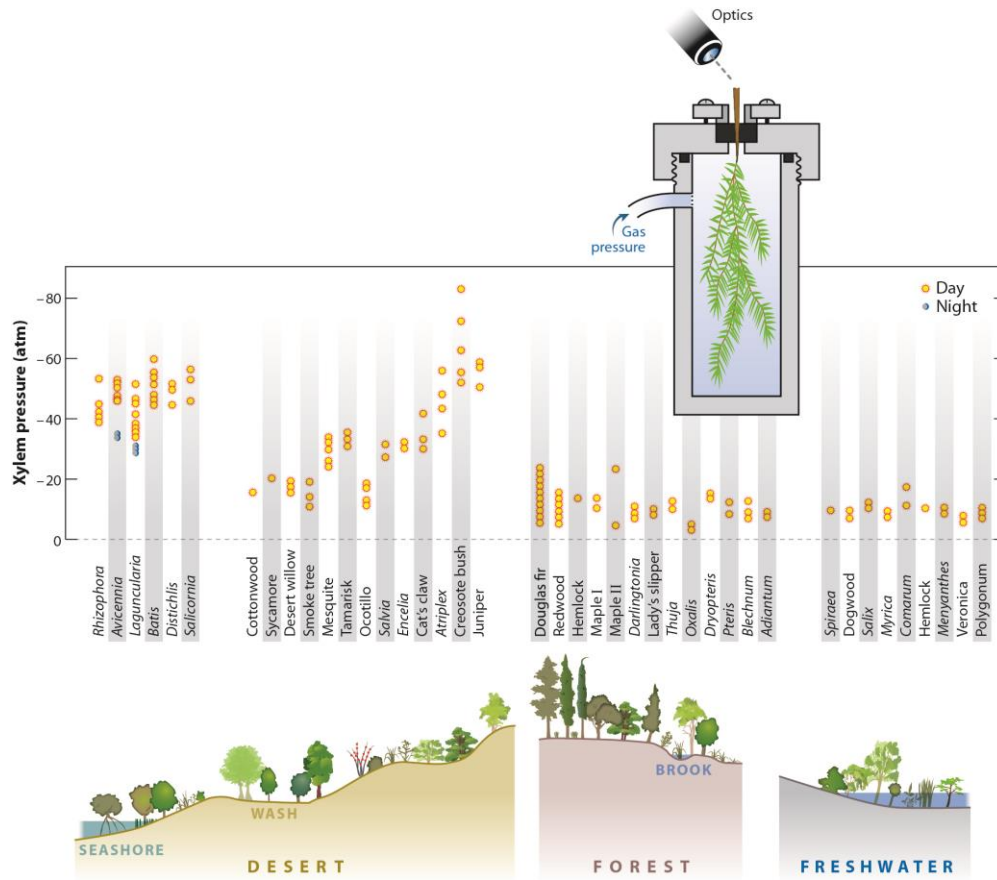


**Figure 3:** Range of minimum xylem leaf water potentials ( $\Psi_{\text{leaf}}$ ) observed in plants from diverse ecosystems (Stroock et al. 2014).

Plants thrive in a range of habitats in diverse ecosystems and agro-ecosystems requiring them to be well-adapted to their specific environmental conditions. In terms of water availability, the three ecosystems shown in Fig. 3 comprise the full range of minimum plant water potentials that have been measured, from  $\Psi_{\text{leaf}} > -0.1$  MPa to  $< 8$  MPa (Scholander et al. 1965). The movement of water from soil to the atmosphere through plants occurs via the so-called 'Soil-Plant-Atmosphere Continuum' (SPAC), essentially a continuum to transport water passively, i.e. without the need for metabolic energy. This transport is the result of differences

in total water potential ( $\Psi_w$ ) between the soil and the atmosphere, the plant being merely the conduit in the pathway for water movement. The Cohesion-Tension theory, originally proposed by Dixon and Joly (1895), postulates that water moves under tension from roots to leaves driven by capillary forces in the cell walls within the leaf substomatal cavities in response to evaporation from the leaf surface. Water moves from regions of high  $\Psi_w$  in the soil and roots, to regions of low  $\Psi_w$  in the leaves on its path to the atmosphere, the difference in  $\Psi_w$  between the soil and atmosphere setting the driving force for water transport in the SPAC.

The lowest water potential along the SPAC is found in the atmosphere; this water potential is defined by the relative humidity and temperature (contributing to vapor pressure deficit, or VPD). The water potential in the atmosphere at 50% RH at 20°C is approximately -94 MPa (using Eq. 1.3). The difference in  $\Psi_w$  between the atmosphere, the leaf boundary layer ( $\Psi_w \sim -7$  MPa), and sub-stomatal cavities and mesophyll surfaces ( $\Psi_w \sim -1$  MPa) moves water from inside the leaf out to the atmosphere to allow for photosynthesis. The matric potential in the leaf mesophyll (due to adsorption and capillarity) is lowered. In turn, capillary water in the interstitial spaces of the mesophyll pulls on bulk water in xylem vessels connected to the leaf and down to the root, lowering the pressure potential,  $\Psi_w^p$ . Lower  $\Psi_w^p$  in the xylem within roots lowers the matric potential  $\Psi_w^m$  of the root cells ( $\Psi_w \sim -0.6$  MPa) in contact with the soil vapor and liquid water ( $\Psi_w \sim -0.3$  MPa). The lowered matric potential of root tissue results in water being pulled out of the soil. As seen from the typical values for  $\Psi_w$  given at each stage of the SPAC, water moves from higher values of  $\Psi_w$  to lower values of  $\Psi_w$ .

When water availability from the soil is limiting, some plants are able to adapt to the drought stress. Osmotic adjustment or osmoregulation is one means by which certain higher

plants maintain turgor in their cells under conditions of decreasing water potential (Hsiao et al. 1976; Turner and Jones 1980; Davies and Zhang 1991). These changes can occur by either accumulation of solutes within the cytoplasm of cells, or by modifying the distribution of solutes, ions, etc. between cells. The changes in stomatal opening are due to changes in osmotic potential of the guard cells. Plants differ in their ability to osmotically-adjust from only a few bars to almost 100 bars of osmotic potential (Morgan 1984). Grapevines have been reported to osmotically-adjust to water stress up to 4 bar, primarily by accumulating inorganic ions (Patakas et al. 2002), glucose and fructose (Düring 1985).

## **1.5 Grapevine Physiological Responses to Water Stress**

### **1.5.1 Vegetative and reproductive responses**

Grapevines (*Vitis* spp.) are versatile plants that can be grown in a wide range of soil and climatic conditions (Nagarajah 1989). Traditionally, grapevines have been grown in non-irrigated arid to semi-arid regions such as the Mediterranean and, hence, are considered to be moderately drought-tolerant (Chaves et al. 2010). Both vegetative and reproductive performance of a grapevine are influenced by the water status of the vine, and it is now widely accepted that a moderate amount of water stress is beneficial for commercial production of red winegrapes such that there is a balance of vegetative and reproductive growth with improved fruit quality (Lovisolo et al. 2010). Irrigation techniques such as deficit irrigation (Chalmers 1981, Chaves et al. 2010) and partial rootzone drying have been developed specifically with this objective in mind, to produce ‘balanced’ vines, and to improve water use efficiency in vineyards (Dry and Loveys 1998, Dry et al. 2001, Santos et al. 2003, Intrigliolo et al. 2009). One of the physiological bases for moderate withholding of water is to reign in excess grapevine shoot growth (or vigor), since excess vigor may have negative effects on fruit

composition (McCarthy 1997; Chapman et al. 2005). In addition to reducing excess vegetative growth, mild water stress in grapevines is reported to also shift the partitioning of carbohydrates away from growing shoot tips and into reproductive structures such as fruit (Souza et al. 2005). It has also been observed that mild to moderate levels of water stress imposed by deficit irrigation do not significantly impact photosynthesis (Flexas et al. 2002, Souza et al. 2005, Chaves et al. 2007) except under severe water stress conditions (Loveys and Kriedemann 1973, Souza et al. 2005). A comprehensive review on deficit irrigation effects in grapevines can be found in Chaves et al. (2010).

Vegetative responses to water stress range from inhibition of root and shoot growth, to decreased canopy gas exchange, and decreased leaf and stem water potentials (Chaves et al. 2003). A reduction in shoot growth and flaccid shoot tips mark the first visible symptoms of water stress in grapevines. Specifically, shoot extension growth has been shown to be more sensitive to water stress than is the formation of new leaves (Matthews et al. 1987, Kliewer et al. 1983). The basis of reduced shoot growth could be due to lower plant growth regulator levels in the shoot apical meristem, e.g. gibberellins, cytokinins, and auxins. The effects of reduced shoot growth results in reduced leaf area per shoot, therefore lowering the photosynthetic capacity of the shoot to produce sugars for its fruit (Reynolds 1994). Reduced leaf area could result in elevated light and temperature levels in the canopy and fruit zone, the latter which would result in sunburn effects to the fruit (e.g. decreased color, flavor) (Kliewer and Lieder 1968, Kliewer and Schultz 1973).

The reproductive growth response to water stress is somewhat less marked than the vegetative growth response (Rühl and Alleweldt 1985). An early pioneering study by Buttrose (1974) established that water-stressed grapevines had lower bud fruitfulness, possibly as a

consequence of lower vine carbohydrate availability due to decreased photosynthesis (Buttrose 1969), as well as lower inflorescence initiation, if water stress was early in the phenology, prior to or around bloom. Shortly after bloom, water stress can result in lower fruitset (Alexander 1965) and, consequently, decrease yields (Hardie and Considine 1976). After fruitset, water stress can result in decreased berry size (due to less cell division and expansion), and sometimes even result in berry abscission (Nagarajah 1989). The decrease in yield is reportedly due to smaller and lighter clusters (due to decreased berry weight), and not due to fewer clusters per shoot (Kliewer et al. 1983). This is consistent with another study on Gewürztraminer grapevines (Reynolds et al. 2005). Following véraison, the commencement of ripening as well as color change in red grape varieties, water stress appears to have little impact on yield (Matthews et al. 1987). In my work with water-stressed 'Riesling' grapevines, I characterized the relationship between water status, as indicated by midday stem water potential ( $\Psi_{\text{md}}$ ), and physiological and reproductive attributes such as leaf gas exchange, shoot growth rates, and hydraulic performance, in a single growing season, corroborating the reports of less sensitivity of reproductive growth compared to vegetative growth (Fig. 4). This figure indicates that gas exchange and berry size decrease linearly as  $\Psi_{\text{md}}$  decreases, while for shoot growth rate, there appears to be an inflection point around -0.5 MPa, suggesting a water potential threshold at this value, i.e. shoot growth is very sensitive to water stress at  $\Psi_{\text{md}} < -0.5$  MPa.

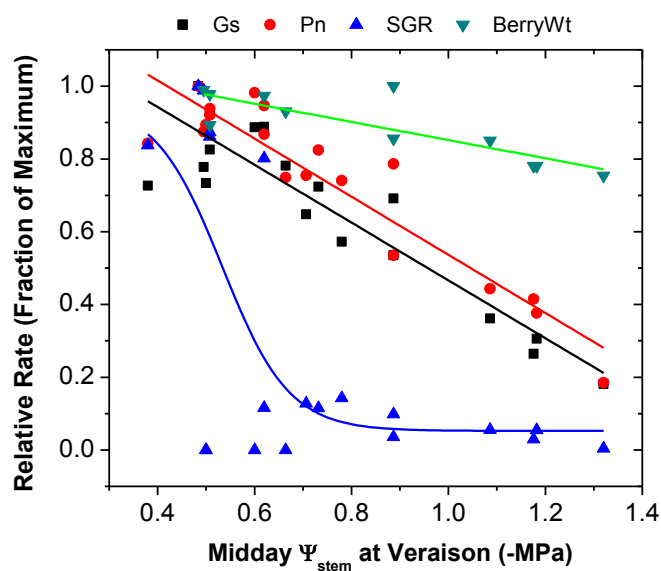


**Figure 4:** Relationship between ‘Riesling’ grapevine midday stem water potential ( $\Psi_{stem}$ ) and various physiological and fruit growth parameters ( $G_s$ =stomatal conductance,  $P_n$ =net assimilation (photosynthesis), SGR=shoot growth rate, BerryWt=average berry weight at harvest) as measured in long shoots over a 4-week period around veraison (2-weeks pre-veraison and 2-weeks post-veraison) in 2011 in the Finger Lakes region of NY.

The effects of mild- to moderate water stress on grape composition include increased grape soluble solids (probably a concentration-by-dehydration effect), increased berry skin tannins and anthocyanins, less fruity aromas in white wines but more fruity in red wines, higher concentrations of phenolic-free glycosyl glucose (Koundouras et al. 2009, Roby et al. 2004, Bindon 2007, Chapman et al. 2005, Myburg 2006, des Gaschons et al. 2005, Choné et al. 2001a). These effects are highly variable depending on variety, environmental conditions, soil type, rootstock, and irrigation level and strategy (Iland et al. 2011). A comprehensive review of the effects of various environmental and vineyard management practices, including of the effects of irrigation, on berry and wine composition can be found in Reynolds (2010). In my research with Riesling grapevines, I looked into the effects of vine water stress on grape size (berry weight) and berry composition (soluble solids) on shoots of various lengths (Ch. 3).

### 1.5.2 Xylem hydraulic conductance and its measurement

In the flow pathway between roots and leaves, roots are reported to have the lowest hydraulic conductance or the highest hydraulic resistance (Vandeleur et al. 2009). Specific hydraulic resistances in the xylem that determine flow arise primarily due to perforation plates (axial flow), bordered pits (radial flow), and the presence of tyloses, parenchymal cell outgrowths into the lumens of xylem vessels that are responses to wounding or pathogen infections (Canny 1997). Since the flow of sap in xylem is generally laminar (small Reynolds Number, the ratio of inertial to viscous forces), the effects of friction on the xylem wall is likely to be non-negligible, as is the case in pipe flow (Denn 1980). In laminar flow in cylindrical pipes such as xylem, the well-established Hagen-Poiseuille equation can be used to determine the hydraulic conductance (or its inverse, resistance),  $K$  ( $\text{kg s}^{-1}$ ), as:

$$K = \frac{\pi \Delta p \cdot D^4}{128 L \eta} \quad (1.12)$$

where  $\Delta p$  is the pressure difference between the two ends of the xylem segment (Pa),  $D$  is the xylem lumen diameter (m),  $L$  is the length of the xylem segment (m), and  $\eta$  is the shear viscosity (Pa s). From this relationship, it can be seen that conductance scales as diameter to the fourth power making large vessels greatly more efficient than small vessels at transporting water. From Eq. 1.12, the hydraulic conductivity,  $L_p$  ( $\text{kg m MPa}^{-1} \text{ s}^{-1}$ ), the conductance per unit pressure drop per distance ( $dP/dL$ ), can be determined (Tyree and Ewers 1989):

$$L_p = \frac{K}{\Delta p/L} = \frac{\pi D^4}{128 \eta} \quad (1.13)$$

Finally, the specific conductivity,  $L_s$  ( $\text{kg m}^{-1} \text{MPa}^{-1} \text{s}^{-1}$ ), can be calculated by normalizing the hydraulic conductivity by the cross-sectional area of the stem segment,  $A_s$  ( $\text{m}^2$ ) (Tyree and Ewers 1989).  $L_s$  is a useful measure of the efficiency of xylem vessels to transport water. In grapevines, Lovisolo and Schubert (1998) found that water stress resulted in lower shoot hydraulic conductivity, lower shoot specific conductivity, and lower leaf specific conductivity the same season water stress was imposed. The same authors found that water stress resulted in smaller xylem vessels, which they speculated would lower vulnerability to embolisms. In my study of the hydraulic performance of Riesling grapevines, I measured the hydraulic conductivity of shoots of various lengths to determine their ability and efficiency to transport water (Ch. 3).

### **1.5.3 Ultrasonic acoustic emissions to quantify xylem cavitation**

The C-T Theory of sap ascent in plants is based on the negative pressures (tensions,  $P_{liq}$ ) in sap that rises from roots to leaves. These tensions can pull air in from adjacent vessels through inter-vessel bordered pits in a process known as air-seeding (Zimmermann 1983), resulting in cavitation (water is replaced with vapor) of the xylem vessel element. Once cavitation occurs, the vapor expands filling the entire xylem vessel, becoming embolized and, therefore, non-conducting to sap. Since the early 20<sup>th</sup> century, audible ‘clicks’ from cavitations in the form of acoustic emissions (AE) have been detected in a variety of synthetic and biological systems using a microphone connected to an amplifier (Dixon 1914, Temperley 1947, Milburn and Johnson 1966). Milburn and Johnson (1966) found a correlation between the number of low frequency AEs (0.2-2 kHz) and water status of plant tissue; they were able to also show that decreasing the transpiration of the plant by bagging leaves in a polyethylene bag resulted in fewer ‘clicks’. It should be noted that while AEs have been detected from

xylem cavitations in the audible frequency range (0.2–2 kHz), this range makes the detection of acoustic signals from plants difficult due to interference from sounds in nature, laboratory, and instruments (Tyree and Dixon 1983). Fortunately, plant-derived AEs can also be detected at the ultrasonic range of around 150 kHz. Milburn and Johnson (1966) suggested that the likely source of ultrasonic AE (UAE) signals was xylem cavitations although considered the possibility that tissue fracture, breakage of bordered pits, or collapsing of cell walls of tracheid or vessel elements could be contributing to the sounds. Tyree and Dixon (1983) measured AE signals in the 0.1-1 MHz high frequency range and speculated that the source of the vibrations associated with ‘clicks’ were due to either oscillations in the hydrogen bonds of water, elastic oscillations in cell walls, torus aspiration (in gymnosperms), or structural failure of sapwood. Another complicating factor is the possibility that a single UAE event (detected) could represent more than one vessel simultaneously cavitating (Jackson 1996). Since cavitations result in oscillations or reverberations of sound, it is quite possible that multiple events could represent fewer actual cavitations. Sanford and Grace (1985) proposed that this issue can be resolved by estimating the number of vessel elements in a particular stem segment, and measuring the number of AE events on a well-hydrated stem segment that is left to dry on a bench although they did not specifically do this.

Cavitation from freezing and thawing of stems in a variety of trees was observed using UAE signals (Raschi et al. 1989). In field-grown irrigated and non-irrigated corn, Tyree et al. (1986) found that UAE events occurred in non-irrigated plants when  $\Psi_{\text{leaf}}$  fell below -1.8 MPa, while in well-irrigated plants, UAE events started below  $\Psi_{\text{leaf}}$  of -1.0 MPa. In fruit crops, higher numbers of UAEs were observed in drought-stressed apples, especially those with dwarfing rootstocks (Jones 1989). In cut roses, the rate of UAEs increased in conjunction with transpiration when stems were dehydrated in a gas exchange chamber (Spinarova et al. 2007).

The only known study measuring acoustic emissions on grapevines was by Chouzouri and Schultz (2005). The researchers subjected potted grapevines to varying levels of water stress and found that stomatal conductance decreased concomitantly with increased AEs as soil water level decreased, and that different cultivars had different sensitivities to water stress as determined by their different UAE rates. The technique of acoustic emissions measurement correlated well with hydraulic conductance measurements as a method to quantify xylem embolisms (Lo Gullo and Salleo 1991). A comprehensive review of acoustic emissions and detection techniques in plants is provided by Jackson (1996). Measurement of UAEs in field-grown grapevines was used in my research to quantify the rate of cavitations in xylem vessels of shoots within a single grapevine.

## **1.6 The need to measure water potential in plants and soils**

Water potential provides a physical basis by which the status of water in soils and plants can be comparably quantified. A number of studies have reported a close relationship between plant water potential and plant physiological and reproductive processes (Shackel 2007, Naor 2006, Flexas et al. 1999). In grapevines, vine water status, as indicated by its average seasonal stem water potential, has been reported to be a useful predictor of ripening and the quality of grapes and wine (van Leeuwen et al. 2009).

Since the soil water potential may be difficult to sample accurately due to spatial heterogeneity and sampling techniques, in many cases researchers will measure the water potential of a plant at pre-dawn, while there is little or no transpiration, to get an indication of the integrated water status of the soil around the roots. The concept is that when the plant is not transpiring, the soil and plant are both in equilibrium. Thus, the plant becomes a sensor of the soil water potential around the roots. However, predawn stem water potential ( $\Psi_{pd}$ ) may

not correlate as well to tree physiology in heterogeneous soils as under near-zero water loss, the wettest soil will re-hydrate the plant and control the pre-dawn water potential (Ameglio et al. 1999). However, under maximum water flux around midday, a small portion of wet soil may not be able to support the transpiration due to limitations in the conductivity of the soil, leading to drying around the roots. Consequently,  $\Psi_{md}$  may not always be correlated with  $\Psi_{pd}$  in heterogeneous soils. In my study on the effect of soil moisture deficit on grapevine physiology,  $\Psi_{pd}$  was used as an estimate of the moisture status of the soil as the soil was dried down during the growing season, while  $\Psi_{md}$  was used to estimate the water status of the vine during periods of maximum stress when other physiological, e.g. gas exchange, parameters were measured.

### **1.6.1 Rationale of measuring stem water potential in plants**

A number of soil- and plant-based measures exist for the characterization of plant water status. Soil-based measures of water have been shown to be useful for irrigation scheduling purposes (Liu et al. 2012, Madile et al. 2012, Abrisqueta et al. 2012, Dabach et al. 2013), since the amount of soil water sets the upper bound on plant available water (refer to Sec. 1.3 on soil water relations for an explanation). There are several drawbacks of using soil water potential to estimate plant water status or potential. Soil heterogeneity can mean that discrete sampling point measurements are not representative of a larger area (Jones 2007). For example, a neutron probe sample in one hectare only samples only 0.0005% of the soil assuming 1 meter of depth (15-25 cm sphere of influence); tensiometers sample much less. Furthermore, differences in rooting patterns, hydraulic architectures, and resistances between plant species and varying evaporative demands can result in rather different plant water status for the same soil moisture level. This is especially true for lianas such as grape that do not

have a programmed architecture but grow roots wherever conditions are most suitable. For measurements of soil water content all the above limitations apply, as well as the variable relationship between water content and water potential.

As many biochemical processes depend on cell turgor ( $\Psi_w^p$ ) of living cells, it would seem reasonable to use  $\Psi_w^p$  as a measure of plant water status. However, turgor only captures one component of the total water potential,  $\Psi_w$ , within living cells. In particular, differences in osmotic potentials and the stomatal strategies of various plants under water stress, e.g. isohydric vs. anisohydric, can make the use of  $\Psi_w^p$  as a measure of stress rather difficult (Jones 2007). A plant-based measure of water status should be more closely related to key physiological processes of the plant (e.g. photosynthesis, growth, crop productivity) rather than soil- and atmosphere-based (e.g. evapotranspiration) measures (Shackel 2007).

Midday stem water potential ( $\Psi_{stem}$ ) is often used in physiological studies to estimate the water status of plants. The advantage of using  $\Psi_{stem}$  is that it can be measured in various tissues as well as multiple times during the day. Patakas et al. (2005) showed that  $\Psi_{pd}$  tended to underestimate the average level of stress in the plant, while midday leaf water potential ( $\Psi_{leaf}$ ) responded to dynamic fluctuations in general and local environmental parameters (VPD, incident radiation, and specific leaf exposure) as well as stomatal adjustments and was, therefore, not well-correlated to the level of stress in the plant. The same researchers found  $\Psi_{stem}$  to be least susceptible to local environmental fluctuations and to be the best integrator of the water status of the entire plant as many leaves are all interacting to give the stem water potential. Naor (2006) reached a similar conclusion based on his review of studies undertaken on various orchard crops -- that both  $\Psi_{pd}$  and  $\Psi_{stem}$  were more closely related to physiological processes than was  $\Psi_{leaf}$ . Shackel (2007) found similar results in his study of almond and

grapevines. In a comparison of several crop water stress measurement techniques and indices, researchers reported that  $\Psi_{\text{leaf}}$  (as measured with a pressure chamber) was subject to spatial and temporal sampling limitations, and was both destructive and disruptive to the crop leaf community (O’Toole et al. 1984). Choné et al. (2001b) found in grapevines that  $\Psi_{\text{stem}}$  was the first indicator of water stress (and correlated well to leaf transpiration), followed by  $\Psi_{\text{pd}}$ , whereas  $\Psi_{\text{leaf}}$  was not well-correlated to soil moisture.

Table 1 in Jones (2007) provides an excellent summary of the relative value of different water status measures for the purposes of water transport, drought adaptation, plant breeding, and irrigation scheduling. Given the numerous advantages of measuring  $\Psi_{\text{stem}}$  highlighted above, I adopted this measure to quantify the water status of grapevines used in my drought stress study (Ch. 3).

## 1.7 Techniques to measure water potential in plants and soils, and their limitations

### 1.7.1 Current instruments

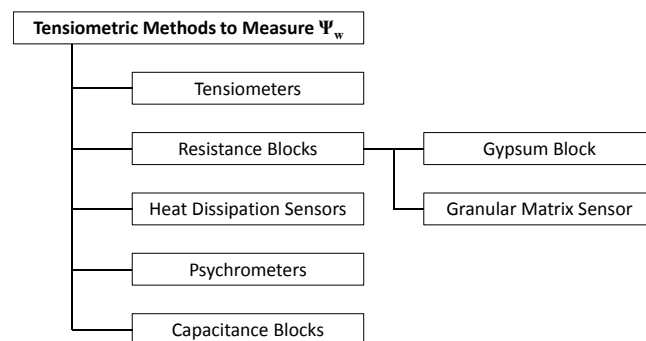


**Figure 5:** Tensiometric methods to measure soil water potential,  $\Psi_w$ .

Numerous techniques to measure soil and plant  $\Psi_w$  exist that are used to varying extents in commercial agriculture and research. Various tensiometric techniques are used to measure soil  $\Psi_w$  (Fig. 5). A tensiometer is an instrument originally developed for field use by Livingston (1908) and Lorenzo Richards (Richards 1931), and measures the hydrostatic pressure ( $P_{liq} < 0.1$  MPa) of a fixed internal volume of water that is in thermodynamic equilibrium with an external vapor phase ( $P_{liq} \approx \Psi_w^{liq} = \Psi_w^{vap}$ ) through a porous ceramic exchange tip (pore diameter  $\sim 2.5$   $\mu\text{m}$ ) (Cassel and Klute 1986). In soils,  $\Psi_w^{vap}$  is set by equilibration with its matric potential that accounts for adsorption and capillarity effects. As water in the instrument attempts to leave through the porous ceramic, the adhesive forces of water create an air-water meniscus within the pores, preventing the water from escaping until its Laplace (capillary, or bubbling) pressure is overcome. Since the maximum tensile strength of water is predicted to be around -190 MPa (Caupin et al. 2012), the factor determining the measurement range of the tensiometer is, therefore, the largest pore size within the ceramic tip (Eqs. 1.8-1.9). Most commercially-available soil tensiometers have a range from  $0 > \Psi_w > -85$  kPa, which is adequate for most soil moisture measurements in the context of irrigated agriculture (Cassel and Klute 1986) even though the wilting point (soil  $\Psi_w$ ) of many crops is around -1.5 MPa (Ahuja and Nielsen 1990). Ridley and Burland (1993) developed a tensiometer based on a -1500 kPa porous ceramic plate coupled to an electronic pressure transducer (pressure limit 3.5 MPa), and were able to measure soil suction pressures down to the limit of the porous ceramic plate, i.e. -1.5 MPa, with a response time of  $\sim 4$  min. Mendes and Buzzi (2013) developed a similar device as Ridley and Burland rated at 1500 kPa; their device had a larger volume (1100  $\text{mm}^3$  or 1.1 mL) compared to the Ridley and Burland model (10  $\text{mm}^3$  or 0.10 mL). The authors found no effect of the larger volume (hence, 'high capacity') on device performance as long as the liquid was pre-pressurized for several days prior to bringing under tension.

Another approach to tensiometry was developed by Peck and Rabbidge (1966, 1967, 1969) based on replacing the water inside the tensiometer with an osmotic solution that would raise the internal hydrostatic pressure ( $P_{liq} > 0.1$  MPa) to a maximum value corresponding to a zero matric potential, i.e. saturated soil. Upon soil drying,  $P_{liq}$  would decrease from its maximum positive value by an amount corresponding to the matric potential of the soil. More recently, a similar polymer tensiometer that extends the range of measurement range of  $\Psi_w$  to -1.6 MPa was developed based on the principle of increased osmotic pressure inside the instrument (de Rooij et al. 2009, Durigon et al. 2011). For unknown reasons, none of these tensiometers were commercialized even though they appeared promising in terms of measurement range.

Thermocouple psychrometry is another technique to measure water potential in both plants and soils (Boyer 1966, Dixon and Tyree 1984). The principle is that the tissue of interest is placed in a sealed chamber in which the humidity of the air is set by the tissue. The wet bulb depression or temperature difference between a wet and dry thermocouple as a result of the water status of the tissue can be used to estimate the tissue water potential via calibration with Antoine's equation or data on the saturation curve. While this device can be used to measure the osmotic potential of plant tissues (by disruption of cell walls) as osmometry, it is fairly difficult to set up correctly, requires highly precise temperature measurements, has long equilibration times (~ 8 h), and is, therefore, only practical for laboratory use (Jones 1992). They have a useful range of -100 kPa to -10 MPa (-100 bar), limited precision in the wet range, difficult to install, and are sensitive to temperature changes (Spanner 1951; Richards and Ogata 1958). *In situ* psychrometry of leaf water potential correlated linearly to the pressure chamber technique across a number of plant species, but overestimated the water potential in species that had high epidermal resistances (Turner et al. 1984).

Other techniques to measure soil water potential include resistance, capacitance, and heat dissipation measurements within porous blocks that are in equilibrium with the soil water (Fig. 5). Resistance blocks include granular matrix sensors (e.g. Watermark) and gypsum blocks in which changes in electrical resistance within the block correspond to changes in water content. Capacitance blocks (e.g. Decagon MPS-2) measure the charge time between parallel plates (within the porous block that is used as a dielectric), which is related to the moisture content. Commercially-available RH sensors based on capacitive sensing include Humiscan (General Eastern) and HMP 243 (Vaisala). These devices have an accuracy based on the RH being measured and are generally more accurate below 90% RH. For example, the Humiscan is reported to have an accuracy of  $\pm 1\%$  RH between 0-90% RH, and  $\pm 2\%$  RH above 90% RH. This translates to an error of between 1.3 – 2.7 MPa in the measurement of water potential. Similarly, the HMP 243 is reported to have an accuracy of  $\pm 0.1^\circ\text{C}$  in dewpoint measurement, translating to over  $\pm 0.6$  MPa in water potential. Decagon's MPS-2 has a reported range of -0.01 to -0.5 MPa with an accuracy of  $\pm 25\%$ . Heat dissipation sensors work by measuring the heat flow (heat pulse applied and temperature measured internally) across the porous block that is proportional to the water content. In all the above methods, water potential is obtained from water content using a moisture retention curve for the specific soil type.

Water potential or the activity of water can also be measured using an optical dewpoint measurement system, which measures the temperature of the condensate formation (dew point) on a chilled mirror. This is the gold-standard of water activity measurements and is known as the chilled mirror hygrometer, commercially available as 'Aqualab' Model 4TE (Decagon Devices, Inc., Pullman, WA), Model S8000 (Michell Instruments, U.K.), and DewMaster and Model 200M (EdgeTech, Marlborough, MA). Similar to a psychrometer, a sample of unknown water potential is placed in a closed chamber and comes to equilibrium

with the vapor in the chamber. A Peltier cooling system lowers the polished stainless steel mirror temperature (inside chamber) to the dew point of the vapor ( $p_{chamber}=p_{sat}(T)$ ), resulting in a condensation of the vapor on the chilled mirror. Reflection of incident light from the mirror detects the onset of condensation and controls the cooling precisely to maintain evaporation and condensation at the same rate. This dew point, measured by a platinum resistance thermometer (100  $\Omega$  at 0°C), can then be used to determine the activity of the sample. The accuracy of Aqualab 4TE is reported to be  $\pm 0.003 a_w$ , translating to a water potential of  $\pm 0.4$  MPa. Table 3 provides a list of various soil moisture sensors.

In plants, the leaf pressure chamber (Scholander et al. 1965) is very widely used to obtain both  $\Psi_{leaf}$  and  $\Psi_{stem}$  in both indoor and outdoor settings due to its relative portability and ease of use. The concept of this instrument is to place an excised leaf (with the petiole externally-exposed) into a closed chamber connected to a source of compressed air, and, upon slow pressurization of the chamber, to measure the ‘balance’ pressure when the first sign of sap is observed at the cut end. The balance pressure, as measured by an external pressure gauge connected to the chamber, relates to the original  $\Psi_{leaf}$  as (Jones 1992):

$$\Psi_{leaf} = \Psi_w^p + \Psi_w^s \quad (1.14)$$

Since  $\Psi_w^s$ , the apoplastic solute potential, is usually quite small,  $< 0.1$  MPa, this term is generally neglected (Jones 1992). Although the measurements are discrete (in time), destructive, and potential hazards exist with the use of compressed air, the pressure chamber procedure is fairly quick to perform (per leaf) and accurate. It correlates well with another technique, the cell pressure probe (Melcher et al. 1998), which measures the turgor pressure of individual plant cells or xylem tensions by means of a glass microcapillary that contains oil

whose change in pressure (due to turgor when inserted into a cell or tension when inserted into the xylem) is measured using a pressure transducer (Huskin et al. 1978).

Tables 2 and 3 summarize the main instruments currently utilized to measure soil water content and soil water potential, respectively, along with their pros and cons. Table 4 lists the current methods to measure the water status of plants with their pros and cons.

**Table 2: Methods to measure soil water content,  $\theta$ .**

Technique	Principle	Operating Range	Pros	Cons	References
<b>Qualitative Method</b>					
<b>Feel and Appearance</b>	Soil core samples taken at various depths and felt by hand. SWC based on various soil textures.	N/A	Easy to do, inexpensive.	Accuracy within 10-15% of true water content; rocky or stony soils are a problem.	Ley et al. (2009)
<b>Direct Method</b>					
<b>Gravimetric</b>	Over-drying soil cores of known volume at 105°C for 12-24 hrs until a constant mass is attained.	Full range of soil moisture	Low-cost, accurate, works well in uniform soils and not in gravelly, rocky, or shallow soils.	Destructive, time consuming, large sample size required for heterogeneous soils and profiles.	Campbell & Mulla (1990); Ley et al. (2009)
<b>Nuclear Methods</b>					
<b>Neutron scattering (neutron probe)</b>	High energy, fast neutrons from an Am/Be source slowed down (thermalized) after inelastic collisions with hydrogen molecules in soil water; lose kinetic energy; slow neutrons counted by detector. Measures total soil water content based on proper calibration by gravimetric sampling.	0-60% soil moisture	Non-destructive, in-situ	Need uniform soils; rocky or stony soils are problematic; B and Fe rich soils are also trouble; radiation hazard; dense root systems can interfere with actual soil moisture levels; does not work properly in top 8 inches of soil profile as neutrons escape; needs proper calibration in high B or OM soils; expensive (\$3500-\$4500); licensing and training costs to work with a radioactive source.	Gardner (1986)
<b>Gamma Ray Attenuation</b>	Gamma rays from a Cs source attenuated based on soil moisture, bulk density, thickness.	--	Quick; simultaneous measurement of bulk density and water content; non-destructive.	Expensive, radiation hazard; not suitable for field studies, only lab.	Schmugge et al (1980) Water Resour. Res. ; Gardner (1986)

Technique	Principle	Operating Range	Pros	Cons	References
<b>Microwave Methods</b>					
<b>Time Domain Reflectometry</b>	Uses water in the soil between two capacitance probes as a dielectric; high frequency EM wave transmission time across the probes measured, which is inversely proportional to the dielectric constant and water content; dry soil dielectric 2-5; wet soils 30; water 80; air 1, when measured between 30 Mhz and 1 GHz.	5-50% soil moisture	Rapid, easy; one calibration curve for all soils; non-destructive. In situ; shown to be as accurate as gravimetric method (Topp, 1984) once calibrated.	High attenuation in wet or saline soils result in failure to detect signal reflections; poor depth resolution; expensive (\$8000); not suitable for rocky soils.	Patterson & Smith (1981); Topp et al. (1980, 1982)
<b>Frequency Domain Reflectometry</b>	150 Mhz RF frequency waves used to measure soil capacitance, which is related to the dielectric constant of the soil around the probes based on geometry of the electric field around the electrodes, then uses the same technique as TDR to estimate soil water.	0-saturation	Good accuracy when calibrated properly especially in clay or high bulk density soils.	Expensive; Requires a close fitting tube.	Eller and Denoth (1996); Alva et al. (2003); Kinli et al. (2012); Xu et al. (2012)

**Table 3: Methods to measure soil water potential,  $\Psi$ .**

Technique	Principle	Operating Range	Pros	Cons	References
<b>Tensiometers</b>	Water in soil (matric potential) equilibrates with water in porous ceramic cup of tensiometer; drying of soil generates a tension in the water in the cup.	0 to -85 kPa	Very accurate; easy to install; inexpensive (\$75-\$200)	Limited range; only useful for irrigation scheduling; need to keep refilling water regularly; need many measurements in field.	Cassel & Klute (1986)
<b>Pressure Plate</b>	Indirect method; generates moisture release curves; positive pressure applied on soil sample on a porous plate. Moisture release from the soil onto plate is detected which is equal to the applied pneumatic pressure, equal to the negative of soil matric potential.	0 to -1500 kPa	Accurate in the 0-500 kPa range. Allows for simultaneous measurement of multiple samples.	Not suited for low water potentials or in-situ measurement; slow equilibration times on dry samples.	Klute (1986); Madsen et al. (1986); Bruce & Luxmoore (1986)
<b>Thermal Conductivity</b>	Heat dissipation of soil matrix gives the thermal conductivity of the matrix, used to infer water potential.	-10 to -1000 kPa	In-situ, used for irrigation scheduling; precise, easy to install; unaffected by salts.	Limited range; expensive; no spatial averaging; requires complex electronics.	Phene et al. (1971)
<b>Electrical Resistance Methods - Gypsum Blocks</b>	Matrix (gypsum) equilibrates with the soil and the electrical resistance is measured, which is related to the water content related to potential.	-30 to -200 kPa	In-situ; inexpensive (\$5-15 for block, \$200 for meter); easy to install.	Solutes/ions can affect readings; calibration needed; no spatial averaging; limited range; breakdown in alkaline soils or with high soluble salts.	Bouyoucos & Mick (1940)
<b>Filter Paper Method</b>	Filter paper of known water content equilibrated with soil sample for 1-2 days. Filter paper quickly removed from soil sample chamber; loose soil removed; filter paper sealed in a container for weighing and drying.	--	In-situ; inexpensive; simple; accurate.	Not suitable for irrigation scheduling due to large equilibration times required.	Gardner (1937); Hamblin (1981)
<b>Thermocouple Psychrometer</b>	Temperature difference between wet and dry bulbs gives the water potential; measures osmotic and matric potentials.	-100 kPa to -10 MPa	Matric + osmotic potentials; rapid measurement.	Low precision and range; not practical for irrigation scheduling; limited precision in the wet range; sensitive to temperature changes.	Spanner (1951); Richards & Ogata (1958)

**Table 4: Methods to measure plant water status.**

Technique	Principle	Operating Range	Pros	Cons	References
<b>Qualitative Method</b>					
<b>Feel and Appearance</b>	Leaf water status can be estimated by touching and slightly squeezing the leaf blade (lamina) to feel the degree of turgor in the cells. Appearance indicates degree of stress (wilting =high stress).	N/A	Easy to detect, inexpensive.	Only a qualitative estimate; not precise. Some growers use this method to decide when to irrigate. Cannot automate. Yield reduction occurs before visible symptoms.	Jones 2004
<b>Quantitative Methods</b>					
<b>Morphometric</b>	Measurements of growth and development of various organs and their components, e.g. xylem, leaf area, internode length, stem and fruit size.	N/A	Low-cost, easy to do; can be used for irrigation scheduling; very sensitive to water deficits.	Cannot be automated; instrumentation delicate and expensive.	Huguet et al. 1992; Lovisolo and Schubert 1998
<b>Dendrometry</b>	Measurement of trunk diameter or fruit size changes.	N/A	Inexpensive; useful for irrigation scheduling.	Cannot be automated easily	Naor and Cohen 2003; Ortuno et al. 2006
<b>Tissue Water Content (RWC, leaf thickness)</b>	Relative water content or leaf thickness measured with $\alpha$ or $\beta$ -ray sensors. Similar to morphometric measurements.	Full range from hydrated to dessicated	Easy to measure and automate; commercial sensors available.	Instrumentation complex and costly; complicated by isohydric plant, homeostatic regulation.	Jones 2004; Boyer et al. 2008; Bennett et al. 1987; Nakayama and Ehrlir 1964; Mederski 1961
<b>Thermal Sensing</b>	Infrared thermography measures leaf temperature from stomatal conductance (water stress=closed stomates=higher leaf temperature).	N/A	Can characterize large areas quickly; good for screening studies; early warning due to sensitivity of stomates to water stress.	Expensive equipment; prone to averaging error due to remote sensing.	Idso et al. 1981; Jones 2004a, b; Stoll and Jones 2007; Leinonen and Jones 2004
<b>Cell Pressure Probe (<math>\Psi_p</math>) Leaf Patch Clamp (ZIM-probe)</b>	Pulled glass capillary with oil or water inserted into plant cell which responds to cell turgor. Measures pressure component of water potential.	0 to 100 kPa turgor pressure	Shown to be well-correlated with pressure chamber readings.	Only suitable for laboratory setting; cannot be easily automated or used for irrigation scheduling.	Tomos and Leigh 1990; Huesken et al. 1978; Melcher et al. 1998; Rueger et al. 2010; Ehrenberger et al. 2012; Bramley et al. 2013; Angeles et al. 2004; Zimmermann et al. 2008

Technique	Principle	Operating Range	Pros	Cons	References
<b>Pressure Chamber (<math>\psi</math>)</b>	Measures balance pressure of leaf; can be used for stem water potential measurement.	0 to -4 MPa $\pm$ 0.02 MPa	Widely accepted and easy to do.	Destructive measurement; cannot be automated; needs pressurized gas; labor intensive; slow.	Scholander et al. 1965; Sperry et al. 1996
<b>Psychrometer (<math>\psi</math>)</b>	Measures humidity of air in equilibrium with plant tissue sample (can also be done with soils); measures dew point of air with thermocouples.	-0.1 MPa to -10 MPa $\pm$ 0.001 MPa	Precise; valuable output; can be automated; slow to respond; can be embedded in plant tissue.	Large errors associated with imprecise temperature measurements or due to temperature gradients within the psychrometer chamber; expensive; requires specialized skill to install, operate.	Hsiao 1990; Dixon and Tyree 1984; Jones 2004
<b>Acoustic Emissions</b>	Measures ultrasonic sounds from the cavitation of xylem vessels under water stress.	N/A	Sensitive to increasing water stress; very sensitive instrumentation.	Different plants have different thresholds of cavitation. Expensive equipment; not practical for irrigation scheduling; cannot indicate rehydration.	Tyree and Sperry 1989; Jones 1989; Jackson 1996; Sanford 1985
<b>Sap Flow</b>	Provides measure of water flux through plants using heat conduction/balance methods. A measure of the sap/water conductance of the plant.	N/A	Sensitive to water stress; being used by Fruition Sciences (CA) for irrigation scheduling in vineyards. Can be automated.	Indirect estimate of conductance; complex instrumentation requiring technical expertise and calibration per plant.	Fruition Sciences: <a href="http://www.fruitionsciences.com">www.fruitionsciences.com</a> ; Conejero et al. 2007; Ginestar et al. 1998; Green et al. 2003; Fernandez et al. 2008
<b>Porometer</b>	Measures stomatal conductance of a leaf based on water vapor balance in a cuvette.	N/A	Accurate; good for research studies; moderately expensive equipment.	Labor intensive; costly; not automated; not for commercial application.	Jones 2004; Idso 1988; Meidner 1992; Flexas et al. 1992
<b>Chlorophyll Fluorescence</b>	Excess light energy that is not absorbed by leaves for photosynthesis is reflected as longer wavelength light and measured by fluorometers.	N/A	Accurate; can be used for a variety of stress responses, e.g. photosynthetic performance. Easy to measure. Powerful when combined with gas exchange measurements.	Requires expertise in physiology; specialized instrumentation and knowhow to operate; requires good planning and design of experiment otherwise results difficult to interpret.	Maxwell and Johnson 2000; Krause 1991; Flexas 1998; Epron et al. 1992

### 1.7.2 MEMS-based sensors to measure water potential

Microelectromechanical systems (MEMS) represent a family of miniature integrated devices comprising both electrical and mechanical components. MEMS has been an enabling technology for a number of decades and has pervaded applications ranging from biotechnology (DNA amplification), medicine (blood pressure sensors), communications (RF and microwave circuits), and inertial sensing (inertial sensors, accelerometers, gyroscopes), e.g. in cars and smartphones. The advantages of MEMS-based devices include small form factor, low cost due to the economies of scale associated with large-scale IC fabrication, ability to integrate electronics and mechanics, and the availability of a mature toolset based on IC fabrication for their manufacture.

In the context of plants and soils, MEMS-based sensors offer some key advantages for the measurement of water potential over existing techniques. Some of the advantages are:

- Low internal volumes: conventional soil tensiometers have internal volumes ranging from a few mL to > 100 mL. MEMS-based tensiometers would have internal volumes < 1  $\mu$ L which reduces the volume of metastable liquid and, hence, the lowers the probabilities of both impurities and cavitation.
- MEMS materials: silicon and glass are inherently wetting materials that are compatible with water.
- Cleanroom process: microfabrication in a cleanroom minimizes the risk of potential contamination of the internal components of the device. This lowers the probability of cavitation due to impurities on the internal walls of the device.

- Design flexibility: Computer-aided design (CAD) of the devices provide flexibility to make a variety of design configurations on a single wafer, as well as rapid changes to the design, if needed.
- Small form factor: allows for the embedding in plant stems and trunks for direct measurement of stem water potential. Can be used multi-season for the same reason.
- Data acquisition and compatibility: electronic pressure sensor readings can be integrated with existing dataloggers due to simple voltage output. Sensor information can be transmitted wirelessly in real-time using telemetric units to a datalogger, or to a GPRS (General Packet Radio Service) modem connected to an Internet server via a commercial mobile phone network.
- Cost: potential to manufacture sensors at low cost associated with economies of scale associated with mass manufacture.

However, a number of disadvantages or liabilities associated with MEMS exist, including:

- Microfabrication: requires access to cleanroom with extensive suite of fabrication tools and support. Also requires skilled individual with cleanroom fabrication expertise.
- Cost: High initial cost associated with cleanroom process characterization and prototype development. Possible long development time associated with this phase.
- Specialized equipment: Calibration needs to be done for each device since there is variability across a single wafer. Filling microfluidic devices requires specialized equipment (pressure chambers, etc.) to fill water under high pressure.
- Packaging: environmental applications such as moisture sensing in plants and soils require robust packaging to withstand harsh environments (temperature, radiation, resins of plants, contaminants in soils).

- User skill: MEMS devices need to be integrated into existing datalogging systems so require some user familiarity with these systems.

### **1.7.3 The ideal water potential sensor**

Numerous methods exist for the measurement of water status of a given system. The main considerations when selecting an appropriate sensor include application (irrigation scheduling, monitoring, and research), soil type and structure, plant type and range of typical water status levels, measurement range and accuracy, skill level required for operation, robustness, maintenance, and cost.

Given the above-mentioned advantages of MEMS technology for the measurement of soil and plant water potential, there exists an opportunity for the development of a new instrument that is capable of overcoming the limitations of existing moisture sensing technologies in plants and soils. The ideal water potential sensor would be versatile enough to measure both soil and plant  $\Psi_w$  over the full range found in most crops and soils. A small form factor would allow for the embedding in woody plant trunks and stems and measure  $\Psi_w$  to an extended range, while low-cost sensors would allow for many sensors to be deployed with sensor arrays to provide high spatial resolution. The sensor should respond in an appropriate timeframe, ideally in the order of minutes, in order to provide high temporal  $\Psi_w$  data as the plant responds to dynamic environmental conditions. Broad acceptance and use of the sensor would require relatively low unit cost as well as operations cost, be easy to embed into plants and soils, and require little maintenance. Multi-season use would require that the sensors be able to withstand extremes in temperature and precipitation in a given region although low cost may allow changing sensors each season. These features would allow a sensor to be used in a wide

range of applications from precision irrigation of agronomic and horticultural crops, to forest ecology to monitor water fluxes of tree stands and vulnerability of forests to drought, as reported in a recent study by Choat (2012).

## **1.8 Summary**

Water's importance to both physiological and reproductive processes in land plants cannot be overstated. Water directly or indirectly affects seed germination, plant growth and development, and the ability to produce a crop (or fruit). Quantitative information on the water status of plants and soils provides information on a key component of the development physiology of most plants and is a particularly important part of plant biology research (Whalley *et al.* 2013), as well as to growers looking to manage water via irrigation. Yet, precise and direct measurements of water status in plants and soils remains challenging, partly due to the limitations of current instrumentation, or a lack of understanding in their use and limitations (*ibid.*). My doctoral research aimed to address both the above-mentioned issues. First, using the grapevine as a model plant, I set out to establish quantitative relationships between the water status of plants and their physiological and reproductive performance across a range of water status levels from well-watered to highly water-stressed. This information would inform both plant physiology researchers and commercial growers as to the optimum water status in their plants (grapevines) to maximize physiological growth, productivity (yield), and crop quality. Second, in order to obtain continuous and precise measurements of water status of plants for the above-mentioned study, I worked on the development of a prototype water potential (moisture) sensor known as a 'microtensiometer' based on microelectromechanical system (MEMS) technology that would offer a number of key advantages over the existing suite of moisture sensors available for plants and soils. I

envision the microtensiometer being a valuable tool to address outstanding questions in plant ecophysiology, to aid growers in irrigation management improving farm water use efficiency, and to avoid yield and quality losses. The worldwide trend towards greater use of technology and smart sensors to improve viticultural practices and optimize water utilization in vineyards to improve the quantity and quality of grapes has been the primary motivation for the work conducted in my doctoral degree that is described in the following chapters.

The dissertation is organized as follows: Chapter 2 provides a detailed description of the development and testing of a microtensiometer that is a potential technology for the measurement of water potential in a number of contexts including plants and soils. In Chapter 3, I describe the physiological responses of grapevines, specifically between shoots within individual grapevines, to water stress. The goal of this study was to investigate whether grapevine shoots had differing physiological and hydraulic responses to water stress based on their growth or vigor. In Appendix A, I describe a growth chamber study to investigate the reported phenomenon of stomatal oscillations in potted oaks and grapevines under water stress, and whether cavitation events in the xylem contribute to this phenomenon. Appendix B shows the detailed process flow schematic for the fabrication of the microtensiometer. Appendix C provides a list of photolithographic masks used for the fabrication of the microtensiometer. Appendix D shows the calculation of vapor pressure deficit (VPD) from temperature and relative humidity (RH).

## 1.9 References

- Abrisqueta I., Vera J., Tapia L.M., Abrisqueta J.M. & Ruiz-Sanchez M.C. (2012) Soil water content criteria for peach trees water stress detection during the postharvest period. *Agricultural Water Management*, **104**, 62-67.
- Ahuja & Nielsen D.R. (1990) *Irrigation of agricultural crops*. American Society of Agronomy, Madison, Wis., USA.
- Alva A.K., Collins H.P., Fraisse C. & Boydston R.A. (2003) Evaluation of Enviroscan capacitance probes for monitoring soil moisture in center pivot irrigated potatoes. *Zeitschrift fur Bewässerungswirtschaft*, **38**, 93-109.
- Ameglio T., Archer P., Cohen M., Valancogne C., Daudet F.A., Dayau S. & Cruiziat P. (1999) Significance and limits in the use of predawn leaf water potential for tree irrigation. *Plant and Soil*, **207**, 155-167.
- Angeles G., et al. (2004) The Cohesion-Tension theory. *New Phytologist*, **163**, 451-452.
- Antoine C. (1888) Tensions des vapeurs; nouvelle relation entre les tensions et les températures. *Comptes Rendus des Séances de l'Académie des Sciences. Paris.*, **107**, 681-684, 778-780, 836-837.
- Balling A. & Zimmermann U. (1990) Comparative measurements of the xylem pressure of *Nicotiana* plants by means of the pressure probe and pressure bomb. *Planta*, **182**, 325-338.
- Barigah T.S., Charrier O., Douris M., Bonhomme M., Herbette S., Ameglio T., Fichot R., Brignolas F. & Cochard H. (2013) Water stress-induced xylem hydraulic failure is a causal factor of tree mortality in beech and poplar. *Annals of Botany*, **112**, 1431-1437.
- Bennett J.M., Sinclair T.R., Muchow R.C. & Costello S.R. (1987) Dependence of stomatal conductance on leaf water potential, turgor potential, and relative water content in field-grown soybean and maize. *Crop Science*, **27**, 984-990.
- Bouyoucos G.J. & Mick A.H. (1940) An electrical resistance method for the continuous measurement of soil moisture under field conditions. *Technical Bulletin. Michigan Agricultural Experiment Station*, **172**, 38.
- Boyer J.S., James R.A., Munns R., Condon T. & Passioura J.B. (2008) Osmotic adjustment leads to anomalously low estimates of relative water content in wheat and barley. *Functional Plant Biology*, **35**, 1172-1182.

- Bramley H., Ehrenberger W., Zimmermann U., Palta J.A., Ruger S. & Siddique K.H.M. (2013) Non-invasive pressure probes magnetically clamped to leaves to monitor the water status of wheat. *Plant and Soil*, **369**, 257-268.
- Brodersen C.R., McElrone A.J., Choat B., Matthews M.A. & Shackel K.A. (2010) The dynamics of embolism repair in xylem: in vivo visualizations using high-resolution computed tomography. *Plant Physiology*, **154**, 1088-1095.
- Bronick C.J. & Lal R. (2005) Soil structure and management: a review. *Geoderma*, **124**, 3-22.
- Bruce R.R. & Luxmoore R.J. (1986) Water retention: field methods. In: *Methods of soil analysis. Vol. 1. 2nd ed.* (ed A. Klute), pp. 663-686. American Society of Agronomy, Madison, WI.
- Buttrose M.S. (1969) Fruitfulness in grapevines: I Effects of light intensity and temperature. *Botanical Gazette*, **130**, 166-173.
- Buttrose M.S. (1974) Fruitfulness in grape-vines: effects of water stress. *Vitis*, **12**, 299-305.
- Campbell G.S. & Mulla D.J. (1990) Measurement of soil water content and potential. In: *Irrigation of agricultural crops* (eds B.A. Stewart & D.R. Nielsen), pp. 127-142. American Society of Agronomy, Madison, Wis., USA.
- Canny M.J. (1995) A new theory for the ascent of sap - cohesion supported by tissue pressure. *Annals of Botany*, **75**, 343-357.
- Canny M.J. (1997) Tyloses and the maintenance of transpiration. *Annals of Botany*, **80**, 565-570.
- Cassel D.K., Klute, A. (1986) Water potential: Tensiometry. In: *Methods of Soil Analysis. Part I: Physical and Mineralogical Methods. Agronomy Monograph No. 9 (2nd edn.)* 563-596. (ed G.S. Campbell, Jackson, R.D., Mortland, M.M., Nielsen, D.R., Klute, A.). Am. Soc. Agron. Inc., Madison, Wisconsin.
- Caupin F., Arvengas A., Davitt K., Azouzi M.E., Shmulovich K.I., Ramboz C., Sessoms D.A. & Stroock A.D. (2012) Exploring water and other liquids at negative pressure. *Journal of Physics-Condensed Matter*, **24**.
- Chalmers D.J., Mitchell P.D. & Vanheek L. (1981) Control of peach-tree growth and productivity by regulated water supply, tree density, and summer pruning. *Journal of the American Society for Horticultural Science*, **106**, 307-312.
- Chapman D.M., Roby G., Ebeler S.E., Guinard J.X. & Matthews M.A. (2005) Sensory attributes of Cabernet Sauvignon wines made from vines with different water status. *Australian Journal of Grape and Wine Research*, **11**, 339-347.

- Charlton M.D.B., Lau H.W. & Parker G.J. (1996) *High aspect ratio photo-assisted electro-chemical etching of silicon and its application for the fabrication of quantum wires and photonic band structures*. Paper presented at the Microengineering Applications in Optoelectronics, IEE Colloquium.
- Chaves M.M., Santos T.P., Souza C.R., Ortuno M.F., Rodrigues M.L., Lopes C.M., Maroco J.P. & Pereira J.S. (2007) Deficit irrigation in grapevine improves water-use efficiency while controlling vigour and production quality. *Annals of Applied Biology*, **150**, 237-252.
- Chaves M.M., Zarrouk O., Francisco R., Costa J.M., Santos T., Regalado A.P., Rodrigues M.L. & Lopes C.M. (2010) Grapevine under deficit irrigation: hints from physiological and molecular data. *Annals of Botany*, **105**, 661-676.
- Choat B., et al. (2012) Global convergence in the vulnerability of forests to drought. *Nature*, **491**, 752-756.
- Chone X., Leeuwen C.v., Chery P., Ribereau-Gayon P. & van Leeuwen C. (2001a) Terroir influence on water status and nitrogen status of non-irrigated Cabernet Sauvignon. Vegetation development, must and wine composition. *South African Journal for Enology and Viticulture*, **22**, 8-15.
- Chone X., Leeuwen C.v., Dubourdieu D., Gaudillere J.P. & van Leeuwen C. (2001b) Stem water potential is a sensitive indicator of grapevine water status. *Annals of Botany*, **87**, 477-483.
- Conejero W., Alarcon J.J., Garcia-Orellana Y., Nicolas E. & Torrecillas A. (2007) Evaluation of sap flow and trunk diameter sensors for irrigation scheduling in early maturing peach trees. *Tree Physiology*, **27**, 1753-1759.
- Conejero W., Mellisho C.D., Ortuno M.F., Moriana A., Moreno F. & Torrecillas A. (2011) Using trunk diameter sensors for regulated deficit irrigation scheduling in early maturing peach trees. *Environmental and Experimental Botany*, **71**, 409-415.
- Cutler J.M., Rains D.W. & Loomis R.S. (1977) Importance of cell size in water relations of plants. *Physiologia Plantarum*, **40**, 255-260.
- Dabach S., Lazarovitch N., Simunek J. & Shani U. (2013) Numerical investigation of irrigation scheduling based on soil water status. *Irrigation Science*, **31**, 27-36.
- Davies W.J. & Zhang J.H. (1991) Root signals and the regulation of growth and development of plants in drying soil. *Annual Review of Plant Physiology and Plant Molecular Biology*, **42**, 55-76.

- de Rooij G.H., van der Ploeg M.J., Gooren H.P.A., Bakker G., Hoogendam C.W., Huiskes C., Kruidhof H. & Koopal L.K. (2009) Measuring very negative water potentials with polymer tensiometers: principles, performance and applications. *Biologia*, **64**, 438-442.
- Denn M.M. (1980) *Process fluid mechanics*. Prentice-Hall, Englewood Cliffs, N.J.
- des Gachons C.P., Leeuwen C.v., Tominaga T., Soyer J.P., Gaudillere J.P., Dubourdiou D., des Gachons C.P. & van Leeuwen C. (2005) Influence of water and nitrogen deficit on fruit ripening and aroma potential of *Vitis vinifera* L. cv Sauvignon Blanc in field conditions. *Journal of the Science of Food and Agriculture*, **85**, 73-85.
- Dixon H.H., Joly, J. (1895) On the ascent of sap. *Philosophical Transactions of the Royal Society of London Series B-Biological Sciences*, **186**, 563-576.
- Dixon M.A. & Tyree M.T. (1984) A new stem hygrometer, corrected for temperature-gradients and calibrated against the pressure bomb. *Plant Cell and Environment*, **7**, 693-697.
- Dry P.R. & Loveys B.R. (1998) Factors influencing grapevine vigour and the potential for control with partial rootzone drying. *Australian Journal of Grape and Wine Research*, **4**, 140-148.
- Dry P.R., Loveys B.R., McCarthy M.G. & Stoll M. (2001) Strategic irrigation management in Australian vineyards. *Journal International des Sciences de la Vigne et du Vin*, **35**, 129-139.
- Durigon A., Gooren H.P.A., Lier Q.d.J.v. & Metselaar K. (2011) Measuring hydraulic conductivity to wilting point using polymer tensiometers in an evaporation experiment. *Vadose Zone Journal*, **10**, 741-746.
- Düring H. (1985). Osmotic adjustment in grapevines. *Acta Horticulturae (ISHS)*, **171**, 315-330.
- Ehrenberger W., Rueger S., Fitzke R., Vollenweider P., Guenthardt-Goerg M., Kuster T., Zimmermann U. & Arend M. (2012) Concomitant dendrometer and leaf patch pressure probe measurements reveal the effect of microclimate and soil moisture on diurnal stem water and leaf turgor variations in young oak trees. *Functional Plant Biology*, **39**, 297-305.
- Eller H. & Denoth A. (1996) A capacitive soil moisture sensor. *Journal of Hydrology (Amsterdam)*, **185**, 137-146.
- Eller C.B., Lima A.L. & Oliveira R.S. (2013) Foliar uptake of fog water and transport belowground alleviates drought effects in the cloud forest tree species, *Drimys brasiliensis* (Winteraceae). *New Phytologist*, **199**, 151-162.

- Epron D., Dreyer E. & Breda N. (1992) Photosynthesis of oak trees (*Quercus petraea* (Matt) Liebl.) during drought under field conditions: diurnal course of net CO<sub>2</sub> assimilation and photochemical efficiency of photosystem II. *Plant, Cell and Environment*, **15**, 809-820.
- FAO (January 2013) Aquastat. United Nations Food and Agriculture Organization. <http://www.fao.org/nr/water/aquastat/main/index.stm>
- Fernandez J.E., Green S.R., Caspari H.W., Diaz-Espejo A. & Cuevas M.V. (2008) The use of sap flow measurements for scheduling irrigation in olive, apple and Asian pear trees and in grapevines. *Plant and Soil*, **305**, 91-104.
- Fisher J.C. (1948) The fracture of liquids. *Journal of Applied Physics*, **19**, 1062-1067.
- Flexas J., Bota J., Escalona J.M., Sampol B. & Medrano H. (2002) Effects of drought on photosynthesis in grapevines under field conditions: an evaluation of stomatal and mesophyll limitations. *Functional Plant Biology*, **29**, 461-471.
- Flexas J., Escalona J.M. & Medrano H. (1998) Down-regulation of photosynthesis by drought under field conditions in grapevine leaves. *Australian Journal of Plant Physiology*, **25**, 893-900.
- Flexas J., Escalona J.M. & Medrano H. (1999) Water stress induces different levels of photosynthesis and electron transport rate regulation in grapevines. *Plant, Cell and Environment*, **22**, 39-48.
- Gardner R. (1937) A method of measuring the capillary tension of soil moisture over a wide moisture range. *Soil Science*, **43**, 277-283.
- Gardner W.H. (1986) Water content. In: *Methods of soil analysis. Part 1. Physical and mineralogical methods* (ed A. Klute). Soil Science Society of America, Inc., Madison, Wisconsin.
- Ginestar C., Eastham J., Gray S. & Iland P. (1998) Use of sap-flow sensors to schedule vineyard irrigation. II. Effects of post-veraison water deficits on composition of Shiraz grapes. *American Journal of Enology and Viticulture*, **49**, 421-428.
- Green S., Clothier B. & Jardine B. (2003) Theory and practical application of heat pulse to measure sap flow. *Agronomy Journal*, **95**, 1371-1379.
- Hamblin A.P. (1981) Filter-paper method for routine measurement of field water potential. *Journal of Hydrology, Amsterdam*, **53**, 355-360.
- Hsiao T.C. (1973) Plant responses to water stress. *Annual Review of Plant Physiology and Plant Molecular Biology*, **24**, 519-570.

- Hsiao T.C., Acevedo E., Fereres E. & Henderson D.W. (1976) Stress metabolism - water stress, growth, and osmotic adjustment. *Philosophical Transactions of the Royal Society of London Series B-Biological Sciences*, **273**, 479-500.
- Huguet J.G., Li S.H., Lorendeau J.Y. & Pelloux G. (1992) Specific micromorphometric reactions of fruit trees to water stress and irrigation scheduling automation. *Journal of Horticultural Science*, **67**, 631-640.
- Husken D., Steudle E. & Zimmermann U. (1978) Pressure probe technique for measuring water relations of cells in higher plants. *Plant Physiology*, **61**, 158-163.
- Idso S.B., Allen S.G. & Choudhury B.J. (1988) Problems with porometry: measuring stomatal conductance of potentially transpiring plants. *Agricultural and Forest Meteorology*, **43**, 49-58.
- Idso S.B., Reginato R.J., Jackson R.D. & Pinter P.J., Jr. (1981) Measuring yield-reducing plant water potential depressions in wheat by infrared thermometry. *Irrigation Science*, **2**, 205-212.
- Iland P., Dry P.R., Proffitt T. & Tyerman S.D. (2011) *The grapevine: from the science to the practice of growing vines for wine*. Patrick Iland Wine Promotions, Campbelltown, Adelaide, S. Aust.
- Intrigliolo D.S. & Castel J.R. (2009) Response of *Vitis vinifera* cv. 'Tempranillo' to partial rootzone drying in the field: water relations, growth, yield and fruit and wine quality. *Agricultural Water Management*, **96**, 282-292.
- IPCC (2007) The AR4 synthesis report. Fourth Assessment Report. *United Nations Intergovernmental Panel on Climate Change*. [http://www.ipcc.ch/publications\\_and\\_data/ar4/syr/en/contents.html](http://www.ipcc.ch/publications_and_data/ar4/syr/en/contents.html)
- Jackson G.E. & Grace J. (1996) Field measurements of xylem cavitation: Are acoustic emissions useful? *Journal of Experimental Botany*, **47**, 1643-1650.
- Javot H. & Maurel C. (2002) The role of aquaporins in root water uptake. *Annals of Botany*, **90**, 301-313.
- Jones H.G. (1990) Physiological aspects of the control of water status in horticultural crops. *HortScience*, **25**, 19-26.
- Jones H.G. (1992) *Plants and microclimate: a quantitative approach to environmental plant physiology*. Cambridge University Press, Cambridge [England]; New York, NY, USA.

- Jones H.G. (2004) Application of thermal imaging and infrared sensing in plant physiology and ecophysiology. In: *Advances in Botanical Research Incorporating Advances in Plant Pathology, Vol 41* (ed J.A. Callow), pp. 107-163.
- Jones H.G. (2004) Irrigation scheduling: advantages and pitfalls of plant-based methods. *Journal of Experimental Botany*, **55**, 2427-2436.
- Jones H.G. (2007) Monitoring plant and soil water status: established and novel methods revisited and their relevance to studies of drought tolerance. *Journal of Experimental Botany*, **58**, 119-130.
- Jones H.G., Higgs K.H. & Bergamini A. (1989) The use of ultrasonic detectors for water-stress determination in fruit trees. *Annales Des Sciences Forestieres*, **46**, S338-S341.
- Jones H.G., Stoll M., Santos T., Sousa C.d., Chaves M.M. & Grant O.M. (2002) Use of infrared thermography for monitoring stomatal closure in the field: application to grapevine. *Journal of Experimental Botany*, **53**, 2249-2260.
- Kinzli K.D., Manana N. & Oad R. (2012) Comparison of laboratory and field calibration of a soil-moisture capacitance probe for various soils. *Journal of Irrigation and Drainage Engineering*, **138**, 310-321.
- Kliewer M.W. (1968) Effect of temperature on the composition of grapes grown under field and controlled conditions. *Proceedings. American Society for Horticultural Science*, **93**, 797-806.
- Kliewer W.M., Freeman B.M. & Hossom C. (1983) Effect of irrigation, crop level and potassium fertilization on Carignane vines. I. Degree of water stress and effect on growth and yield. *American Journal of Enology and Viticulture*, **34**, 186-196.
- Kliewer W.M. & Schultz H.B. (1973) Effect of sprinkler cooling of grapevines on fruit growth and composition. *American Journal of Enology and Viticulture*, **24**, 17-26.
- Koch G.W., Sillett S.C., Jennings G.M. & Davis S.D. (2004) The limits to tree height. *Nature*, **428**, 851-854.
- Koundouras S., Hatzidimitriou E., Karamolegkou M., Dimopoulou E., Kallithraka S., Tsialtas J.T., Zioziou E., Nikolaou N. & Kotseridis Y. (2009) Irrigation and rootstock effects on the phenolic concentration and aroma potential of *Vitis vinifera* L. cv Cabernet Sauvignon grapes. *Journal of Agricultural and Food Chemistry*, **57**, 7805-7813.
- Kramer P.J.B.J.S. (1995) *Water relations of plants and soils*. Academic Press, San Diego.
- Krassow H., Campabadal F. & Lora-Tamayo E. (2000) Wafer level packaging of silicon pressure sensors. *Sensors and Actuators A-Physical*, **82**, 229-233.

- Krause G.H. & Weis E. (1991) Chlorophyll fluorescence and photosynthesis: the basics. *Annual Review of Plant Physiology and Plant Molecular Biology*, **42**, 313-349.
- Lambers H.C.F.S.P.T.L. (1998) *Plant physiological ecology*. Springer, New York.
- Leeuwen C.v., Tregouat O., Chone X., Bois B., Pernet D., Gaudillere J.P. & van Leeuwen C. (2009) Vine water status is a key factor in grape ripening and vintage quality for red Bordeaux wine. How can it be assessed for vineyard management purposes? *Journal International des Sciences de la Vigne et du Vin*, **43**, 121-134.
- Leinonen I. & Jones H.G. (2004) Combining thermal and visible imagery for estimating canopy temperature and identifying plant stress. *Journal of Experimental Botany*, **55**, 1423-1431.
- Ley T.W., Stevens R.G., Topielec R.R. & Neibling W.H. (2009) Soil water monitoring & measurement. In: *Irrigation factsheet PNW0475*. Washington State University.
- Liu H., Yang H., Zheng J., Jia D., Wang J., Li Y. & Huang G. (2012) Irrigation scheduling strategies based on soil matric potential on yield and fruit quality of mulched-drip irrigated chili pepper in Northwest China. *Agricultural Water Management*, **115**, 232-241.
- Livingston B.E. (1908) A simple atmometer. *Science*, **28**, 319-320.
- Loveys B.R. & Kriedemann P.E. (1973) Rapid changes in abscisic acid-like inhibitors following alterations in vine leaf water potential. *Physiologia Plantarum*, **28**, 476-479.
- Lovisollo C., Perrone I., Carra A., Ferrandino A., Flexas J., Medrano H. & Schubert A. (2010) Drought-induced changes in development and function of grapevine (*Vitis* spp.) organs and in their hydraulic and non-hydraulic interactions at the whole-plant level: a physiological and molecular update. *Functional Plant Biology*, **37**, 98-116.
- Lovisollo C. & Schubert A. (1998) Effects of water stress on vessel size and xylem hydraulic conductivity in *Vitis vinifera* L. *Journal of Experimental Botany*, **49**, 693-700.
- Madile A.K., Singh P.K., Sharma H.C., Singh R.P. & Ganga J. (2012) Tensiometer based drip irrigation scheduling for enhancing water productivity of capsicum (*Capsicum annum* L.) under polyhouse. *Indian Journal of Soil Conservation*, **40**, 41-45.
- Madsen H.B., Jensen C.R. & Boysen T. (1986) A comparison of the thermocouple psychrometer and the pressure plate methods for determination of soil water characteristic curves. *Journal of Soil Science*, **37**, 357-362.
- Matthews M.A., Anderson M.M. & Schultz H.R. (1987) Phenologic and growth responses to early and late season water deficits in Cabernet franc. *Vitis*, **26**, 147-160.

- Maxwell K. & Johnson G.N. (2000) Chlorophyll fluorescence - a practical guide. *Journal of Experimental Botany*, **51**, 659-668.
- McCarthy M.G. (1997) The effect of transient water deficit on berry development of cv Shiraz (*Vitis vinifera* L.). *Australian Journal of Grape and Wine Research*, **3**, 102-108.
- Mederski H.J. (1961) Determination of internal water status of plants by beta ray gauging. *Soil Science*, **92**, 143-146.
- Meidner H. (1992) Developments in mass flow porometry. *Journal of Experimental Botany*, **43**, 1309-1314.
- Melcher P.J., Meinzer F.C., Yount D.E., Goldstein G. & Zimmermann U. (1998) Comparative measurements of xylem pressure in transpiring and non-transpiring leaves by means of the pressure chamber and the xylem pressure probe. *Journal of Experimental Botany*, **49**, 1757-1760.
- Mendes J. & Buzzi O. (2013) New insight into cavitation mechanisms in high-capacity tensiometers based on high-speed photography. *Canadian Geotechnical Journal*, **50**, 550-556.
- Milburn J.A. (1973) Cavitation in *Ricinus* by acoustic detection: induction in excised leaves by various factors. *Planta*, **110**, 253-265.
- Milburn J.A. (1973) Cavitation studies on whole *Ricinus* plants by acoustic detection. *Planta*, **112**, 333-342.
- Milburn J.A. (1996) Sap ascent in vascular plants: Challengers to the cohesion theory ignore the significance of immature xylem and the recycling of Munch water. *Annals of Botany*, **78**, 399-407.
- Milburn J.A. & Johnson R.P.C. (1966) Conduction of sap. 2. Detection of vibrations produced by sap cavitation in *Ricinus* xylem. *Planta*, **69**, 43-52.
- Moller M., Alchanatis V., Cohen Y., Meron M., Tsipris J., Naor A., Ostrovsky V., Sprintsin M. & Cohen S. (2007) Use of thermal and visible imagery for estimating crop water status of irrigated grapevine. *Journal of Experimental Botany*, **58**, 827-838.
- Morgan, J.M. (1984) Osmoregulation and water stress in higher plants. *Annu. Rev. Plant Physiol. Plant Mol. Biol.* **35**, 299-319.
- Myburg P.A. (2006) Juice and wine quality responses of *Vitis vinifera* L. cvs. Sauvignon blanc and Chenin blanc to timing of irrigation during berry ripening in the coastal region of South Africa *South African Journal of Enology and Viticulture*, **27**, 1-7.

- Nagarajah S. (1989) Physiological responses of grapevines to water stress. *Acta Horticulturae*, 249-256.
- Nakayama F.S. & Ehrlner W.L. (1964) Beta ray gauging technique for measuring leaf water content changes and moisture status of plants. *Plant Physiology*, **39**, 95-98.
- Naor A. (2006) Irrigation scheduling and evaluation of tree water status in deciduous orchards. *Horticultural Reviews*, **32**, 111-165.
- Naor A. & Cohen S. (2003) Sensitivity and variability of maximum trunk shrinkage, midday stem water potential, and transpiration rate in response to withholding irrigation from field-grown apple trees. *HortScience*, **38**, 547-551.
- Naor A., Gal Y. & Peres M. (2006) The inherent variability of water stress indicators in apple, nectarine and pear orchards, and the validity of a leaf-selection procedure for water potential measurements. *Irrigation Science*, **24**, 129-135.
- Nobel P.S. (2005) *Physicochemical and environmental plant physiology*. Elsevier Academic Press, Amsterdam; Boston.
- Or D. (2001) Who invented the tensiometer? *Soil Science Society of America Journal*, **65**, 1-3.
- Ortuno M.F., Garcia-Orellana Y., Conejero W., Ruiz-Sanchez M.C., Alarcon J.J. & Torrecillas A. (2006) Stem and leaf water potentials, gas exchange, sap flow, and trunk diameter fluctuations for detecting water stress in lemon trees. *Trees: Structure and Function*, **20**, 1-8.
- O'Toole J.C., Turner N.C., Namuco O.P., Dingkuhn M. & Gomez K.A. (1984) Comparison of some crop water stress measurement methods. *Crop Science*, **24**, 1121-1128.
- Patakas A., Nikolaou N., Zioziou E., Radoglou K. & Noitsakis B. (2002) The role of organic solute and ion accumulation in osmotic adjustment in drought-stressed grapevines. *Plant Science*, **163**, 361-367.
- Patakas A., Noitsakis B. & Chouzouri A. (2005) Optimization of irrigation water use in grapevines using the relationship between transpiration and plant water status. *Agriculture Ecosystems & Environment*, **106**, 253-259.
- Patterson D.E. & Smith M.W. (1980) The use of time domain reflectometry for the measurement of unfrozen water content in frozen soils. *Cold Regions Science and Technology*, 205-210.
- Peck A.J. & Rabbidge R.M. (1966) Soil water potential - Direct measurement by a new technique. *Science*, **151**, 1385-1386.

- Peck A.J. & Rabbidge R.M. (1967) Note on an instrument for measuring water potentials particularly in soils. *Australian Journal of Instrumentation & Control*, **23**, 59.
- Peck A.J. & Rabbidge R.M. (1969) Design and performance of an osmotic tensiometer for measuring capillary potential. *Soil Science Society of America Proceedings*, **33**, 196-202.
- Phene C.J., Hoffman G.J. & Rawlins S.L. (1971) Measuring soil matric potential in situ by sensing heat dissipation within a porous body. 1. Theory and sensor construction. *Soil Science Society of America Proceedings*, **35**, 27-33.
- Phene C.J., Rawlins S.L. & Hoffman G.J. (1971) Measuring soil matric potential in situ by sensing heat dissipation within a porous body. 2. Experimental results. *Soil Science Society of America Proceedings*, **35**, 225-229.
- Pickard W.F. (1981) The ascent of sap in plants. *Progress in Biophysics & Molecular Biology*, **37**, 181-229.
- Plante A.F. & McGill W.B. (2002) Soil aggregate dynamics and the retention of organic matter in laboratory-incubated soil with differing simulated tillage frequencies. *Soil & Tillage Research*, **66**, 79-92.
- Reynolds A.G. (2010) *Managing wine quality*. Woodhead Publishing, Oxford.
- Reynolds A.G. & Naylor A.P. (1994) 'Pinot noir' and 'Riesling' grapevines respond to water stress duration and soil water-holding capacity. *HortScience*, **29**, 1505-1510.
- Reynolds A.G., Parchomchuk P., Berard R., Naylor A.P. & Hogue E. (2005) Gewurztraminer grapevines respond to length of water stress duration. *International Journal of Fruit Science*, **5**, 75-94.
- Richards L.A. (1931) *Capillary conduction of liquids through porous mediums*, Cornell University.
- Richards L.A. & Ogata G. (1958) Thermocouple for vapor pressure measurement in biological and soil systems at high humidity. *Science*, **128**, 1089-1090.
- Ridley A.M. & Burland J.B. (1993) A new instrument for the measurement of soil-moisture suction. *Geotechnique*, **43**, 321-324.
- Ristic R., Downey M.O., Iland P.G., Bindon K., Francis I.L., Herderich M. & Robinson S.P. (2007) Exclusion of sunlight from Shiraz grapes alters wine colour, tannin and sensory properties. *Australian Journal of Grape and Wine Research*, **13**, 53-65.

- Roby G., Harbertson J.F., Adams D.A. & Matthews M.A. (2004) Berry size and vine water deficits as factors in winegrape composition: anthocyanins and tannins. *Australian Journal of Grape and Wine Research*, **10**, 100-107.
- Ruhl E. & Alleweldt G. (1985) Investigations into the influence of time of irrigation on yield and quality of grape-vines. *Acta Horticulturae*, 457-462.
- Sancho-Knapik D., Peguero-Pina J.J., Farinas M.D., Alvarez-Arenas T.G. & Gil-Pelegrin E. (2013) Ultrasonic spectroscopy allows a rapid determination of the relative water content at the turgor loss point: a comparison with pressure-volume curves in 13 woody species. *Tree Physiology*, **33**, 695-700.
- Sandford A.P. & Grace J. (1985) The measurement and interpretation of ultrasound from woody stems. *Journal of Experimental Botany*, **36**, 298-311.
- Santos T.P.d., Lopes C.M., Rodrigues M.L., Souza C.R.d., Maroco J.P., Pereira J.S., Silva J.R. & Chaves M.M. (2003) Partial rootzone drying: effects on growth and fruit quality of field-grown grapevines (*Vitis vinifera*). *Functional Plant Biology*, **30**, 663-671.
- Schmugge T.J., Jackson T.J. & McKim H.L. (1980) Survey of methods for soil moisture determination. *Water Resources Research*, **16**, 961-979.
- Scholander.P.F., Hammel H.T., Bradstre.E.D. & Hemmings.E.A. (1965) Sap pressure in vascular plants - Negative hydrostatic pressure can be measured in plants. *Science*, **148**, 339-346.
- Shackel K.A. (2007) Water relations of woody perennial plant species. *Journal International des Sciences de la Vigne et du Vin*, **41**, 121-129.
- Slatyer R.O. & Taylor S.A. (1960) Terminology in plant- and soil-water relations. *Nature*, **187**, 922-924.
- Smart D.R., Carlisle E., Goebel M. & Nunez B.A. (2005) Transverse hydraulic redistribution by a grapevine. *Plant, Cell and Environment*, **28**, 157-166.
- Solomon S. (2010) *Water: the epic struggle for wealth, power, and civilization*. Harper, New York.
- Soltani A., Sinclair T.R. (2012) Modeling physiology of crop development, growth and yield. CABI, Wallingford, Oxfordshire, UK; Cambridge, MA.
- Souza C.R.d., Maroco J.P., Santos T.P.d., Rodrigues M.L., Lopes C., Pereira J.S., Chaves M.M., de Souza C.R. & dos Santos T.P. (2005) Control of stomatal aperture and carbon uptake by deficit irrigation in two grapevine cultivars. *Agriculture, Ecosystems & Environment*, **106**, 261-274.

- Spanner D.C. (1951) The Peltier effect and its use in the measurement of suction pressure. *Journal of Experimental Botany*, **2**, 145-168.
- Sperry J.S., Saliendra N.Z., Pockman W.T., Cochard H., Cruiziat P., Davis S.D., Ewers F.W. & Tyree M.T. (1996) New evidence for large negative xylem pressures and their measurement by the pressure chamber method. *Plant Cell and Environment*, **19**, 427-436.
- Spinarova S., Hendriks L., Steinbacher F., Schmid O. & Hauser B. (2007) Cavitation and transpiration profiles of cut roses under water stress. *European Journal of Horticultural Science*, **72**, 113-118.
- Stoll M. & Jones H.G. (2007) Thermal imaging as a viable tool for monitoring plant stress. *Journal International des Sciences de la Vigne et du Vin*, **41**, 77-84.
- Stroock A.D., Pagay, V.V., Zwieniecki, M.A., Holbrook, N.M. (2014) The physicochemical hydrodynamics of vascular plants. *Annu. Rev. Fluid Mech.*, **46**, 615-642.
- Studdert G.A. & Echeverria H.E. (2000) Crop rotations and nitrogen fertilization to manage soil organic carbon dynamics. *Soil Science Society of America Journal*, **64**, 1496-1503.
- Temperley H.N.V. (1947) The behavior of water under hydrostatic tension. 3. *Proceedings of the Physical Society of London*, **59**, 199-208.
- Tomos A.D. & Leigh R.A. (1999) The pressure probe: A versatile tool in plant cell physiology. *Annual Review of Plant Physiology and Plant Molecular Biology*, **50**, 447-472.
- Topp G.C., Davis J.L. & Annan A.P. (1980) Electromagnetic determination of soil water content: measurements in coaxial transmission lines. *Water Resources Research*, **16**, 574-582.
- Topp G.C., Davis J.L. & Annan A.P. (1982) Electromagnetic determination of soil water content using TDR: I. Applications to wetting fronts and steep gradients. *Soil Science Society of America Journal*, **46**, 672-678.
- Topp G.C., Davis J.L. & Annan A.P. (1982) Electromagnetic determination of soil water content using TDR: II. Evaluation of installation and configuration of parallel transmission lines. *Soil Science Society of America Journal*, **46**, 678-684.
- Turner N.C. & Jones M.M. (1980) Turgor maintenance by osmotic adjustment: A review and evaluation. In: *Adaptation of plants to water and high temperature stress* (eds N.C. Turner & P.J. Kramer), pp. 87-103. Wiley, New York.

- Turner N.C., Spurway R.A. & Schulze E.D. (1984) Comparison of water potentials measured by in situ psychrometry and pressure chamber in morphologically different species. *Plant Physiology*, **74**, 316-319.
- Tyerman S.D., Niemietz C.M. & Bramley H. (2002) Plant aquaporins: multifunctional water and solute channels with expanding roles. *Plant, Cell and Environment*, **25**, 173-194.
- Tyree M.T. (1997) The Cohesion-Tension theory of sap ascent: current controversies. *Journal of Experimental Botany*, **48**, 1753-1765.
- Tyree M.T. & Ewers F.W. (1991) Tansley review No 34 The hydraulic architecture of trees and other woody plants. *New Phytologist*, **119**, 345-360.
- Tyree M.T. & Sperry J.S. (1989) Characterization and propagation of acoustic emission signals in woody plants -- towards an improved acoustic emission counter. *Plant Cell and Environment*, **12**, 371-382.
- van den Honert T.H. (1948) Water transport in plants as a catenary process. *Discussions of the Faraday Society*, **3**, 146-153.
- Vandeleur R.K., Mayo G., Sheldon M.C., Gilliam M., Kaiser B.N. & Tyerman S.D. (2009) The role of plasma membrane intrinsic protein aquaporins in water transport through roots: diurnal and drought stress responses reveal different strategies between isohydric and anisohydric cultivars of grapevine. *Plant Physiology*, **149**, 445-460.
- van Leeuwen C., Tregoat O., Chone X., Bois B., Pernet D. & Gaudillere J.P. (2009) Vine water status is a key factor in grape ripening and vintage quality for red Bordeaux wine. How can it be assessed for vineyard management purposes? *Journal International Des Sciences De La Vigne Et Du Vin*, **43**, 121-134.
- van't Hoff J.H. (1885) Lois de l'equibre chimique dans 'etat dilue, gazez on dissons. *Kongliga Svenska Vetenskaps-Akademiens Handlingar*, **17**, 21.
- Wang Z., Quebedeaux B. & Stutte G.W. (1995) Osmotic adjustment: effect of water stress on carbohydrates in leaves, stems and roots of apple. *Australian Journal of Plant Physiology*, **22**, 747-754.
- Wang Z. & Stutte G.W. (1992) The role of carbohydrates in active osmotic adjustment in apple under water stress. *Journal of the American Society for Horticultural Science*, **117**, 816-823.
- Warrick A.W. (1990) Nature and dynamics of soil water. In: *Irrigation of agricultural crops. Agronomy No. 30* (eds B.A. Stewart & D.R. Nielsen), pp. xxvii, 1218 p. American Society of Agronomy, Madison, WI.

Xu J., Ma X., Logsdon S.D. & Horton R. (2012) Short, multineedle frequency domain reflectometry sensor suitable for measuring soil water content. *Soil Science Society of America Journal*, **76**, 1929-1937.

Zimmermann M.H. (1983) *Xylem Structure and the Ascent of Sap*. Springer-Verlag, New York, USA

Zimmermann U., Haase A., Langbein D. & Meinzer F. (1993) Mechanisms of long-distance water transport in plants. A reexamination of some paradigms in the light of new evidence. *Philosophical Transactions of the Royal Society of London Series B-Biological Sciences*, **341**, 19-31.

## **CHAPTER 2: A microtensiometer for the continuous measurement of very negative pressures of liquid water**

### **Abstract**

Tensiometers sense the chemical potential of water (or water potential) in an external phase of interest by measuring the pressure in an internal volume of liquid water in equilibrium with that phase. For sub-saturated phases, the internal pressure is below atmospheric and frequently negative; the liquid is under tension. Here, we present the initial characterization of a new tensiometer based on a microelectromechanical pressure sensor and a nanoporous membrane. We explain the mechanism of operation, fabrication, and calibration of this device. We show that these microtensiometers operate stably out to water potentials below -10 MPa, a tenfold extension of the range of current tensiometers. Finally, we present use of the device to perform an accurate measurement of the equation of state of liquid water at pressures down to -18 MPa. We conclude with a discussion of outstanding design considerations, and of the opportunities opened by the extended range of stability and the small form factor in sensing applications and in fundamental studies of the thermodynamic properties water.

### **2.1 Introduction**

In both natural and technological contexts, the degree of saturation with respect to water often plays a central role in defining a system's properties and function. For example, in the atmosphere, relative humidity is a critical meteorological indicator, and is important to evaporative demand on soil, bodies of water, and the biosphere<sup>1</sup>. In the context of plants and agriculture, water saturation in the soil and atmosphere controls viability, growth potential, yield, and quality of crop.<sup>2-4</sup> Balanced with osmotic forces in cells, cell turgor is maintained as

it is critical for plant growth and function. In foods, water activity affects taste, texture, and stability with respect to bacterial and fungal growth.<sup>5-8</sup> In chemical and biological processes, the osmotic strength of aqueous solutions controls the kinetics and thermodynamics of reactions and the stability of cells, proteins, and materials.<sup>5, 9-14</sup>

The chemical potential of water,  $\mu_w$  [ $\text{J mol}^{-1}$ ], within a phase or host material provides the most generally useful measure of the degree of hydration. This thermodynamic state variable quantifies the free energy of water molecules and thus their accessibility for chemical reactions and physical exchange with other phases or materials. For example, regardless of the local mode of transport, we can express the driving force for mass transfer as a gradient of chemical potential. In the following, we will characterize the chemical potential of water with two convenient state variables: 1) activity,  $a_w$ , the relative humidity of a vapor in equilibrium with the phase of interest ( $a_w = p/p_{sat}(T)$ , where  $p$  and  $p_{sat}(T)$  are the vapor pressure and saturation vapor pressure, respectively); 2) Water potential,  $\Psi_w$  [MPa], the deviation of the chemical potential from its value at saturation divided by the molar volume of liquid water ( $\Psi_w = (\mu_w - \mu_0(T))/v_{w,liq}$ ); this measure, with units of pressure, is widely used in the plant and soil science communities. The typical water potential range of plants and soils is  $-0.01 > \Psi_w > -3.0$  MPa ( $0.9999 > a_w > 0.978$ ), while a typical relative humidity in the atmosphere is around 50% ( $a_w \cong 0.5 \equiv \Psi_w \cong -67$  MPa at 20°C).

For *in situ* measurements, many methods of hygrometry exist: capacitance,<sup>15</sup> resistance,<sup>16</sup> thermal conductivity,<sup>17</sup> psychrometric,<sup>18-20</sup> and tensiometric.<sup>21, 22</sup> Capacitance, resistance, and dielectric methods measure the corresponding electronic property of a calibrated material within the sensor that is allowed to reach its equilibrium hydration with the phase of interest.

These methods allow for small form factors (e.g.  $< 1 \text{ cm}^2$  sensing areas), but generally provide moderate to low accuracy ( $\pm 0.002$  in activity;  $\pm 0.3 \text{ MPa}$  in water potential) for drier conditions ( $a_w < 0.9$ ), and become either slow in response or less accurate above this range.<sup>16</sup> <sup>23</sup> Despite their limited accuracy, resistive (gypsum block)<sup>24</sup> and capacitive (frequency domain reflectometry sensors)<sup>25, 26</sup> sensors are widely used to measure water status in soils for irrigation scheduling.

Psychrometric methods measure the dew point temperature with a psychrometric (wet bulb) thermocouple in equilibrium with the sample of interest through a vapor phase. The range of commercial psychrometers is reported by the manufacturer to be 0.9999 to 0.93 in activity and -0.01 to -10 MPa in water potential with an accuracy of  $\pm 0.001$  in activity and  $\pm 0.1 \text{ MPa}$  in water potential.<sup>27</sup> Of note, Dixon and Tyree developed a stem psychrometer for the continuous measurement of water potential of plant stems; this technique was shown to be in good agreement with the pressure chamber technique.<sup>28</sup>

Tensiometers, as we will discuss in detail in the following section, operate on the principle of equilibration between a sub-saturated vapor with a bulk volume of water via a microporous ceramic membrane that is able to support capillary pressures across an air-liquid interface (Fig. 2). Commercially-available tensiometers have a small range of 1 to 0.9988 in activity or 0 to -0.16 MPa in water potential with an excellent accuracy of  $\pm 5 \times 10^{-4} \text{ MPa}$  in water potential;<sup>29</sup> they fail due to invasion of air or cavitation beyond this range. Despite the extremely limited range and large form factors of conventional tensiometers (sensing area  $> 10 \text{ cm}^2$ ), their unmatched accuracy near saturation means that they are used extensively to monitor the water potential in soils for irrigation scheduling for annual crops that require moist conditions to grow.<sup>30</sup> In research contexts, a number of groups have extended the range

of operation of tensiometers. They have pursued two strategies: 1) Ridley and Burland first introduced the use of porous membranes with smaller pore sizes to achieve stability out to  $\Psi_w = -1.5$  MPa ( $a_w \cong 0.99$ ),<sup>31, 32</sup> these “high capacitance tensiometers” have had similar form factors as those of conventional tensiometers; 2) Peck and Rabbidge first introduced the use of osmotic solutions within the internal volume of the tensiometers to extend the stability limit,<sup>33, 34</sup> more recently, this approach has been refined and demonstrated out to  $\Psi_w = -1.6$  MPa ( $a_w = 0.988$ ) with a reduced form factor ( $1.5 \text{ cm}^2$ ).<sup>35-37</sup>

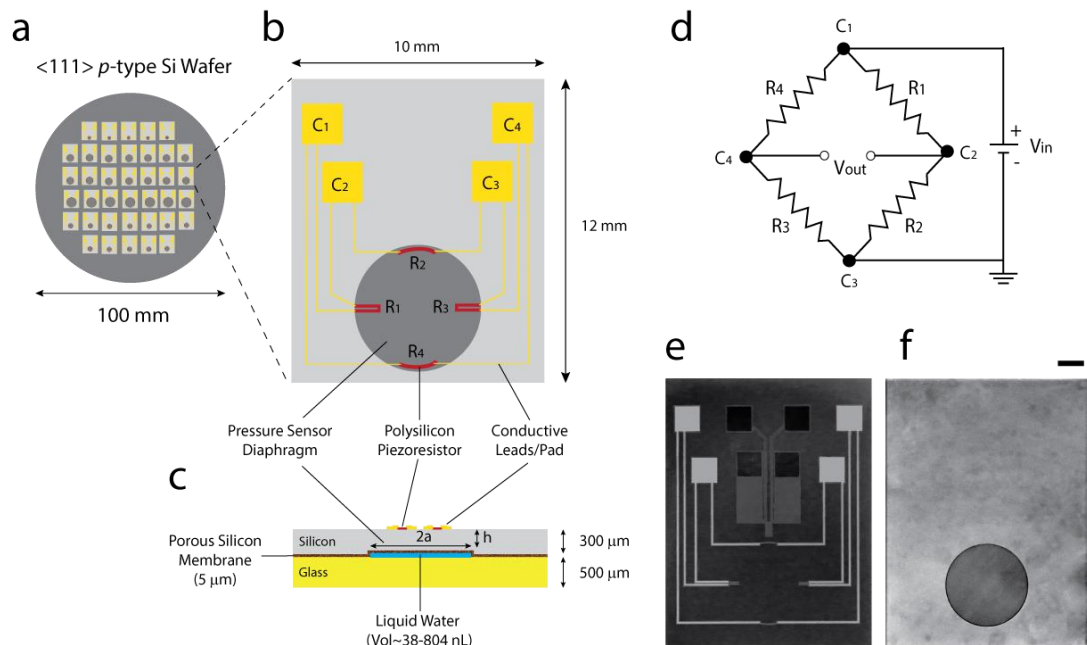
The range, accuracy, and fundamental limitations of these various hygrometric approaches are summarized in Table 1.

**Table 1:** Comparison of conventional methods of hygrometry.

Method	Range $\Psi_w$ (MPa), $a_w$	Accuracy ( $\pm\Psi_w$ MPa; $\pm a_w$ )	Response Time	Measurement Area/Volume	Limitations
Psychrometry <sup>27</sup>	$\Psi_w$ : -0.01 to -10 $a_w$ : 0.9999 to 0.93	$\Psi_w$ : $\pm 0.1$ $a_w$ : $\pm 0.001$	1 min	< 5 cm <sup>2</sup>	Temperature-sensitive, installation expertise required
Electro-Magnetic <sup>16, 23</sup>	$\Psi_w$ : -0.01 to -0.5 $a_w$ : 0.9999 to 0.996	$\Psi_w$ : $\pm 0.13$ $a_w$ : $\pm 9 \times 10^{-4}$	10-60 min	> 30 cm <sup>2</sup>	Low accuracy
Tensiometry <sup>29</sup>	$\Psi_w$ : +0.2 to -0.16 $a_w$ : 1 to 0.999	$\Psi_w$ : $\pm 5 \times 10^{-4}$	30 min	> 10 cm <sup>2</sup>	Small range, requires maintenance

The tensiometric approach presents a promising route to accurate measurements of chemical potential across the range near saturation ( $a_w > 0.9$ ,  $\Psi_w > -13.5$  MPa), if the stability limit can be significantly extended. Furthermore, the development over the past decades of robust Microelectromechanical systems (MEMS) for sensing pressure provides a route to reduce dramatically the form factor of tensiometers,<sup>38</sup> a smaller sensor could allow for measurements with higher spatial resolution and for embedding of the sensor within complex

samples such as the vascular system of living plants. A MEMS approach may also help extend the stability limit by: 1) minimizing the internal volume of the liquid that is placed at reduced pressure; 2) minimizing the presence of impurities that could destabilize the liquid by nucleating bubbles; and, 3) allowing for the formation of the exchange membrane in well-defined, nanoporous materials such as porous silicon. In an effort to exploit these opportunities, we have developed a MEMS-based ‘microtensiometer’.



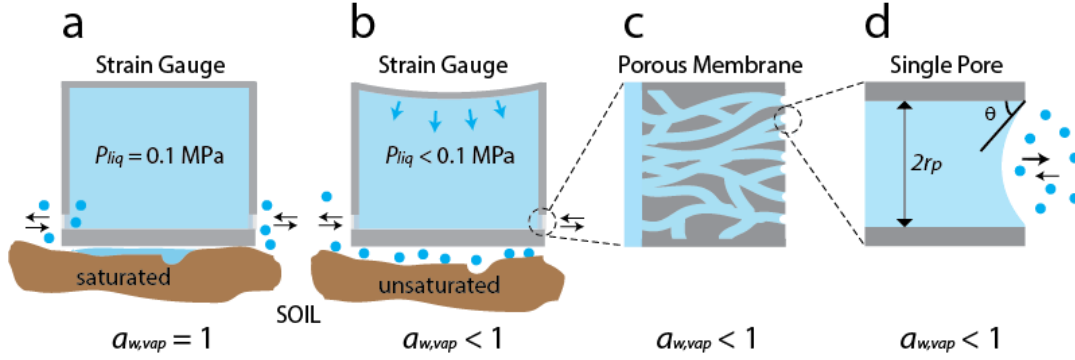
**Figure 1:** Microtensiometer. **(a)** Organization of tensiometers on a 4” p-type <111> silicon wafer. Wafer contains 38 sensors with diaphragms of various diameters: 1.4 mm (5), 2 mm (12), 4 mm (14), and 6.8 mm (7). **(b-c)** Top (b) and cross-sectional (c) views of a sensor with a 4 mm-diameter diaphragm. Aluminum leads and contact pads are shown in yellow and polysilicon resistors are shown in red. In (b), contact pads for Wheatstone bridge are labeled C<sub>1</sub>-C<sub>4</sub> and resistors are labeled R<sub>1</sub>-R<sub>4</sub>. In (c), the diaphragm radius and thickness are labeled a and h, respectively. **(d)** Wheatstone bridge configuration of piezoresistors and connections for applied (V<sub>in</sub>) and measured (V<sub>out</sub>) voltages. Labels of contact pads and resistors correspond to those in (b). **(e)** Photo showing top-view of an individual fabricated sensor (die) with 4 mm-diameter diaphragm. Patterned oxide for a platinum resistance thermometer (PRT) is visible in the center, top of the die. No PRT was fabricated on the microtensiometers described in this paper. **(f)** Bottom-view of device shown in (e) showing the porous silicon membrane surface and circular cavity of depth ~ 25 μm. Scale bar = 1.5 mm.

Fig. 1 presents an overview of our approach: Fig. 1a shows the layout of dies on each wafer, with 38 devices with four different diameters of diaphragm (1.4, 2, 4, and 6.8 mm) to provide a range of sensitivities. Figs. 1b-c show the top and cross-section views of a single device: a circular cavity hosts the internal volume of liquid; the layer of silicon above this cavity serves as the diaphragm; a thin layer of PoSi that covers the entire bonded surface of the silicon serves as the membrane; and a Wheatstone bridge of piezoresistors formed of polysilicon on the outer surface of the silicon serve as a strain gauge. Fig. 1d presents the architecture of the Wheatstone bridge. Figs. 1e-f show micrographs of the front- and back-side of a microtensiometer, respectively. Fig. 1e also shows the top center region with patterned oxide, a dielectric material for electrical isolation; this oxide will be used in the future to incorporate a platinum resistance thermometer (PRT); the PRT was not fabricated on the sensors characterized here.

In this paper, we describe the operating principle and fabrication of this microtensiometer, and characterize its stability, transient response, and use as a sensor in a laboratory environment. We conclude with a discussion of outstanding challenges and proposals of future applications that could address open questions in the thermodynamics of liquids, in plant and soil science (agriculture, plant physiology, ecology), and in materials such as food stuffs and concrete.

## 2.2 Background and theory

### 2.2.1 Working principle of tensiometry



**Figure 2:** Concept of tensiometry. **(a)** Bulk liquid in equilibrium ( $P_{liq} = p_{vap} \cong 0.1 \text{ MPa}$ ) with a saturated vapor ( $a_w = 1$ ; tensiometer placed in a sample, e.g. saturated soil) through a porous membrane (shown in light grey on two lower sides of the cavity); liquid-vapor equilibrium exists and no evaporation occurs from the bulk liquid. **(b)** Sub-saturated vapors ( $a_{w,vap} < 1$ ; tensiometer placed in unsaturated soil as an example) lower the hydrostatic pressure in the bulk liquid ( $P_{liq} < 0.1 \text{ MPa}$ ) until the capillary pressure of the air-liquid meniscus in the membrane is exceeded, resulting in evaporation of the bulk liquid. Changes in hydrostatic pressure are measured by measuring the deflection of a flexible diaphragm (strain gauge shown as curved plate on top side of cavity). **(c)** Porous membrane at the interface of the cavity couples external vapor with bulk water inside the cavity. **(d)** Close-up of a single pore within the membrane showing a concave air-liquid interface;  $r_p$  is the pore radius and  $\theta$  is the contact angle of the liquid with the wall of the membrane.

Tensiometry is based on the coupling of liquid water to vapor via a wettable porous membrane. The concept is illustrated in Fig. 2. Chemical equilibration occurs between a macroscopic volume (large enough volume to minimize interactions with walls that might affect the thermodynamic properties of the liquid; smallest cavity dimension  $> 1 \mu\text{m}$ )<sup>39</sup> of pure liquid inside a cavity within the tensiometer and a vapor that itself is in equilibrium with the chemical potential of the phase of interest outside the device (Eq. 1; Fig. 2).

$$\mu_{w,liq}(T, P_{liq}) = \mu_{w,vap}(T, p_{vap}) = \mu_{sample} \quad (1)$$

When exposed to a sub-saturated external phase, the pure water in the tensiometer will evaporate from the external surface of the membrane. This loss of fluid will reduce the pressure in the bulk phase ( $P_{liq}$ ) within the cavity (Figs. 2b-d). This reduction of pressure will

lower the chemical potential ( $\mu_{liq}$ ) of the internal liquid. If the liquid phase remains intact, the pressure will decrease until the internal and external chemical potentials are equal and transfer of water will cease. The pressure at which this equilibrium will occur can be found by expanding the expressions for the chemical potential of the pure liquid and vapor (ideal gas) in Eq. 1:

$$\begin{aligned} \mu_0(T) + \int_{P_{atm}}^{P_{liq}} v_{w,liq}(P'_{liq}, T) dP'_{liq} + RT \ln(a_{w,liq}) \\ = \mu_0(T) + RT \ln(a_{w,vap}) = \mu_{sample} \end{aligned} \quad (2)$$

where  $\mu_0(T)$  [J mol<sup>-1</sup>] is the chemical potential of water on the vapor-liquid coexistence line (in the presence of  $P_{atm}$  of air) at temperature  $T$  [K],  $v_{w,liq}$  [m<sup>3</sup> mol<sup>-1</sup>] is the molar volume of the liquid,  $R = 8.314$  [J mol<sup>-1</sup> K<sup>-1</sup>] is the ideal gas constant, and  $a_w = p_{vap}/p_{sat}(T)$  = relative humidity (%) / 100 is the activity of the vapor at temperature,  $T$ . If we take the liquid to be inextensible ( $v_{w,liq} = \text{constant}$ ), we can solve Eq. 2 for the internal pressure of water inside the tensiometer cavity,  $P_{liq}$ , at equilibrium ( $a_{w,liq} = a_{w,vap} = a_w$ ):

$$P_{liq} = P_{atm} + \frac{RT}{v_{w,liq}} \ln(a_w) = P_{atm} + \frac{\mu_{sample} - \mu_0}{v_{w,liq}} = P_{atm} + \Psi_w \quad (3)$$

We note that Eq. 3 provides approximate relations between the water potential of a phase, its activity, and the pressure within a pure liquid at equilibrium with that phase:<sup>40</sup>

$$\Psi_w = P_{liq} - P_{atm} = \frac{RT}{v_{w,liq}} \ln(a_w) \quad (4)$$

The relations in Eq. 4 hold within the approximation of constant molar volume of the liquid. We recognize in Eq. 4 that the water potential is the pressure difference across the diaphragm of the tensiometer (Figs. 2a-b). In other words, a tensiometer provides a direct, approximate measurement of water potential. Eq. 4 also allows us to understand the unusual sensitivity of

tensiometry near saturation: for  $a_w = 1 + \Delta a_w$  with  $\Delta a_w \ll 1$ , we have at room temperature ( $T = 293 \text{ K}$ ):

$$\Psi_w \cong \frac{RT}{v_{w,liq}} \Delta a_w \cong 135 \Delta a_w \text{ [MPa]} \quad (5)$$

As an example, for a 1% reduction in activity from saturation ( $\Delta a_w = -0.01$ ), the diaphragm of the tensiometer experiences a difference of pressure (from Eq. 5),  $\Psi_w = P_{w,liq} - P_{atm} \cong 1.3 \text{ MPa}$ . With appropriate design of the diaphragm and strain gauge, pressure differences as small as  $10^{-6} \text{ MPa}$  can be achieved,<sup>41</sup> allowing for extreme sensitivity to small changes in saturation.

The approximation of constant molar volume that led to Eq. 4 provides an over estimate in the magnitude of the water potential, but this error is less than 0.5% for  $\Psi_w > -22 \text{ MPa}$  ( $a_w > 0.85$ ) at  $20^\circ\text{C}$ . As indicated in Eq. 2, in order to achieve an exact determination of chemical potential,  $\mu_{sample}$  from the measurement of  $P_{liq}$  requires knowledge of the Equation of State (EoS) of the liquid along the isotherm at reduced pressure. The few existing measurements of thermodynamic properties of water at reduced pressure<sup>42</sup> suggest that the EoS of the IAPWS<sup>43</sup>,<sup>44</sup> provides accurate predictions at  $20^\circ\text{C}$  and down to  $P_{liq} \cong -20 \text{ MPa}$ .

### 2.2.2 Stability limit of tensiometers

As the pressure in the bulk, internal liquid,  $P_{liq}$ , drops below ambient,  $P_{atm} \cong 0.1 \text{ MPa}$ , it becomes susceptible to the invasion of air through the pores and to cavitation (formation of gas bubbles). Invasion of air will occur through the membrane when:

$$|P_{liq} - P_{atm}| > \frac{2\sigma \cos\theta_r}{r_{p,max}} \quad (6)$$

where  $\sigma$  is the surface tension of water [ $0.072 \text{ N m}^{-1}$ ],  $\theta_r$  [rad] is the receding contact angle of the liquid with the pore wall,  $r_{p,max}$  [m] is the radius of the largest pore that spans the membrane. The threshold in Eq. 6 represents the Young-Laplace pressure across a curved meniscus; for nanoscopic pores, it can only serve as a rough estimate of the threshold.<sup>45</sup> For  $p_{sat} < P_{liq} < P_{atm}$ , the internal liquid will be supersaturated with respect to air unless it has been degassed, and, therefore, be prone to cavitation by formation of bubbles of air. For lower pressures,  $P_{liq} < p_{sat}$ , the liquid will also be superheated and prone to cavitation via the formation of bubbles of vapor (boiling).<sup>44</sup> In the absence of pre-existing pockets of gas within the cavity, these two modes of cavitation will be kinetically limited and the liquid will be metastable.<sup>46, 47</sup> In conventional tensiometers, with macroscopic internal volumes and membranes with micrometer-scale pores, the stability limit tends to be  $|P_{liq} - P_{atm}| < 0.1 \text{ MPa}$ , or  $a_{w,vap} > 0.999$ . Work by our group suggests that this limit can be extended significantly ( $|P_{liq} - P_{atm}| > 20 \text{ MPa}$ ;  $a_{w,vap} < 0.86$ ) with the use of nanoporous membranes and smaller internal volumes.<sup>48</sup> This possibility motivated our construction of a microtensiometer to benefit from this extended range.

### 2.2.3 Piezoresistive pressure sensor

To measure the internal hydrostatic pressure of water, the microtensiometer uses the widely-developed diaphragm-based pressure transducer in which a pressure difference across the diaphragm results in its deflection, and the resulting strain is measured through piezoresistors. Specifically, our transducer consists of four doped polysilicon piezoresistors (Fig. 2b,  $R_1$ - $R_4$ ) in a Wheatstone bridge configuration (Fig. 2d) that sit atop a millimeter-sized circular diaphragm (Figs. 2b-c). The voltage response (output,  $V_{out}$ ) of the Wheatstone bridge for a given input or excitation voltage ( $V_{in}$ ) is a function of the resistance change of the

individual piezoresistors in response to stresses in the longitudinal ( $\sigma_l$ , along direction of current) and transverse ( $\sigma_t$ , perpendicular to direction of current) directions. Stress in the radial direction is function of the applied pressure ( $\Delta P$ ) as well as diaphragm dimensions (thickness,  $h$ ; radius,  $a$ ).<sup>49</sup> In our setup, all piezoresistors have the same value and thus  $V_{out}=0$  V when  $\Delta P=0$ . For equal magnitude resistances, the Wheatstone bridge response ( $\Delta V_{out}/\Delta V_{in}$ ) as a function of applied pressure ( $\Delta P$ ), diaphragm dimensions, and longitudinal and transverse piezoresistive coefficients,  $\pi_l$  and  $\pi_t$ , can be calculated as:

$$\frac{\Delta V_{out}}{\Delta V_{in}} \approx \frac{3a^2}{8h^2} (\pi_l(1-\nu) + \pi_t(\nu-1))\Delta P \quad (7)$$

where  $\nu$  is the Poisson Ratio of polysilicon ( $\sim 0.23$ ).

#### 2.2.4 Porous silicon membrane

Porous silicon (PoSi) has desirable characteristics for high-performance nanoporous membranes due to the ability to form nanoscopic pores allowing for high capillary pressures to be generated in the liquid phase. It is also possible to tune its pore size and morphology by varying the substrate crystal orientation, substrate composition (doping), current density of electrochemical etching, and etchant composition and concentration, making it a versatile material for a membrane.<sup>57</sup> Furthermore, as an inorganic membrane, it has the advantage over organic membranes of robustness and easy integration with other substrates such as glass.

PoSi is formed by anodic dissolution of single crystalline silicon in hydrofluoric acid (HF; Fig. 4a).<sup>57</sup> As described in the previous section (2.1), a PoSi membrane is made on the backside of the microtensiometer by electrochemical etching of *p*-type silicon (Fig. 1c, Fig.

4a). A key design criteria of the membrane was to obtain relatively homogenous pores with diameters in the order of several nanometers such that large capillary pressures could be generated in the bulk liquid (based on Eq. 6).

For example, pores of diameter 2 nm can generate over 70 MPa of tension in the liquid ( $P_{liq} < -70$  MPa). Additionally, it was desirable to have a solid membrane surface that was highly wettable (hydrophilic) with the receding contact angle of the liquid with the pore wall,  $\theta_r \sim 0^\circ$  (Eq. 6). The high wettability of PoSi results from the formation of a thin layer of native oxide on its surface, producing low contact angles with water ( $\theta_r < 10^\circ$ )<sup>61,62</sup> and aiding in the generation of high capillary pressures. The concentration of dopant used (boron for *p*-type silicon) as well as the applied anodization potential are known to affect pore morphology and branching.<sup>57,60</sup> Low current densities have been reported to produce smaller pores compared to high current densities, which produce more mesoporous structures.<sup>61,63</sup> Additionally, higher HF (etchant) concentrations have been known to aid in forming smaller pores.<sup>61-63</sup> The dilution of HF with either hydrochloric acid (HCl) or ethanol (EtOH) can also influence the structural properties of PoSi<sup>64,65</sup>; HCl results in sharper features and less in-depth inhomogeneities<sup>66</sup>, while EtOH results in thicker PoSi with greater mechanical strength.<sup>67</sup> The mechanical properties of PoSi, in particular, its Young's modulus depend on the type of doping (p- or n-type) and the current density used for electrochemical etching. PoSi based on moderately-doped *p*-type silicon have relatively high Young's modulus values ranging from 11 to 19 GPa depending on the current density used.<sup>68</sup>

## **2.3 Material and Methods**

### **2.3.1 Materials**

Double-side polished silicon wafers (4" diameter, 325  $\mu\text{m}$  thickness, *p*-type doping, resistivity range 1-10  $\Omega\text{-cm}$ ; University Wafer, <http://www.universitywafer.com>); Borofloat 33 glass wafer, double-side polished (4" diameter, 500  $\mu\text{m}$  thickness, Prime grade; University Wafer, <http://www.universitywafer.com>). Reagents used: hydrofluoric acid (49% w/w, in  $\text{H}_2\text{O}$ ; Sigma-Aldrich), ethanol (95% v/v; Sigma-Aldrich). Power supply for electrochemical etching: Agilent DC power supply (Model: 6613C, Agilent technologies, Santa Clara, CA). Microfabrication tools used in the cleanroom including oxide and thin-film deposition furnaces, photolithographic tools (resist spinner, contact aligner, wafer developer), wet etching reagents, dry etching tools (RF plasma etchers, oxygen plasma asher), PECVD thin film deposition, evaporator and sputtering tools (thin film metal deposition), high-temperature annealing tool, substrate bonder, and wafer dicing saw. Process characterization tools included profilometer, Filmmetrics thin film thickness analyzer, 4-point probe (wafer resistivity), and current-voltage (I-V) testing tool (resistor linearity).

### **2.3.2 Mask designs**

Photolithographic masks for the fabrication of the microtensiometer were made in the cleanroom of the Cornell Nanoscale Science and Technology Facility (CNF), Ithaca, NY. Individual mask (images) were designed using L-Edit computer-aided design software (Tanner EDA, Monrovia, CA). Using a high-resolution pattern generator (Model DWL 2000, Heidelberg Instruments, Heidelberg, Germany), the mask images were transferred to a 5"×5" fused-silica (quartz) plate ("photomask") coated with  $\sim 100$  nm chromium and photoresist.

Following pattern transfer (exposure), the photoresist on the exposed masks was developed and the chromium layer wet-etched. A complete list of masks used in the fabrication process is provided in Appendix C.

### 2.3.3 Fabrication

Fabrication of the microtensiometer was done in the cleanroom of the CNF. The process flow for the fabrication of a microtensiometer is shown in Fig. 3; a detailed version can be found in supplemental section, Fig. S1. A moderately-doped (1-10  $\Omega$ -cm resistivity) *p*-type  $\langle 111 \rangle$  double-side polished silicon wafer (100 mm-diameter, 325  $\mu\text{m}$ -thickness) was used. After standard RCA cleaning,  $\sim 1 \mu\text{m}$  of thermal oxide ( $\text{SiO}_2$ ) was grown in a furnace at 1000°C for electrical isolation (Fig. 3-i). Doped *p*<sup>+</sup> polysilicon ( $\text{B}_2\text{H}_6\text{:SiH}_4 \sim 0.045$ ) of thickness  $\sim 900 \text{ nm}$  was then deposited over the  $\text{SiO}_2$  using a LPCVD furnace at 620°C and 400 mTorr. The wafer was then annealed in argon at 900°C for 30 min to enhance the polysilicon strain response and relax residual stresses. Typical sheet resistivities of the LPCVD polysilicon were 200-250  $\Omega$ /square (pre-annealing) and 100-160  $\Omega$ /square (post-annealing). The polysilicon and  $\text{SiO}_2$  layers were then patterned using photolithography and dry (plasma) etching to form the piezoresistors (dimensions 1100  $\mu\text{m} \times 30 \mu\text{m} \times 1 \mu\text{m}$ ) and metal insulation pattern, respectively (Fig. 3-ii). After removing the backside  $\text{SiO}_2$  layer, a  $\sim 25 \mu\text{m}$  deep cavity was patterned and etched on the backside of the silicon wafer using deep reactive ion etching (Bosch process; Fig. 3-iii).

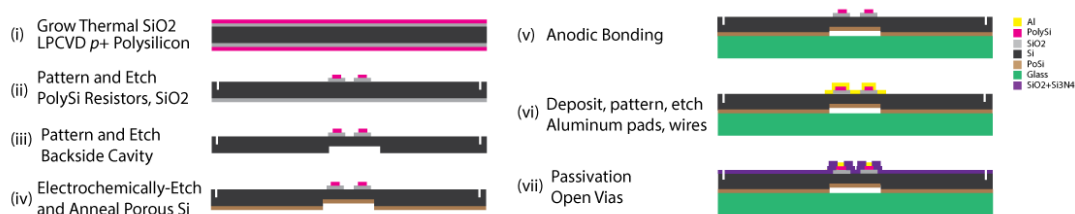


**Figure 3:** Microtensimeter fabrication process flow (abridged). A detailed process flow is provided in Appendix B.

The vapor exchange membrane of nanoporous silicon (PoSi) was then formed on the backside of the silicon wafer (Fig. 3-iv). The setup for the fabrication of PoSi used a custom-built electrochemical etch cell made of polytetrafluoroethylene (PTFE or Teflon) (Fig. 4a). To ensure electrical contact of the silicon wafer to the anode, the wafers were dipped in 6:1 buffered oxide etch (BOE) solution for 1 min to remove the native oxide, and then coated with  $\sim 200$  nm of aluminum by evaporation on the frontside of the wafer. The backside of the silicon wafer was then placed in contact with the etchant, a 50:50 (v/v) solution of 49% hydrofluoric acid (HF) and 95% ethanol (EtOH) in the etch cell. Electrochemical etching was done under constant current density of  $20 \text{ mA/cm}^2$  for 5 minutes using an Agilent DC power supply (Model 6613C, Agilent Technologies, Palo Alto, CA), resulting in a PoSi layer of approximately  $5 \mu\text{m}$  in thickness (Figs. 1c, 4b) with a pore diameter of 1-5 nm (Fig. 4d). After removing the aluminum on the topside of the wafer, the PoSi was annealed at  $700^\circ\text{C}$  for 30 sec in an  $\text{O}_2$  environment in order to replace the hydride-terminated silicon bonds ( $\text{SiH}_4$ ) with  $\text{O}_2$ -terminated silicon to form  $\text{SiO}_2$ ; this prevents the PoSi from degassing while bonding.

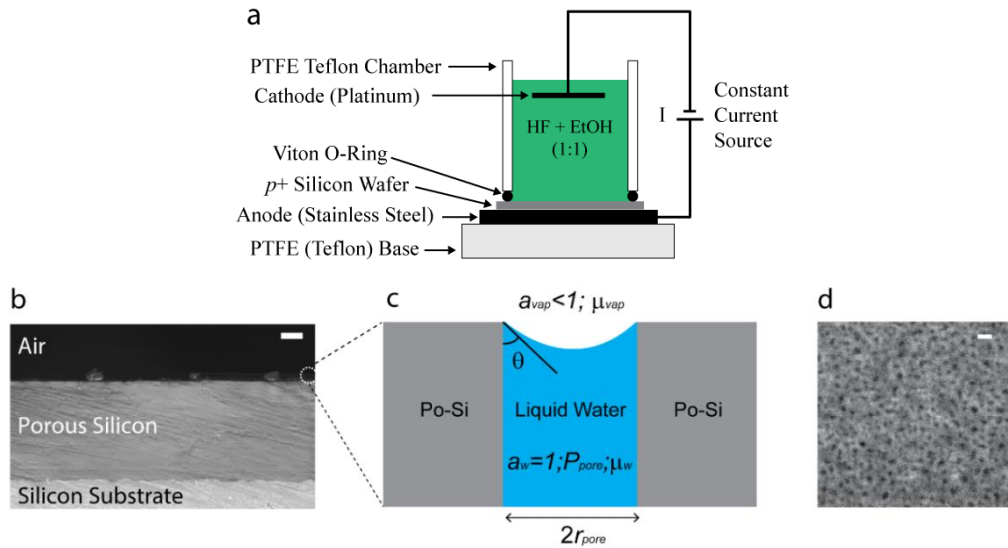


**Figure 4:** Nanoporous silicon membrane. **(a)** Electrochemical etch cell (cross-section) used for the formation of porous silicon. **(b)** Scanning electron micrograph cross-section of porous silicon membrane; scale bar = 1  $\mu\text{m}$ . **(c)** Schematic of an individual pore cross-section within the porous silicon membrane showing the liquid-vapor interface, the contact angle of water with the membrane wall ( $\theta$ ), and pore radius ( $r_{pore}$ ). **(d)** Nanoporous silicon (grey), top view, showing surface pores (dark spots) with diameters ( $2r_{pore}$ ) ranging from 1-5 nm; scale bar = 10 nm.

After annealing, the PoSi side of the wafer was anodically-bonded to a 100 mm diameter and 500  $\mu\text{m}$  thick borofloat glass wafer in vacuum at 400°C (Fig. 3-v) as follows: (i) the glass wafer was cleaned in a standard SC1 solution (29%  $\text{NH}_4\text{OH}$  and 30%  $\text{H}_2\text{O}_2$  in water at 70°C) for 10 minutes to remove any organic materials, while the silicon wafer was cleaned by rinsing with acetone and isopropyl alcohol; (ii) the silicon and glass wafers were dried and plasma cleaned in an oxygen plasma asher (RF 150 W, 4 min, 70 sccm); and, (iii) the silicon wafer (PoSi side) was anodically-bonded to the borofloat glass wafer using an anodic bonder (Model Sb8e, Süss Microtec, Garching, Germany).

After bonding, the electrical connections to the piezoresistors were formed. Following a short ( $\sim 15$  s) 30:1 BOE dip, a thin-film of aluminum ( $\sim 250$  nm) was evaporated on the frontside of the bonded wafer, patterned, and wet etched using a solution of phosphoric,

acetic, and nitric acids @ 50°C to form the contact pads and wires (Figs. 1b-c, Fig. 3-vi). Aluminum was selected as the thin-film metal as it makes ohmic contact with polysilicon. Following aluminum deposition, the metal was annealed at 400°C in a rapid thermal anneal tool in a H<sub>2</sub>/N<sub>2</sub> (forming gas) atmosphere for 2 min to improve the I-V linearity as well as decrease the contact resistance between aluminum and polysilicon.<sup>50, 51</sup> Electrical isolation and protection of the electronics on the topside of the silicon wafer was achieved by depositing a stack of PECVD oxide (SiO<sub>2</sub>; 400 nm), nitride (Si<sub>3</sub>N<sub>4</sub>; 200 nm), and oxynitride (SiO<sub>2</sub> + 15% Si<sub>3</sub>N<sub>4</sub>; 100 nm) at 200°C. This low deposition temperature was important to prevent debonding of the wafer. Vias were then opened over the metal pads using photolithography and dry etching (Fig. 3-vii). Lastly, individual devices (Fig. 1e-f) were released from the wafer by dicing with a wafer saw. A detailed process flow is given in Appendix B.

### **2.3.4 External electrical connections and measurements**

A custom-built jig (dimensions: 2.5 cm × 2.5 cm × 1.3 cm) made of rigid acrylic with gold spring-loaded electrical pins was used for the sensor calibration (in positive pressures of air) and testing at both ambient and controlled relative humidities (see next section for calibration and testing setup; Fig. 5). The jig allowed for exchange of vapor through the nanoporous membrane while the pressure sensor was operated. The Wheatstone bridge of the pressure sensor was excited on pads P<sub>1</sub> and P<sub>3</sub>, while the output voltage was measured on pads P<sub>2</sub> and P<sub>4</sub>. Pad 3 was grounded, so that the voltage difference between P<sub>1</sub> and P<sub>3</sub> was always the positive applied voltage on P<sub>1</sub>,  $V_{in}$ . An excitation voltage of 0.1 V was used for the pressure sensor, and based on an effective bridge resistance of 3 kΩ, resulted in a total current of less than 40 μA. Low operating currents were desirable to reduce Ohmic heating of the resistors. The jig (with the microtensiometer inside) was connected to an Agilent DC power supply

(Model 6611C, Agilent Technologies, Palo Alto, CA) and an Agilent digital multimeter (DMM, Model 34401A). Both the DMM and power supply were connected to a digital acquisition (DAC) board (National Instruments, Austin, TX) and PC running LabView (v.7 Express, National Instruments Corp., Austin, TX).

### Calibration of pressure sensor

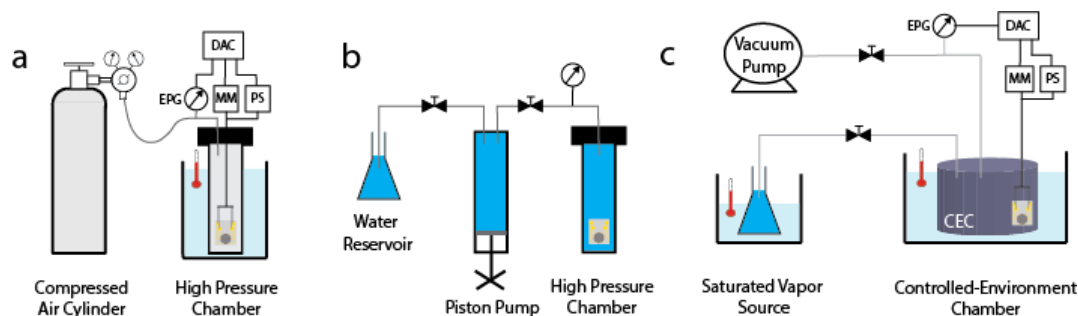


**Figure 5:** Experimental setup for calibration, filling, and testing of the microtensiometer. **(a)** Positive pressure of air used to calibrate pressure sensor to  $P_{air} > 10$  MPa at constant temperature. DAC=Data acquisition card + computer; MM=digital multimeter; PS=digital power supply; EPG=electronic pressure gauge. **(b)** Filling under high pressure ( $P_{liq} > 5$  MPa) of water. **(c)** Controlled environment chamber (CEC; dark grey air-tight cylinder) used to equilibrate sensor with sub-saturated vapor stream or saturated salts for testing.

The electrical response to differences in pressure across the diaphragm was performed with the application of elevated, positive pressures in air to the outside of each device, with the cavity still filled with air. In order to block the flow of air into the device upon pressurization, the device was submerged under water for ~15 minutes such that the membrane took up water by capillarity, but the cavity remained filled with air. The liquid in the pores of the membrane blocked entry of air into the internal cavity during exposure to elevated gas pressures. This configuration leads to the same deflection of the diaphragm as occurs during operation of the tensiometer with liquid at reduced pressure within the cavity. For the calibration, a wired device was placed in a high-pressure chamber (leaf pressure chamber (PMS Instrument Co., Albany, OR) for pressures up to 3 MPa, or a HIP chamber

(High Pressure Equipment Company, Erie, PA) for pressures up to 10 MPa) (Fig. 5a). To monitor pressure in the high pressure chamber, a precision pressure gauge (Model: TJE (5000 psig), Honeywell Sensotec, Columbus, OH) connected to a PC running LabView was used.

### **2.3.5 Filling**

Following calibration, devices were placed in vacuum for at least four hours to dry the membrane and evacuate air from the internal cavity. This evacuation reduced the initial supersaturation with air of the liquid water that we forced into the cavity for device filling. We note that dissolution of a volume of air at atmospheric pressure into an equal volume of liquid water occurs at a pressure of  $\sim 6$  MPa at room temperature ( $20^{\circ}\text{C}/293.15^{\circ}\text{K}$ ); upon returning the solution to atmospheric pressure it would have a metastability equivalent to  $\sim 5.9$  MPa of tension (calculated using data of air solubility in water at  $293.15^{\circ}\text{K}$ )<sup>52</sup>. The devices were filled by placing them in an HIP pressure chamber (same as used for calibration) filled entirely with deionized water (resistivity 7-18 M $\Omega$ ) over 12-72 hours (Fig. 5b). The time to fill the devices depended on their internal volumes; the 6.8-mm diaphragm devices required over three days to fill completely. Higher filling pressures were avoided for these devices due to the risk of diaphragm fracture from the high applied strain. For the smaller diaphragm devices (1.4 and 2-mm diameter), filling pressures over 10 MPa could be applied; these could be filled within 12 hours.

### **2.3.6 Operation**

Testing of the sensor was done using the experimental setup depicted in Fig. 5c. Two approaches were used to set the vapor activity of the chamber: (1) saturated salt solutions were placed inside the environment chamber (dark grey) enclosed with the microtensiometer to

equilibrate; (2) a stream of vapor (generated by an evacuated reservoir of water at controlled temperature) was delivered into the environment chamber (Fig. 5c). In the second system, the vapor activity to which the sensor was exposed was measured with a vacuum gauge (Model ASD 2002; Adixen, Annecy, France); this vapor pressure was varied by controlling the relative resistances to flow with valves upstream of the environment chamber and upstream of the vacuum pump (Fig. 5c). In both approaches, the environment chamber with the microtensiometer was placed in a temperature-controlled water bath to maintain isothermal conditions. Using either of these approaches, the temperature and vapor activity of the chamber were known, and the liquid pressure inside tensiometer was measured, equivalent to the water potential ( $\Psi_w$ ) or chemical potential ( $\mu_w$ ) at the given temperature:  $\mu_w(a_w, T) \leftrightarrow P(a_w, T)$ .

## **2.4 Results and discussion**

### **2.4.1 Pressure sensor calibration**

Fig. 6a shows the normalized voltage response ( $\Delta V_{\text{out}}/\Delta V_{\text{in}}$ ) of four microtensiometers with diaphragms of different diameters to the application of elevated gas pressure (see *Calibration* in Methods); all four devices came from the same wafer. All pressure sensors showed excellent linearity up to the highest pressures tested (10 MPa). Devices with larger diaphragms had a lower pressure limit for fracture compared to devices with smaller diaphragms and hence were calibrated to lower pressures (Table 2).

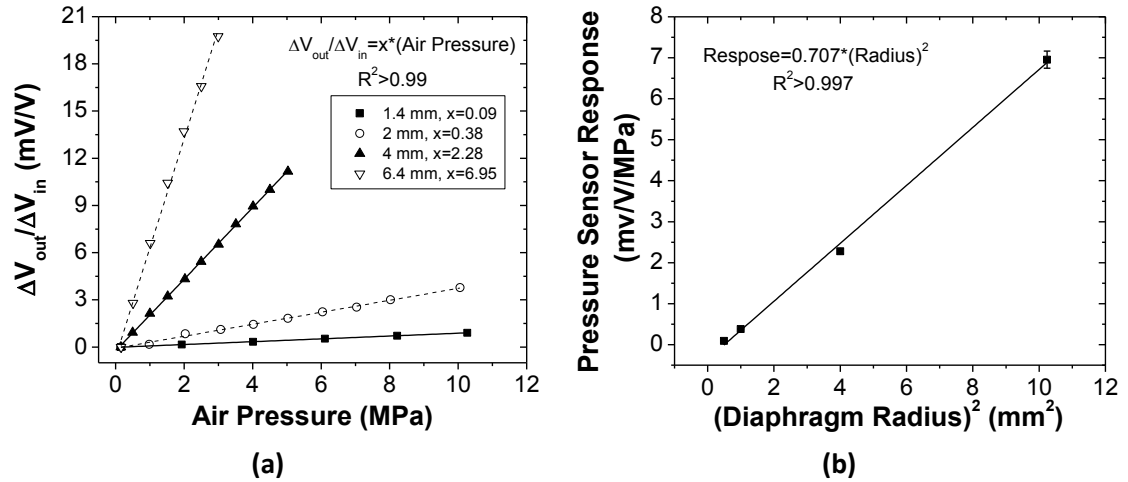


**Figure 6:** Pressure sensor calibration: **(a)** Microtensimeter calibrations using positive pressures of air. ‘x’ [mV/V/MPa] is the slope of the calibration linear regression line, representing the pressure sensor voltage response to applied pressure. Higher values of ‘x’ indicate greater sensitivity to pressure. **(b)** Pressure sensor response showing the relationship of response (as maximum longitudinal stress,  $\sigma_l$ ) to diaphragm radius<sup>2</sup>, in agreement with plate deflection theory.

As predicted by Eq. 7, increasing the diameter of the diaphragm increased the sensitivity, from 0.09  $\mu\text{V V}^{-1} \text{MPa}^{-1}$  in the 1.4 mm-diameter diaphragm to 6.95  $\text{mV V}^{-1} \text{MPa}^{-1}$  for the 6.8-mm one. The electronic noise of our pressure sensors, based on an average value measured from several devices on the same wafer, was less than 0.01 MPa or 0.05% of full-scale (data not shown here).

**Table 2:** Pressure difference (MPa) across diaphragm as a function of diaphragm size and predicted strain. Typical strain at failure for silicon is approximately 4.3% (Petersen 1982).

Strain (%)	Diaphragm Diameter (mm)			
	1.4	2	4	6.8
0.1	76.1	26.1	3.3	0.7
0.2	152.3	52.2	6.5	1.3
0.4	304.5	104.5	13.1	2.7

Fig. 6b presents the response per applied pressure ( $((\Delta V_{\text{out}}/\Delta V_{\text{in}})/\Delta P)$ , slopes from Fig. 6a) for the same devices as a function of the square of the diaphragm radius. The linearity of this plot indicates that the electromechanical response was consistent across these four devices

taken from different locations on the wafer. Based on Eq. 7 and the slope in Fig. 6b, the piezoresistive coefficient ( $\pi_l(1 - \nu) + \pi_t(\nu - 1)$ ) was calculated as  $1.7 \times 10^{-10} \text{ Pa}^{-1}$ . This value corroborates with values reported in the literature for *p*-type polysilicon of between  $1.3 \times 10^{-10} \text{ Pa}^{-1}$  and  $1.8 \times 10^{-10} \text{ Pa}^{-1}$ .<sup>53, 54</sup>

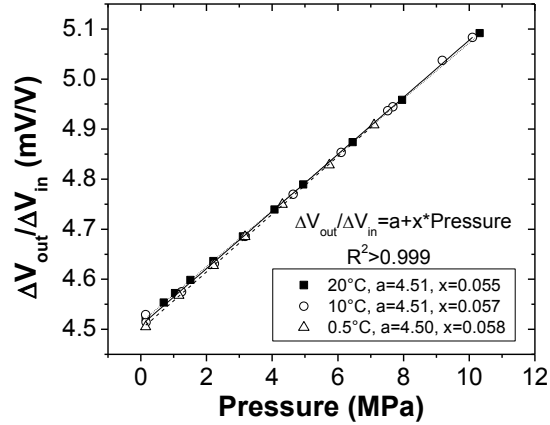


**Figure 7:** Microtensimeter pressure sensor calibrations showing sensor output voltage as a function of applied air pressure at 20°C, 10°C, and 0.5°C. ‘a’ [mV/V] is the voltage offset at 0 MPa pressure, and ‘x’ [mV/V/MPa] is the slope of the linear regression representing the pressure sensor voltage response to applied pressure.

Polysilicon piezoresistors have high temperature dependence as indicated by their temperature coefficient of resistance (TCR= 0.01% /°C or 0.3 Ω/°C).<sup>55</sup> We tested the microtensimeter pressure sensor response to positive air pressure during three calibration runs at different temperatures: 0.5°C, 10°C, and 20°C (Fig. 7). At all three temperatures, there was nearly no change in either slope (x) or offset (a) of the device, and the pressure response was highly linear ( $R^2 > 0.999$ ). The lack of temperature-dependence of the pressure sensor was an important design criteria and advantage of using a balanced Wheatstone bridge, one in which all four piezoresistors had similar resistances. In our experience with unbalanced bridges where the resistors had very different resistances, or if a resistor was disconnected

from the bridge due to a fabrication defect, the temperature-dependence of the pressure sensor was significant.

#### 2.4.2 Membrane stability limit

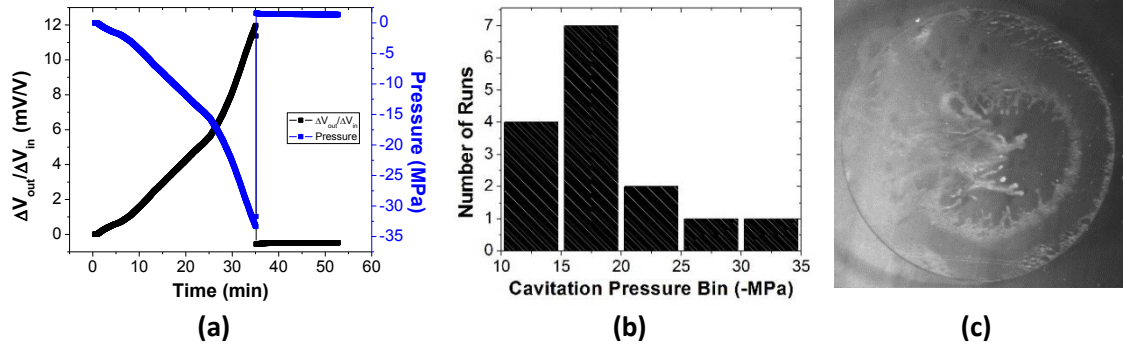


**Figure 8:** (a) Membrane stability limit determined by placing microtensimeter (2-mm diameter diaphragm) at ambient relative humidity ( $a_w \sim 0.6 \equiv \Psi_w \sim -54$  MPa). (b) Statistics of the stability limit of microtensimeters showing the number of runs of devices that cavitated at each negative pressure bin (15 runs with 10 sensors). (c) Snapshot of cavitation ( $P_{liq} = P_{cav}$ ) in the microtensimeter liquid cavity resulting in a rapid increase of liquid pressure to near ambient ( $P_{liq} \rightarrow \sim 0.1$  MPa). Cavitation image captured using a high-speed camera (MotionPro HS-3, Redlake Imaging, Cheshire, CT) at 3000 fps.

Following calibration and filling with degassed water, the stability limit of the microtensimeter nanoporous silicon membrane was tested by placing a water-filled device in ambient conditions ( $T \sim 20^\circ\text{C}$ ,  $a_w \sim 0.6 \equiv P_{liq} \sim -54$  MPa; Eq. 6). Fig. 8a shows the time-dependent response of a microtensimeter with a 2-mm diameter diaphragm during drying; the voltage response ( $\Delta V_{out}/\Delta V_{in}$ ) is shown on the left axis and the calibrated pressure on the right axis. After a period of  $\sim 35$  minutes, the device cavitated and the response returned rapidly toward its baseline. In this extreme case, cavitation occurred at a liquid pressure approaching  $-33$  MPa. To the best of our knowledge, this represents the largest tension ever recorded directly (as a mechanical stress) within a liquid by any method.<sup>56</sup> Fig. 8b presents a histogram of the stability limits measured across 15 independent experiments with 10 different devices. No device failed at a pressure above  $-10$  MPa and most held to beyond  $-15$  MPa. This

range of tensions is an order of magnitude larger than that reported previously for tensiometers.

Most devices we tested were able to withstand multiple cycles ( $> 5$ ) of filling and cavitation. On occasion, particularly for devices with large diaphragms (4 and 6.8 mm-diameters), cavitation led to de-bonding from the bonded interface between glass and silicon. The perturbation due to cavitation sometimes shifted the zero of the Wheatstone bridge, as can be seen in the time-traces in Fig. 8a. Such shifts may have occurred due to changes in the contact resistances leading to the piezoresistors caused by the rapid release of tension.

One can gain an appreciation for the violence of the cavitation process in the snapshot from a high speed video presented in Fig. 8c (see Supplemental Movie). This frame is from  $\sim 0.3$  ms after the onset of cavitation of a microtensiometer with a 4 mm-diameter diaphragm as viewed through the glass (rear) side. The lighter grey regions are clouds of gas bubbles that were advected through the cavity.

We cannot draw any definitive conclusions about the mechanism of cavitation in these devices. The invasion of air through the porous membrane could be the origin. The range of stability limits reported in Fig. 8b corresponds to a range of pore diameters of 9 nm (-33 MPa) to 27 nm (-10 MPa) based on the Young-Laplace equation (Eq. 6 with a receding contact angle,  $\theta_r = 0$ ). From the micrograph in Fig. 4d, it is plausible that pores of these diameters transverse the membrane from the edge to the cavity. Nucleation mechanisms may also play a role. Previous measurements of the stability of water by our group by vapor-liquid equilibrium via organic membranes<sup>47</sup> and by many others using a variety of methods<sup>56</sup> have found a limit

between -20 and -30 MPa. Further work is necessary to distinguish between these possibilities.

### 2.4.3 Transient responses to sub-saturated vapor

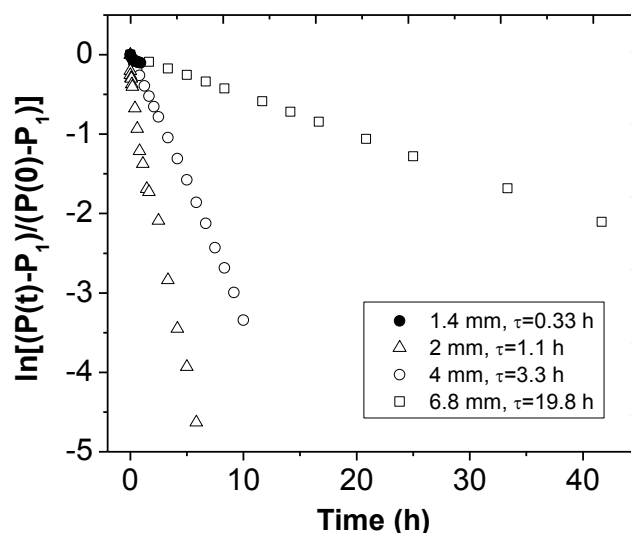


**Figure 9:** Natural log plot of unaccomplished fluid pressure inside cavity of devices of several diaphragm sizes. Slopes of the linear regressions were used to estimate time constants of equilibration,  $\tau$ , indicated in the legend (slope =  $-1/\tau$ ).

In order to test the response of the microtensiometer to external changes in activity, calibrated microtensiometers of all sizes (from the same wafer) were filled with water and allowed to equilibrate with sub-saturated vapors (at different activities). The time constant,  $\tau$ , associated with the transient response was calculated from the slope of the natural log plot of the unaccomplished fluid pressure inside the device (Fig. 9). The time constants for equilibration varied based on the diaphragm size and hence volume of liquid water inside the microtensiometer cavity; devices with larger diaphragms (or cavities) took longer to equilibrate with the external activity than devices with smaller diaphragms. The time constant

of equilibration is associated with the capacitance effect of bulk water inside the cavity as well as poroelasticity of the porous silicon membrane and water within the membrane pores.

#### 2.4.4 Response to sub-saturated salts and vapors

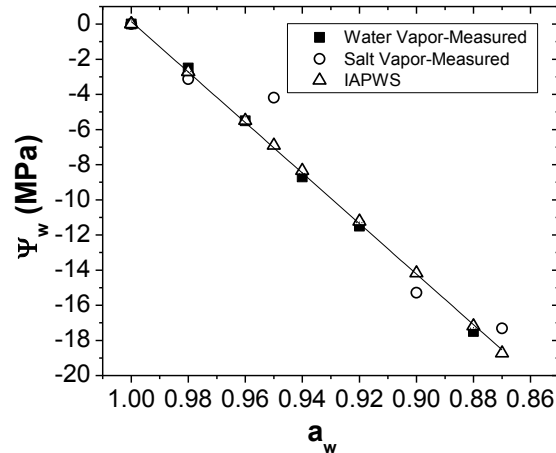


**Figure 10:** Measured and IAPWS-95 calculated water potentials ( $\Psi_w$ , MPa) at various vapor activities ( $a_w$ ) as defined by saturated salt solutions (open circles) and partial pressures of saturated water vapor (filled squares) in an enclosed chamber. All measurements at 20°C.

The response of a microtensiometer with a 2-mm diameter diaphragm to sub-saturated vapor was obtained using two different approaches. In the first approach, a filled device was equilibrated with the vapor of a series of saturated salts of well-defined activities ( $a_{w,vap} \leq 0.98$ ) in a closed temperature-controlled chamber (Fig. 5c). The activity of the individual salts was measured with an Aqualab chilled mirror hygrometer (Model 3TE, Decagon Devices, Inc., Pullman, WA). With the exception of small deviations in measurement in a couple of salts, the microtensiometer was able to precisely measure the activity of the salt (Fig. 10, open circles). The higher measured activity of salt of  $a_w=0.95$  could be due to small leaks in the environment chamber seal (O-ring) such that saturated vapor from the water bath would have entered the chamber and raised the activity of the vapor as defined by the salt.

In a second experiment, we used a saturated vapor stream and controlled the vapor pressure in the closed environment chamber to define the vapor activity (Fig. 5c). The partial pressure of vapor was dynamically controlled such that upon equilibration of the microtensiometer with the sub-saturated vapor, the vapor pressure was reduced to a lower value (lower activity). The microtensiometer response (Fig. 10, filled squares) was accurate as compared with IAPWS-95 calculated values of pressure from activity and temperature.<sup>43</sup> Continuous measurements of the activity of water, as we have demonstrated here, were previously only possible with instruments that had limited range or accuracy at high activities of water, or were not portable. Our device allows for the continuous measurement of water activity down to  $a_w \sim 0.85$  ( $P_{liq} \sim -22$  MPa), an attractive feature since it spans the entire range of activities relevant to living systems (e.g. plants) and the environment (e.g. soils).

## 2.5 Applications

The microtensiometer has numerous potential applications in physical and environmental systems where water activity measurements are required. The large tensions that are capable of being generated inside our device by virtue of the nanoporous membrane and small form factor allow for the study of the physical and thermodynamic properties of water under tension at both ambient and potentially super-cooled temperatures. Only few studies have been able to obtain the equation of state (EoS) of water under tension experimentally owing to the challenge of generating metastable states of water and measuring the thermodynamic properties in that state.<sup>40</sup> With the microtensiometer, obtaining the EoS of stretched liquid water is now experimentally possible by directly measuring the liquid pressure at a known vapor activity and temperature ( $\mu_w \leftrightarrow P(a_{w,vap}, T)$ ), allowing for the validation of empirical models of EoS as

well as molecular dynamics simulations of the phase diagram of water in the stretched region ( $P_{liq} < 0$ ).

Practical applications of the microtensiometer include continuous measurement of water potential ( $\Psi_w \leftrightarrow a_w$ ) in plants and soils that extends the range of current instruments by orders of magnitude. The ability to obtain continuous high spatial resolution  $\Psi_w$  data will allow for efficient water management decision-making in multiple agricultural, forestry, and ornamental horticultural uses. Coupled with existing irrigation systems, the microtensiometer could be a valuable tool for precision irrigation, and could be deployed as sensor arrays using wireless mesh networks in large farms to maximize the efficiency of water usage. The small form factor of the microtensiometer allow for embedding in plant tissue (stems), and its extended range of measurement provides a safety factor that may allow multi-season use once deployed. In the ecological context, water tension measurements in the capillaries (xylem) of trees have been reported to be essential in the evaluation of drought-sensitivity of forests and thus drought effects on globally-critical forest mass and energy fluxes.<sup>69</sup> Microtensiometers could be used to provide dynamic  $\Psi_w$  data to calculate fluxes of water through large forest canopies to inform models and improve our understanding of the water use of forests, which was previously unattainable. The microtensiometer can also be used as a ‘dipping’ osmometer to measure the water activity of solutions having varying solute concentrations, as well as of foods where the precise measurement of water activity is crucial in determining the texture and microbial stability of the food.<sup>9</sup> Finally, the rate of drying in concrete is directly related to its strength and durability. In one study, low water potentials ( $\Psi_w < -5$  MPa) were measured in drying slabs of concrete; these values resulted in the highest values of shrinkage compared to

that at higher water potentials.<sup>70</sup> It is, therefore, desirable to be able to control the rate of shrinkage or drying by monitoring  $\Psi_w$  in order to minimize stresses and increase strength.

For the above-mentioned applications, custom-built application-specific packaging has been and will continue to be developed such that the sensor is able to interact with the environment without compromising the electronics or sensor responsiveness. We are aware that gradients of temperature between the liquid water inside the sensor ( $T_{sens}$ ) and the vapor source ( $T_{vap}$ ) can affect the measurement of activity or water potential; an error of  $\sim 7.7$  MPa/ $^{\circ}\text{C}$  is predicted at  $25^{\circ}\text{C}$ .<sup>28</sup> In order to control for this error, we have thus far tested the device in isothermal conditions where  $T_{vap} \approx T_{sens}$ ; this was feasible due to the small form factor of the device, the high thermal conductivity of silicon ( $149 \text{ W m}^{-1} \text{ K}^{-1}$ ), and the use of a temperature-controlled testing chamber. For applications in which thermal gradients cannot be controlled, such as when embedded in outdoor plants, we have designed an integrated platinum resistance thermometer (outline shown in Fig. 1e-f) to correct the measured tension for temperature differences between the source (e.g. plant tissue) and the sensor.

## 2.6 Conclusions

In this paper, we present the fabrication, operation, and test results of the first generation microtensiometer. Our results indicate that the device was capable of accurately measuring across a very large range of water activities (down to  $a_w \cong 0.76$ ;  $P_{liq} \cong -33$  MPa). To the best of our knowledge, this is the lowest reported negative pressure directly measured in liquid water to date. Factors that likely contribute to the ability of the device to measure out to the extended range of activities include the small form factor, therefore small internal volumes and possibly fewer sites of nucleation within the cavity, and the nanoporous membrane that

allows for large capillary pressures to be generated within its pores. The small form factor of the device also aids its versatility, allowing use in a variety of environmental applications (e.g. continuous water potential monitoring in trees), as well as a portable osmometer for water activity measurements of solutions, food products, and concrete. The MEMS-based design allows for scalability and large-scale manufacturing to lower costs via economies of scale.

The ability to measure high liquid tensions allows for open questions in the thermodynamics of stretched liquid water to be answered, e.g. measurement of the equation of state of water in the negative pressure regime. Future designs of the microtensiometer can be optimized to lower transient response times by tuning specific properties of the nanoporous membrane, and modifying the geometry of the device, in particular decreasing the liquid volumes represented by the internal cavity and membrane. Gradients in temperature between the source and the device can be measured in the future using an integrated platinum resistance thermometer to correct the water activity measurement in non-isothermal environments. Application-specific packaging needs to be developed in order to utilize this device in specific contexts. The microtensiometer should be a valuable tool for the measurement of water activity in several physical, biological, and environmental applications.

## **2.7 References**

1. J. Peixoto and A. H. Oort, *Journal of Climate*, 1996, **9**, 3443-3463.
2. H. G. Jones, *Plants and microclimate : a quantitative approach to environmental plant physiology*, Cambridge University Press, Cambridge England ; New York, NY, USA, 1992.
3. P. A. Shirke and U. V. Pathre, *Journal of Experimental Botany*, 2004, **55**, 2111-2120.
4. T. Hirasawa and T. C. Hsiao, *Field Crops Research*, 1999, **62**, 53-62.

5. M. J. Blandamer, J. B. F. N. Engberts, P. T. Gleeson and J. C. R. Reis, *Chemical Society Reviews*, 2005, **34**, 440-458.
6. J. A. Troller and J. H. B. Christian, *Water activity and food*, Academic Press, New York, 1978.
7. N. Abdullah, A. Nawawi and I. Othman, *Journal of Stored Products Research*, 2000, **36**, 47-54.
8. G. Ayerst, *Journal of Stored Products Research*, 1969, **5**, 127-141.
9. A. Schiraldi, D. Fessas and M. Signorelli, *Polish Journal of Food and Nutrition Sciences*, 2012, **62**, 5-13.
10. E. Wehtje and P. Adlercreutz, *Biotechnology and Bioengineering*, 1997, **55**, 798-806.
11. V. Gekas, C. Gonzalez, A. Sereno, A. Chiralt and P. Fito, *International Journal of Food Properties*, 1998, **1**, 95-112.
12. N. Asaad, M. J. den Otter and J. B. F. N. Engberts, *Organic & Biomolecular Chemistry*, 2004, **2**, 1404-1412.
13. N. Asaad and J. B. F. N. Engberts, *Journal of the American Chemical Society*, 2003, **125**, 6874-6875.
14. M. Starzak and M. Mathlouthi, *Food Chemistry*, 2006, **96**, 346-370.
15. L. Makkonen and T. Laakso, *Boundary-Layer Meteorology*, 2005, **116**, 131-147.
16. F. Aziz, M. H. Sayyad, K. Sulaiman, B. H. Majlis, K. S. Karimov, Z. Ahmad and G. Sugandi, *Measurement Science & Technology*, 2012, **23**.
17. D. Roveti, *Sensors Magazine*, 2001.
18. G. J. W. Visscher, *Measurement Science & Technology*, 1995, **6**, 1451-1461.
19. S. D. Wullschleger, M. A. Dixon and D. M. Oosterhuis, *Plant Cell and Environment*, 1988, **11**, 199-203.
20. C. G. Enfield and J. J. C. Hsieh, *Water Resources Research*, 1971, **7**, 1349-1353.
21. L. A. Richards, *Soil Science*, 1942, **53**, 241-248.
22. F. J. Veihmeyer, N. E. Edlefsen and A. H. Hendrickson, *Plant Physiology*, 1943, **18**, 66-78.

23. C. L. Cutting, A. C. Jason and J. L. Wood, *Journal of Scientific Instruments*, 1955, **32**, 425-431.
24. E. Stenitzer, *Theoretical and Applied Climatology*, 1993, **48**, 159-165.
25. A. Fares and A. K. Alva, *Soil Science Society of America Journal*, 2000, **64**, 311-318.
26. L. R. Parsons and W. M. Bandaranayake, *Soil Sci. Soc. Am. J.*, 2009, **73**, 1378-1385.
27. ICT International, PSY1 Psychrometer, <http://www.ictinternational.com.au>.
28. M. A. Dixon and M. T. Tyree, *Plant Cell and Environment*, 1984, **7**, 693-697.
29. Delta-T Devices, SWT-4 and SWT-5 - Water Filled Tensiometers, <http://www.deltat.co.uk>, Accessed December 3, 2013.
30. S. J. Richards and A. W. Marsh, *Proc. Soil Sci. Soc. Amer.*, 1961, **25**, 65-69.
31. A. M. Ridley, J. B. Burland, F. A. M. Marinho and R. J. Chandler, *Geotechnique*, 1994, **44**, 551-556.
32. Y. Guan and D. G. Fredlund, *Canadian Geotechnical Journal*, 1997, **34**, 604-614.
33. A. J. Peck and R. M. Rabbidge, *Soil Science Society of America Proceedings*, 1969, **33**, 196-202.
34. A. J. Peck and R. M. Rabbidge, *Science*, 1966, **151**, 1385-1386.
35. G. H. de Rooij, M. J. v. d. Ploeg, H. P. A. Gooren, G. Bakker, C. W. Hoogendam, C. Huiskes, H. Kruidhof, L. K. Koopal, M. J. v. der Ploeg, G. H. de Rooij and M. J. van der Ploeg, *Biologia*, 2009, **64**, 438-442.
36. M. J. van der Ploeg, H. P. A. Gooren, G. Bakker, C. W. Hoogendam, C. Huiskes, L. K. Koopal, H. Kruidhof and G. H. de Rooij, *Hydrology and Earth System Sciences*, 2010, **14**, 1787-1799.
37. G. Bakker, M. J. van der Ploeg, G. H. de Rooij, C. W. Hoogendam, H. P. A. Gooren, C. Huiskes, L. K. Koopal and H. Kruidhof, *Vadose Zone Journal*, 2007, **6**, 196-202.
38. W. P. Eaton and J. H. Smith, *Smart Materials & Structures*, 1997, **6**, 530-539.
39. J. N. Israelachvili, *Intermolecular and surface forces*, Academic Press, Burlington, MA, 2011.

40. P. S. Nobel, *Physicochemical and environmental plant physiology*, Academic Press, Inc., San Diego, 1991.
41. S. Beeby, *MEMS mechanical sensors*, Artech House, Boston, 2004.
42. K. Davitt, E. Rolley, F. Caupin, A. Arvengas and S. Balibar, *Journal of Chemical Physics*, 2010, **133**.
43. W. Wagner and A. Pruss, *Journal of Physical and Chemical Reference Data*, 2002, **31**, 387-535.
44. IAPWS, Fredericia, Denmark, 1996.
45. P.-G. de Gennes, F. Brochard-Wyart and D. Quéré, *Capillarity and wetting phenomena: drops, bubbles, pearls, waves*, Springer, New York, 2004.
46. P. G. Debenedetti, *Metastable liquids: concepts and principles*, Princeton University Press, Princeton, N.J., 1996.
47. T. D. Wheeler and A. D. Stroock, *Langmuir*, 2009, **25**, 7609-7622.
48. T. D. Wheeler and A. D. Stroock, *Nature*, 2008, **455**, 208-212.
49. V. Kaajakari, *Practical MEMS*, Small Gear Pub., Las Vegas, Nev., 2009.
50. J. T. Baek, H. H. Park, B. T. Ahn, C. H. Jun, Y. T. Kim, Y. H. Song and J. Kim, *Japanese Journal of Applied Physics Part 1-Regular Papers Short Notes & Review Papers*, 1998, **37**, 2451-2454.
51. Y. Jiang and X. Zhang, *Journal of Materials Science and Engineering A*, 2012, **2**, 22-28.
52. R. Battino, T. R. Rettich and T. Tominaga, *Journal of Physical and Chemical Reference Data*, 1984, **13**, 563-600.
53. A. Salette, R. Lefevre, C. Déhan, P. Morfouli and L. Montès, *Procedia Engineering*, 2012, **47**, 426-429.
54. P. J. French and A. G. R. Evans, *Solid-State Electronics*, 1989, **32**, 1-10.
55. Y. Kanda, *IEEE Transactions on Electron Devices*, 1982, **29**, 64-70.
56. F. Caupin, A. Arvengas, K. Davitt, M. E. Azouzi, K. I. Shmulovich, C. Ramboz, D. A. Sessoms and A. D. Stroock, *Journal of Physics-Condensed Matter*, 2012, **24**.

57. X. G. Zhang, in *Modern Aspects of Electrochemistry*, eds. C. G. Vayenas, R. White and M. Gamboa-Adelco, Springer US, 2006, vol. 39, ch. 2, pp. 65-133.
58. D. Janssen, R. De Palma, S. Verlaak, P. Heremans and W. Dehaen, *Thin Solid Films*, 2006, **515**, 1433-1438.
59. S. B. Habib, E. Gonzalez and R. F. Hicks, *Journal of Vacuum Science & Technology A*, 2010, **28**, 476-485.
60. R. L. Smith and S. D. Collins, *J. Appl. Phys.*, 1992, **71**, R1-R22.
61. V. Lehmann, R. Stengl and A. Luigart, *Materials Science and Engineering B-Solid State Materials for Advanced Technology*, 2000, **69**, 11-22.
62. R. Herino, G. Bomchil, K. Barla, C. Bertrand and J. L. Ginoux, *Journal of the Electrochemical Society*, 1987, **134**, 1994-2000.
63. X. G. Zhang, *Journal of the Electrochemical Society*, 1991, **138**, 3750-3756.
64. A. A. Hamzah, H. E. Z. Abidin, B. Y. Majlis, M. M. Nor, A. Ismardi, G. Sugandi, T. Y. Tiong, C. F. Dee and J. Yunas, *J Micromech Microeng*, 2013, **23**, 1-9.
65. A. A. Hamzah, H. E. Z. Abidin, J. Yunas, C. F. Dee and B. Y. Majlis, *Proc. Micromechanics and Microsystems Europe Workshop, Sep. 9-12, Ilmenau, Germany*, 2012.
66. S. Zangoie, R. Jansson and H. Arwin, *Appl Surf Sci*, 1998, **136**, 123-130.
67. S. N. Sharma, R. Sharma and S. T. Lakshmikumar, *Physica E-Low-Dimensional Systems & Nanostructures*, 2005, **28**, 264-272.
68. M. K. Oisten and P. L. Bergstrom, *Physica Status Solidi A - Applications and Materials Science*, 2009, **206**, 1278-1281.
69. B. Choat, et al., *Nature*, 2012, **491**, 752-755.
70. K.C. Hover, *Construction and Building Materials*, 2011, **25**, 3003-3013.

### **CHAPTER 3: Vegetative growth, gas exchange, water relations, hydraulic performance, and xylem morphology of varying vigor shoots of *Vitis vinifera* L.**

#### **Abstract**

The vegetative growth of grapevines influences their reproductive performance and the capacity of the vine to ripen the crop. Water availability also plays a key role in this process, moderating the balance between vegetative and reproductive growth. It was hypothesized that differences in vegetative growth of individual shoots within a grapevine on a single cane were due to differences in the water status of those shoots as indicated by their midday stem water potentials,  $\Psi_{md}$ . A combination of leaf pressure chamber, leaf gas exchange, ultrasonic acoustic emissions, stem hydraulic measurements, and histology techniques were used on field-grown 'Riesling' grapevines (*Vitis vinifera* L.) that were subjected to progressive soil moisture deficits during the 2011 and 2012 growing seasons. Differences in  $\Psi_{md}$  were not large enough to explain the large differences in shoot length within a single vine. Longer shoots had greater hydraulic conductivities, but shorter shoots were found to have higher rates of xylem acoustic emissions occurring under less water stress (higher  $\Psi_{md}$ ) than longer shoots. Longer shoots had larger cross-sectional xylem vessel area and somewhat less inter-vessel pitting compared to shorter shoots. These differences could contribute to the higher hydraulic efficiency of long shoots, and with fewer pits per vessel, there may be fewer embolisms. Stomatal conductance and photosynthetic responses to increasing water stress were not different in relation to shoot length. In summary, although there were differences in water status between long and short shoots on the same vine, the differences were not great enough to explain the differences in growth rate of the shoots.

*Abbreviations:*  $\Psi_{pd}$ , predawn water potential;  $\Psi_{md}$ , midday stem water potential;  $G_s$ , stomatal conductance;  $A_n$ , net assimilation or photosynthesis;  $L_p$ , maximum hydraulic conductivity;  $L_s$ , stem-specific hydraulic conductivity;  $VPD$ , vapor pressure deficit;  $L_{cs}$ , cane-shoot hydraulic conductivity;  $R_{cs}$ , cane-shoot hydraulic resistivity.

### 3.1 Introduction

Water availability sets the upper limit on plant vegetative and reproductive growth. In arid and semi-arid regions worldwide that lack adequate rainfall, water is the single most important factor limiting crop production (Tuberosa *et al.* 2007). Water stress elicits a multitude of short- and long-term physiological responses in plants including stomatal closure (short-term), shoot growth inhibition (short-term), osmotic adjustment (long-term), structural modifications of xylem (long-term), and enhanced root growth (long-term; Chaves *et al.* 2003). Differences in shoot growth or stem elongation in plants subjected to water stress have been well-documented. While mild water deficits may elicit little physiological response, particularly in osmotically-adjusting plants such that leaf relative water content and turgor is maintained with little or no change in photosynthesis, severe water deficits may result in loss of turgor in leaves, decreased photosynthetic capacity and quantum yield, and, in extreme cases, leaf desiccation and plant mortality (Flexas *et al.* 1999; Hsiao 1973; Jones 1992; Yordanov *et al.* 2003). Plant water status has been positively correlated with branch extension in conifers (Woodruff and Meinzer 2011), plant height of wheat (Li *et al.* 2011), and shoot growth in grapevines (Schultz and Matthews 1988a; Smart *et al.* 1974). This response is thought to be related to constraints on turgor-driven cell expansion (Lockhart 1965) and possibly cell division (Kirkham *et al.* 1972). Maintaining plant water status can happen via several mechanisms. Use of an Ohm's Law analogy of water potential gradient is helpful:

$$\Delta\Psi_{w,soil-leaf} = E \times R_{hydraulic} \quad (3.1)$$

where  $E$  = transpirative flux and  $R_{hydraulic}$  is the hydraulic resistance along the pathway between the soil and leaf. From Eq. 3.1, maintaining leaf water potential can be accomplished

by: (1) affecting  $E$  primarily via stomatal adjustments, or (2) adjusting  $R_{hydraulic}$  to change resistance along the flow pathway.

The water relations of plants are strongly affected by the behavior of the stomates in relation to stress and the environment. Plants have been classified as either isohydric or anisohydric based on their stomatal response to soil water deficits (Franks *et al.* 2007; Stocker 1956; Tardieu and Simonneau 1998). Isohydric behavior occurs when changes in stomatal conductance compensates for changes in soil or leaf water potential or changes in evaporative demand from the atmosphere (vapor pressure deficit, VPD) to maintain relatively constant minimum shoot water potentials. Under increasing water stress, isohydric plants control water loss and maintain their leaf water potentials ( $\Psi_{leaf}$ ) above a threshold value by closing their stomates. The drawback of this stomatal response is that, if stomates close too much, a reduction of CO<sub>2</sub> assimilation is a consequence (Cochard *et al.* 2002) and, hence, lower carbon fixation and productivity of the plant.

In contrast, anisohydric plants do not close their stomates as much in response to water stress or evaporative demand allowing  $\Psi_{leaf}$  to drop to lower values than isohydric responses. But this behavior may result in hydraulic disruptions in the xylem due to cavitations and ensuing embolisms (Jones and Sutherland 1991; Tyree and Sperry 1988). If a plant has the ability to accumulate osmotic potential to offset the lower total water potential, then turgor may be maintained over a range to maintain function at low water potentials. Studies have shown that the two differing stomatal strategies (isohydric vs. anisohydric) under water stress may exist within individual species (Gibberd *et al.* 2001; Hochberg 2013; Schultz 2003; Soar *et al.* 2006), and even within the same plant under different environmental conditions (A. Lakso, unpublished data). A recent study suggested that anisohydric grapevine cultivars may

be able to recover better from moderate levels of water stress upon re-watering (Pou *et al.* 2012), giving them an advantage over isohydric cultivars in semi-arid or arid regions.

Morphological changes to the vascular structure (xylem) and hydraulic resistance of plants associated with water stress have been observed in various plant species. For example, water stress resulted in smaller xylem vessels (diameter) in several wheat genotypes (Bresta *et al.* 2011), oaks (*Quercus* sp.; Fonti *et al.* 2013), ash (*Fraxinus* sp.; Borger and Kozlowski 1972), apple (Bauerle *et al.* 2011), and *Zinnia elegans* (Twumasi *et al.* 2005). Structural changes in xylem vessels, specifically decreases in conduit diameter that may increase hydraulic resistance, are thought to occur as a protective mechanism to prevent cavitation (Lintunen *et al.* 2013) and are consistent with the hypothesis of a tradeoff in cavitation safety versus transport efficiency of xylem (Carlquist 1988, Hacke *et al.* 2006, Martinez-Vilalta *et al.* 2002, Zimmermann *et al.* 1971).

Cavitations in xylem vessels of plants result from excessive tension which pulls in air through bordered pit membranes (meniscal failure; Sperry *et al.* 1993), a process known as ‘air-seeding’ (Zimmermann 1983). Air-filled or embolized vessels can negatively affect hydraulic conductance (Tyree and Ewers 1991) and, consequently, the growth rate and yield of plants (Brodribb *et al.* 2002, Cochard *et al.* 1997, Hubbard *et al.* 2001, Kramer and Boyer 1995). Embolisms and consequent reduced hydraulic capacity have been cited as being the primary cause of decreased productivity and plant mortality during drought although very few studies have actually documented embolisms (Anderegg *et al.* 2011, Choat *et al.* 2012).

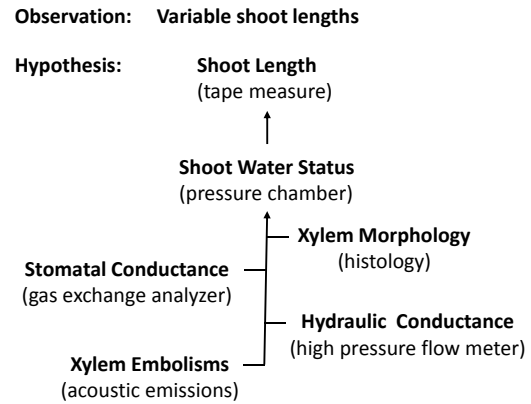
Studies have suggested that cavitations and reduced hydraulic conductivity can be minimized by limiting xylem tensions via a reduction in transpiration by a compensating

isohydric stomatal closure, thereby maintaining xylem water potentials above a threshold of cavitation (Brodribb *et al.* 2003, Bucci *et al.* 2003). Schultz and Matthews (1988b) suggested that embolisms may be an important factor contributing to inhibited shoot growth in grapevines experiencing moderate water stress. This could be the result of stomatal closure and reduced net photosynthesis as found in one study on water-stressed grapevines (Zufferey *et al.* 2011). So, while cavitations in water-stressed plants likely play a role in reducing growth and productivity via decreased hydraulic conductance, only few studies have shown this to be the case at the level of individual organs. The significance of embolisms is that they add to the effect of reduced soil water potentials such that the gradient of water potential between the soil and the atmosphere is increased.

We observed high intra-vine variability of shoot growth along individual canes of *Vitis vinifera* L. that was not based on shoot position along the cane (Fig. 1a), as previously observed (Fregoni and Zioni 1972). An hypothesis for the variation in shoot vigor is variation of shoot water status. This is supported by studies showing a high correlation of early-season shoot length and growth rate and stem water potentials of individual shoots of varying length on the same vine (unpublished data, A. Lakso and A. Coniberti). Variable shoot water status may be due to: (1) differences in stomatal physiology, e.g. isohydry; or, (2) differences in shoot hydraulic architecture, e.g. xylem vessel size and morphology that determine their capacity to transport water; or, (3) differences in the cane-shoot junction resistances (Fig. 1b).



(a)



(b)

**Figure 1:** (a) Typical grapevine showing variability of shoot growth along an individual cane. (b) Observation, hypothesis, and methods (in brackets) used to test hypothesis.

Xylem vessel architecture and size determine the potential hydraulic conductance,  $L_p$ , of the vessel based on the Hagen-Poiseuille relationship of laminar fluid flow in a conduit of uniform dimensions, where  $L_p$  is proportional to the vessel radius to the fourth power (Ch. 1, Eq. 1.12).

The goal of this study was to evaluate possible mechanistic bases for the differences in vegetative growth of adjacent shoots originating within a short distance on a single cane. It was hypothesized that shoot vigor was positively correlated with shoot water status (longer shoots have higher stem water potential than shorter shoots), since superior water status results in increased turgor of cells in the leaves and shoot apical meristem favoring cell expansion and, hence, growth (Boyer 1968, 1993; Cosgrove 1993). The following potential differences were examined for their relative roles in regulating the water status between shoots of different vigor: differences in transpiration regulated by stomata; hydraulic conductance based on the degree of embolisms from water stress-induced air-seeding; hydraulic architectures of the xylem vessels of the different vigor shoots; and, differences in shoot-cane junction resistances. Grapevines were chosen for this study due to their natural range of shoot vigors within a vine, and relatively large diameter vessels of varying sizes (Salleo *et al.* 1985) that

have been observed to have a degree of morphological plasticity in response to water stress (Schultz and Matthews 1988a). Furthermore, grapevines produce a high-value crop whose yield and quality is affected by the vegetative performance of the plant.

## **3.2 Material and Methods**

### **3.2.1 Plant material and site**

Mature grapevines (*Vitis vinifera* L. cv. 'Riesling' grafted onto '101-14' rootstock (*V. riparia* x *V. rupestris*)) planted in 2005 at an experimental vineyard of the New York State Agricultural Experiment Station, Geneva, NY (42.88° N, 77.01° W) were used over two consecutive growing seasons, 2011 and 2012. The vineyard block soil type was a Lima series fine silt loam with high water holding capacity. Inter-row cover crops consisted of a perennial tall fescue (*Festuca arundinacea* Schrub.) and the under-vine 1 m strips were bare from the application of pre-emergent herbicide. Rows were oriented north-south, and the row and vine spacing was 2.7 x 2.1 m (row x vine) resulting in a planting density of 1763 vines ha<sup>-1</sup>. The vines were cane-pruned and shoot thinned to approximately 15 shoots per linear meter of canopy, and trained to a bilateral, vertically shoot-positioned canopy. The canopy was not hedged or topped during the season to allow full expression of shoot growth.

### **3.2.2 Water restriction treatments**

All vines were fully-irrigated until June 15, 2012. On this date, a rain-exclusion plastic tarp ('rain shield') was installed on the vineyard floor over 20 vines in a single row to prevent precipitation from entering the soil and to impose a gradient of water stress on the vines. The rain shield extended to two adjacent rows on either side such that excess rain water would not reach the roots of the measurement row. No supplemental irrigation was applied to the rain-

shielded vines for the remainder of the growing season. The remainder of the vineyard, including six uniform unshielded control vines in a different row, was rain-fed (May to September total rainfall was 478 mm in 2011, and 305 mm in 2012), and received supplemental irrigation as needed to maintain high vine water status (no water stress). Due to the natural ca. 1% slope of the vineyard block, there was a range of soil moisture levels generated amongst the shielded vines that resulted in a range of vine water status. This variation in soil moisture and vine stress allowed us to establish relationships between vine water status and a range of vine physiological parameters described below. In 2011, a similar study was initiated, however, a later start to the rain-shielding – about two weeks after bloom – and a cooler season did not generate significant stress levels until quite late in the season. Due to the earlier start of the rain exclusion treatment in the 2012 growing season as well as a drier season in 2012 compared to 2011, results will be shown from that year unless otherwise stated.

### **3.2.3 Shoot growth measurements**

On each of the 26 vines used for this study, four shoots from the current season per vine were selected after the rain shield was installed (approximately two weeks post-bloom). These four shoots represented two shoot length categories: short shoots (mean length: 40 cm  $\pm$  10 cm) and long shoots (mean length: 120 cm  $\pm$  17 cm). These length cutoffs were chosen such that the majority of shoots (on the cane) were separated into two distinct populations of length extremes. Of the four shoots on each vine, two were on an east-facing part of the canopy and two were on a west-facing part of the canopy. Weekly measurements of shoot length were taken using a meter stick, and the rate of shoot growth per week was calculated from the difference in the shoot lengths every two consecutive weeks.

### 3.2.4 Water status measurements

Stem water potential ( $\Psi_s$ ) measurements were made on one long and short shoot each per vine using a leaf pressure chamber (3000 Series Plant Water Status Console, Soilmoisture Equipment Corp., Santa Barbara, CA) as per the method of Turner (1988). Prior to water status measurements, leaves were enclosed tightly in plastic bags, covered with aluminum foil to stop transpiration, and were allowed to equilibrate with the stem for at least 30 minutes.  $\Psi_s$  was measured either at midday (weekly, between 1200-1500 h;  $\Psi_{md}$ ), or at pre-dawn (five times during growing season, around 0500 h;  $\Psi_{pd}$ ) on the same shoots on each vine (between nodes 2-4).

### 3.2.5 Gas exchange measurements

Leaf gas exchange measurements were conducted weekly on full-expanded, mature, basal leaves on each sentinel shoot that was well-exposed (saturating light levels  $> 1600 \mu\text{mol m}^{-2} \text{s}^{-1}$ ) between 1100-1500 h. Leaves selected for gas exchange measurements were adjacent to those used for  $\Psi_{md}$  measurements. Leaf gas exchange was measured using a CIRAS-1 portable differential  $\text{CO}_2/\text{H}_2\text{O}$  infrared gas analyzer (PP Systems Inc., Amesbury, MA) with a  $2.5 \text{ cm}^2$  broad leaf cuvette using ambient lighting. The relationships between  $\Psi_{md}$ , and leaf stomatal conductance ( $G_s$ ) and net assimilation ( $P_n$ ) of long and short shoots were fitted using an exponential decay function [ $G_s(P_n) = a \exp(-b \Psi_{md})$ ] and non-linear least squares analysis (OriginPro v.8; OriginLab, Northampton, MA).

### 3.2.6 Leaf size and stomatal density

At the end of the growing season, prior to harvest, one mature leaf was sampled from the basal sections of each long and short shoot from equivalent node positions on both types of shoots. Average leaf sizes (i.e. area per leaf) of long and short shoots was determined using a semi-automatic leaf area meter (WinDIAS, Delta-T Devices Ltd., Burwell, Cambridge, UK). Stomatal density was obtained by first removing the tomentum (hair on the lower epidermis of leaves) between the leaf veins with a few drops of warm (ca. 80°C) paraffin wax. The wax was allowed to cool completely before peeling it off the leaf blade. This ‘waxing’ process was repeated 2-3 times until all the hair was removed. To remove chloroplasts and palisade leaf layers that obstruct the visualization of stomates and guard cells, small sections of waxed leaf tissue were placed in hot 5% sodium hydroxide (NaOH) in a boiling water bath for ca. 15 min. The tissue was rinsed 2-3 times with deionized water, then soaked in 50% bleach solution for ca. 20 min, and rinsed again with deionized water. The mostly clear tissue was dehydrated using a series of alcohols (50-75-95-100% v/v, one minute each), and then stained with 1% (v/v) Safranin for ca. 30 sec. The tissue was rinsed twice with absolute ethanol, then Histoclear, and mounted on a microscope glass slide using Permount for observation under a microscope. Counting of stomates was done manually using a hemocytometer and light microscope.

### 3.2.7 Shoot hydraulics measurements

At the end of the growing season, all shoots used for gas exchange and water status measurements were excised and taken to the lab to determine maximum stem hydraulic conductivity,  $L_p$  [ $\text{kg m MPa}^{-1} \text{ s}^{-1}$ ] (Ch. 1, Eq. 1.13).  $L_p$  is obtained by measuring conductance

or flow rate per unit pressure drop [ $\text{kg MPa}^{-1} \text{s}^{-1}$ ] and multiplying it by the stem length [m]. Prior to making conductance measurements, stem diameter [m] and length [m] were measured using calipers and a measuring tape, respectively. Stem diameter was used to calculate stem cross-sectional area,  $A_s$  [ $\text{m}^2$ ]. Stem segments 5-10 cm in length (node positions 1-2, basal section of shoot) were initially rehydrated in deionized water for ca. 1 h.  $L_p$  was measured using a custom-built pressurized flow meter attached to an analytical balance (Model AZ153, Sartorius AG, Göttingen, Germany) connected to a PC running LabVIEW software (v.10.0, National Instruments Corp., Austin, TX). Degassed, deionized water was perfused at 200 kPa through the stems until a steady-state flow rate ( $\pm 5\%$ ) was reached, usually within 2-3 min, after which the mass flow rate data was collected for 3 min. An initial test of the stability of  $L_p$  over time was done for 30 mins; no changes in  $L_p$  were observed after the value stabilized in 2-3 mins. Stem-specific hydraulic conductivity,  $L_s$  [ $\text{kg m}^{-1} \text{MPa}^{-1} \text{s}^{-1}$ ], was calculated from  $L_p$  as per Davis *et al.* (1999) by normalizing  $L_p$  by the transverse area of the stem segment,  $A_s$  [ $\text{m}^2$ ] ( $L_s=L_p/A_s$ ) (Sec. 1.5.2).

In order to determine whether the source of variation in hydraulic resistance between shoots was in the connections (or junctions) between the one-year old cane and the current season's shoot, early in the 2013 growing season, 30 shoots of varying lengths were excised (from the same vines used in the previous two seasons but without water stress) in mid-July with their canes attached, with approximately 2 cm of their cane attached to each side of the shoot junction. The entire shoot with attached cane was re-hydrated in degassed and deionized water for ca. 1 h prior to  $L_p$  measurements. Shoot length, basal shoot diameter, and cane diameters were measured. The cane end of the shoot was trimmed with a razor blade, then placed inside a plastic beaker of degassed and deionized water set inside a very large pressure

chamber (Super Chamber model, PMS Instrument Co., Albany, OR), and sealed around the emerging end of the shoot. The pressure chamber was pressurized to 200 kPa and the exudate collected on an analytical balance with a pre-weighed vial. After a steady-state flow rate was achieved, usually within 2-3 minutes, the analytical balance weight data was collected for 3 min. The  $L_p$  measurement was repeated on the same shoot after the cane was excised in order to determine  $L_p$  of the shoot alone. Specific conductivity was calculated as  $L_p$  normalized by the shoot and cane diameters. Specific resistivity was determined as the inverse of specific conductivity. The difference between the specific resistivity of the cane-shoot combination ( $R_{cs}$ ) and the shoot alone ( $R_s$ ) was used to determine the specific resistivity of the cane-shoot junction,  $R_j$  ( $R_j = R_{cs} - R_s$ ).

### **3.2.8 Xylem air-seeding estimation by acoustic emissions**

The degree of embolization in the xylem vessels of shoots was estimated using continuous measurements of ultrasonic acoustic emissions (Tyree and Dixon 1983) using a Pocket AE-2 portable dual-channel ultrasonic acoustic emissions system (18-bit, 20 MSPS A/D, 1.0 kHz-1.0 Mhz  $\pm$  1.5 dB; Physical Acoustics Corp., Princeton Junction, NJ). The system was equipped with two 150 kHz resonance sensors (R15 $\alpha$ ). The pre-amplifier and thresholds were both set at 40 dB to prevent detection of ultrasonic acoustic emission (AE) events caused by wind and human conversation. The presence of insects, e.g. wasps, near the sensors resulted in AE events, so precautions were taken to ensure that no insects were present around the shoots during the measurement period. Maximum event duration, peak definition time, hit definition time, and hit lockout times were set at 100 ms, 200  $\mu$ s, 800  $\mu$ s, and 1 ms, respectively. These settings were determined based on our characterization tests (described below), using the manufacturer's recommendations as a starting point. Data analysis was performed using

AEwin Replay software (Physical Acoustics Corp., Princeton Junction, NJ) on a Windows-based PC. Recorded data include hit time, counts, amplitude, and absolute energy.

Prior to ultrasonic acoustic emissions (AE) measurements on the experimental vines, we conducted several characterization tests of the AE sensors, described briefly here. First, attenuation of an AE signal was characterized by breaking pencil leads on a dried grapevine shoot at varying distances from the sensor. This provided information on the sensor's ability to detect AE events based on proximity and to inform sensor placement on the shoot for the experiment. Second, a well-hydrated grapevine shoot was excised and AE events were monitored as the shoot was left to dehydrate on a bench. The number of AE events increased rapidly initially, then decreased concurrently with visual signs of leaf wilting. Finally, in order to ensure that AE events were not detected from neighboring shoots on a single cane of a vine, an AE sensor was attached to the basal portion of a shoot of a field-grown grapevine and the pencil lead break test described above was conducted on adjacent shoots. No AE events were detected when a pencil lead was broken on neighboring shoots. AE events were detected on the same shoot with the sensor placed approximately 0.5 m from the AE source. In these studies, we estimate that AE events occurring in the basal 1 m of the shoots were detected.

Prior to AE measurements on each long and short shoot per vine, stem water potential ( $\Psi_{\text{md}}$ ) was measured as described previously. Following  $\Psi_{\text{md}}$  measurement, ca. 2 cm<sup>2</sup> bark was removed from a basal section of the shoot so as to expose the surface of the xylem. A thin film of silicone grease was applied on the acoustic sensor and the sensor was then attached to the exposed region of the shoots using a small metal laboratory clamp covered with plastic coating to maintain tight contact. AE data was collected for 10 minutes per day between 1100 - 1500 h over seven days starting in mid-August when the vine water stress level was high.

Cumulative AE events were calculated from the raw data at each level of water stress or water potential. The relationship between AE and  $\Psi_{md}$  was fitted to an exponential growth function [ $AE = a \exp(b \Psi_{md})$ ] (OriginPro v.8; OriginLab, Northhampton, MA).

### 3.2.9 Xylem anatomical measurements

Stem segments of 5 cm length from individual long and short shoots (following hydraulic measurements) were fixed in a solution of FAA: formaldehyde (37% v/v), glacial acetic acid, ethanol (95% v/v), and deionized water in the ratio 10:5:50:35. Short stem segments were then removed from FAA and dehydrated in 75% (v/v) ethanol (2 min) followed by 95% (v/v) ethanol (2 min) prior to cutting 1 cm segments of stem. Bark was removed from these segments, and longitudinal and transverse segments were cut using a sharp razor blade and embedded in paraffin wax. Transverse and longitudinal sections of thickness 25-40  $\mu\text{m}$  were prepared on a sliding microtome to visualize xylem vessel area and xylem wall features such as inter-vessel bordered pits, respectively. Sections were stained with 0.1% (w/v) thionin blue (stains cell walls) for approximately 20 s, then washed with deionized water before mounting on a glass microscope slide using 50% (v/v) glycerin. Imaging was done of the transverse sections at low magnification using a Wild M5A microscope (Wild Heerbrugg AG, Heerbrugg, Switzerland), and of the longitudinal sections at higher magnification using an Olympus BX60 upright microscope (Olympus America Inc., Center Valley, PA) interfaced with a digital camera (QImaging MicroPublisher 5.0, QImaging, Surrey, BC, Canada). From each transverse image, total xylem vessel number, total transverse lumen area, and largest vessel lumen diameter were obtained using ImageJ software (National Institutes of Health, Bethesda, MD). From this information, average transverse vessel area was calculated. From the longitudinal section images, the frequency of scalariform (number per unit length) and

circular (number per unit area) inter-vessel bordered pits were counted, and the largest circular pit aperture (diameter) was obtained.

### **3.2.10 Fruit measurements**

22 berries per long and short shoot were collected at harvest from vines at a range of stem water potentials. The total weight of berries were measured and divided by the total number of berries to give the average berry weight. The grapes were crushed by hand and must soluble solids (°Brix) were measured using a digital refractometer (Model 300017, Sper Scientific, Scottsdale, AZ). The average sugar content [g] per berry was calculated as the product of the average sugar concentration of the must [g/l] and average berry weight [g].

### **3.2.11 Statistical analysis**

Statistical analyses were performed by analysis of variance (ANOVA) using a linear mixed model that accounts for both fixed and random effects on longitudinal data (repeated measurements over time on each of several subjects; Bates 2005). Seasonal data of  $\Psi_{\text{md}}$  and  $\Psi_{\text{pd}}$  for the two shoot length categories were compared by individual ANOVAs for each measurement day. Linear or non-linear regressions of  $\Psi_{\text{md}}$  and the various physiological and anatomical parameters were determined using Origin Pro graphing software (OriginPro v.8; OriginLab, Northhampton, MA), and statistically analyzed using the mixed model package 'lme4' of the R statistical software package (The R Foundation for Statistical Computing, v. 2.15.2). Results reported as statistically-significant refer to the probability of committing a Type I error at the given significance level ( $P$ -value) for the comparisons of the means of shoot length categories on individual days, or comparisons of the regressions of the shoot length categories.

### 3.3 Results

#### 3.3.1 Water status measurements

Figure 2 shows the seasonal progression of VPD (on the measurement days; see Appendix C for calculation of VPD from temperature and RH), and average water status, shoot growth, and gas exchange of both long and short shoots in 2012. Given the large natural variation in soil and plant water stress levels across the block, data shown is from the 11 most water-stressed vines only. Application of the rain shield resulted in a progressive decline in predawn water potential ( $\Psi_{pd}$ ) and was the same for both long and short shoots (Fig. 2b).  $\Psi_{pd}$  decreased from an initial value of -0.06 MPa early in the season, shortly after fruit set (mid-June), to approximately -0.3 MPa shortly after véraison (mid-August). A slight increase in  $\Psi_{pd}$  following this minimum could have been a result of deep or lateral root growth from stressed vine to access water, lateral water movement after a rainy period, or possibly small leaks in the plastic rain shield late in the season. Maximum daily vine water stress, indicated by the average midday stem water potential ( $\Psi_{md}$ ) of the rain-shielded vines, declined progressively from a maximum of -0.35 MPa early in the season to < -1.6 MPa by the end of the season (Fig. 2c). Throughout the season with the exception of the last measurement day, long shoots had consistently lower  $\Psi_{md}$  values compared to short shoots. Although this difference was small ( $\Delta\Psi_{md} \sim 0.1$  MPa), it was consistent throughout the season and found to be statistically-significant ( $P < 0.05$ ). The seasonal decline in  $\Psi_{md}$  reflected the effect of soil moisture depletion as indicated by  $\Psi_{pd}$  (Fig. 2b).

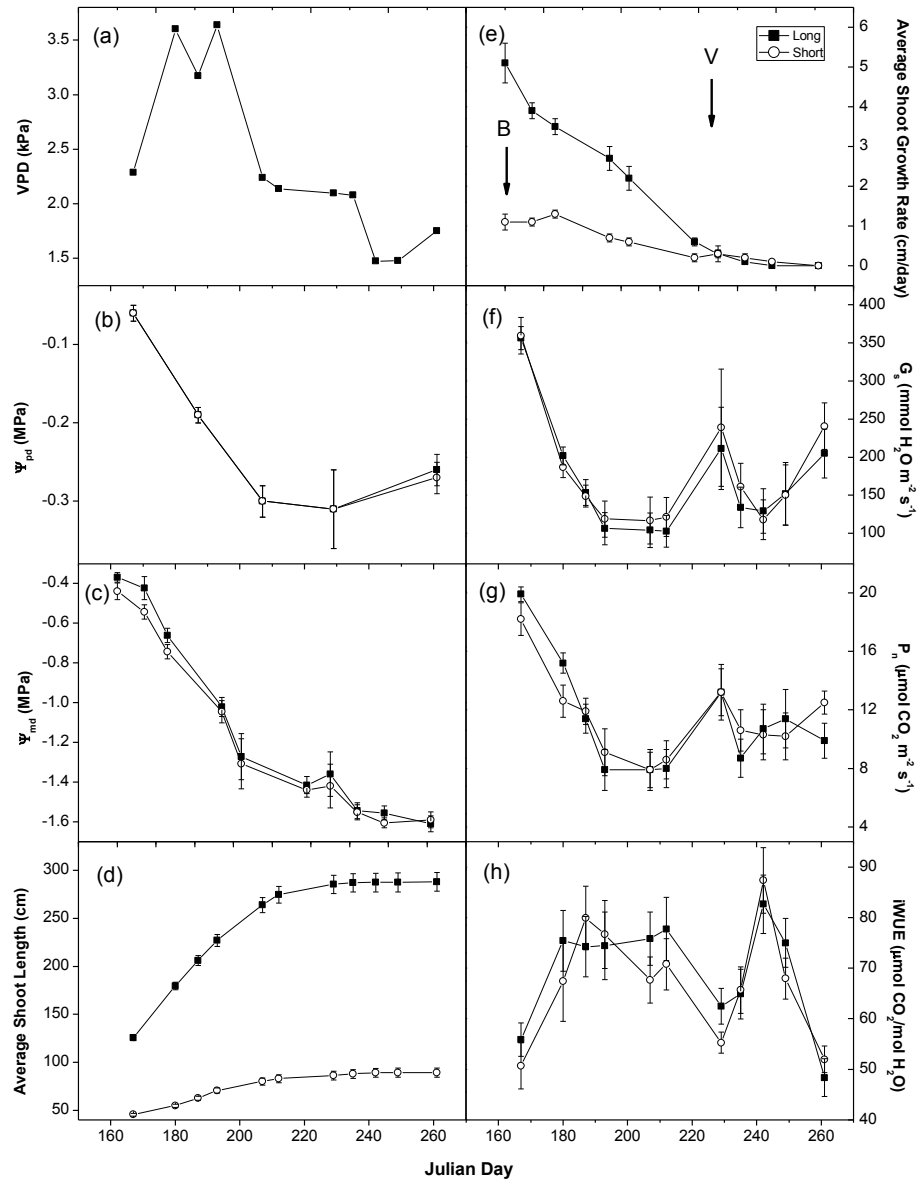


**Figure 2:** 2012 seasonal progression of (a) vapor pressure deficit (VPD); see Appendix D for VPD calculation; (b) pre-dawn water potential ( $\Psi_{pd}$ ); (c) midday stem water potential of rain-shielded vines ( $\Psi_{md}$ ;  $P < 0.05$ ); (d) average shoot length; (e) average shoot growth rate; (f) leaf stomatal conductance ( $G_s$ ); (g) leaf photosynthetic rate ( $A_n$ ); and (h) intrinsic water use efficiency (iWUE) calculated as  $A_n/G_s$  of long and short shoots of 'Riesling' grapevines. Means  $\pm$  S.E. for  $n=22$  shoot length and growth rate measurements, and  $n=11$  gas exchange and stem water potential measurements for each shoot length category on each measurement day from the 11 most water-stressed vines. Arrows with 'B' and 'V' indicate approximate bloom and veraison, respectively.

### 3.3.2 Shoot growth and leaf measurements

Despite progressive water stress during the growing season, long shoots showed a consistently greater growth rate and final length compared to short shoots (Fig. 2d). The average shoot length of long shoots increased over two-fold, from 1.2 m to over 2.9 m, over the course of the growing season, while short shoots grew approximately two-fold, from 0.4 m to 0.8 m in length. Both long and short shoot growth slowed down or stopped by véraison, which is the onset of grape berry ripening (ca. JD 230; Fig. 2d). Short shoots reached 50% of their maximum growth rate of the season approximately one week before long shoots, around JD 207 (Fig. 2e).

Both long and short shoots showed a decline in shoot growth rate (SGR; expressed as a fraction of the maximum) as a function of  $\Psi_{\text{md}}$  (Fig. 3). There was a significant difference ( $P < 0.05$ ) in SGR between long and short shoots, suggesting the greater sensitivity of short shoots to water stress compared to long shoots although other factors may have also limited the growth. The SGRs were 50% of their maximum value when the  $\Psi_{\text{md}}$  value was approximately -1.5 MPa in long shoots, significantly different ( $P < 0.05$ ) from that of short shoots, around -0.7 MPa. The sharp decline in SGR at a  $\Psi_{\text{md}}$  of -0.5 MPa (also indicated in Ch. 1, Fig. 4) suggests a high sensitivity of shoot growth to water stress beyond -0.5 MPa, particularly in short shoots.

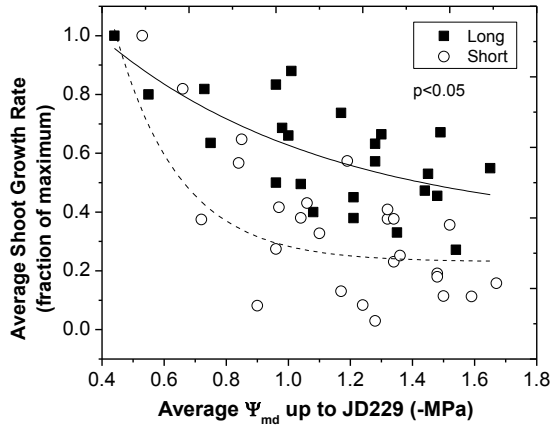


**Figure 3:** Average shoot growth rate as a fraction of maximum growth rate observed for shoot length category vs. average midday stem water potential, both averaged up to Day 229 of growing season when shoot growth slowed down or stopped. Significances are indicated between the regressions of the two shoot length categories (long shoots-solid line, short shoots-dashed line) vs. stem water potential. Non-linear regression equations: Shoot Growth Rate (Long Shoots) =  $(1.12) \cdot \exp(-\Psi_{md}/0.73) + 0.34$ ; Shoot Growth Rate (Short Shoots) =  $(6.62) \cdot \exp(-\Psi_{md}/0.21) + 0.23$ .

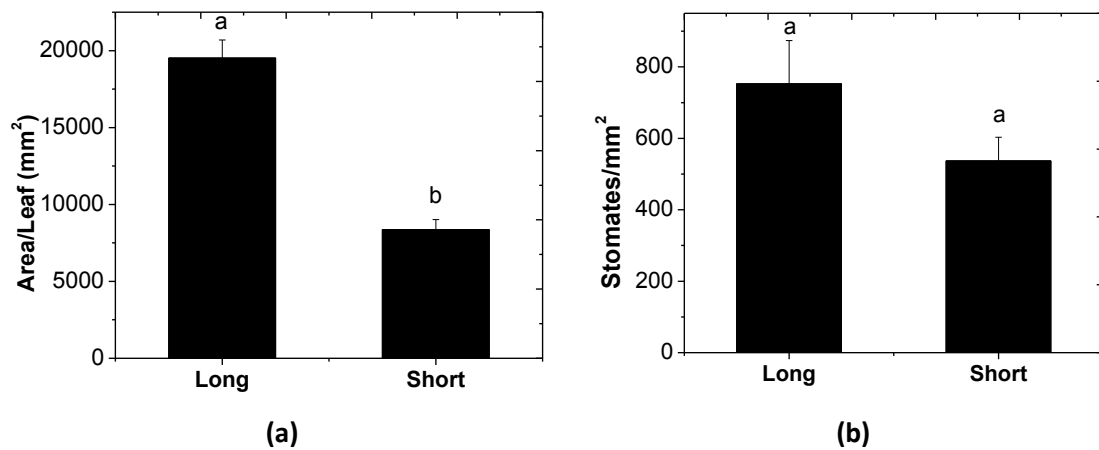


**Figure 4:** (a) Average leaf area of long and short shoots. (b) Average leaf stomatal density of both shoot length categories. 2011 data. Different letters above column means indicate significantly different means at  $p < 0.05$ , Tukey's HSD Test. (n=12)

The average area per leaf from short and long shoots were significantly different (Fig. 4a;  $P < 0.001$ ). Long shoots had an average leaf size that was approximately three times larger than those of short shoots. The average stomatal density (stomates per unit leaf area) of long and

short shoots was 725 and 500 stomates  $\text{mm}^{-2}$ , respectively (Fig. 4b). This difference was, however, statistically non-significant ( $P < 0.1$ ).

### 3.3.3 Gas exchange measurements

There was a similar decline in both  $G_s$  and  $P_n$  of long and short shoots early in the growing season in relation to  $\Psi_{md}$  due to the imposition of the soil moisture deficit (Figs. 2f-g). Concomitantly, the intrinsic water use efficiency ( $iWUE = A_n/G_s$ ) increased by over 50% from its initial value indicating partial stomatal closure that did not reduce  $P_n$  (Fig. 2h). Both  $G_s$  and  $P_n$  declined to their minima by JD 190, around mid-season, and remained stable for over three weeks before increasing to an intermediate level for the remainder of the season.

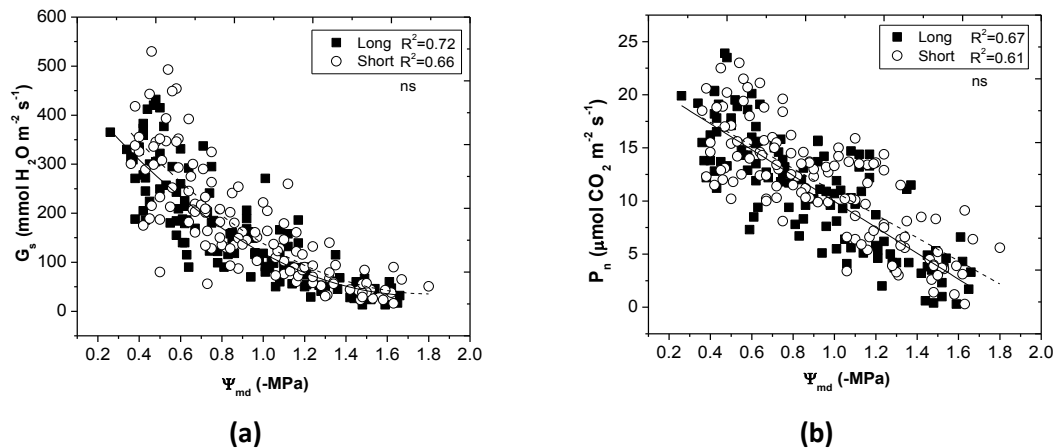


**Figure 5:** (a) Leaf stomatal conductance and (b) net photosynthesis of long and short shoots vs. midday stem water potential. Significances are indicated between the regressions of the two shoot length categories vs. stem water potential. ‘ns’ non-significant difference. Non-linear regression equations for (a):  $G_s(\text{long shoot}) = -527.9(\Psi_{md})^2 + 150.2(\Psi_{md}) + 495.9$ ;  $G_s(\text{short shoot}) = -564.1(\Psi_{md})^2 + 155.6(\Psi_{md}) + 546.6$ . Linear regression equations for (b):  $P_n(\text{long shoot}) = -12.2(\Psi_{md}) + 22.1$ ;  $P_n(\text{short shoot}) = -10.9(\Psi_{md}) + 21.8$ .

There was an overall decreasing trend in all gas exchange parameters –  $G_s$ ,  $P_n$ ,  $iWUE$  – during the course of the growing season. Although the long shoots had slightly lower  $G_s$  and  $P_n$  values, and slightly higher  $iWUE$  values compared to short shoots for part of the season, these

trends were not significantly different ( $P_{G_s} < 0.5$ ;  $P_{P_n} < 0.8$ ;  $P_{iWUE} < 0.2$ ). Short shoots had some of the highest  $G_s$  values, particularly at the highest  $\Psi_{md}$  values, but overall no significant difference ( $P < 0.5$ ) was found between the two shoot length categories (Fig. 5a). A linear decline of  $P_n$  was found as  $\Psi_{md}$  decreased with long and short shoots showing the same relationship (Fig. 5b).

### 3.3.4 Shoot hydraulics measurements

Measurements of maximum stem-specific hydraulic conductivity,  $L_s$  (maximum hydraulic conductivity per stem cross-sectional area;  $L_p/A_s$ ) of long and short shoot segments found highly-significant differences between the two shoot length categories (Fig. 6;  $P < 0.001$ ). Long shoots had up to three orders of magnitude higher specific conductivities compared to short shoots. However, no correlation was found between  $L_s$  and seasonal average midday stem water potential ( $\Psi_{md}$ ) for either of the shoot length categories.

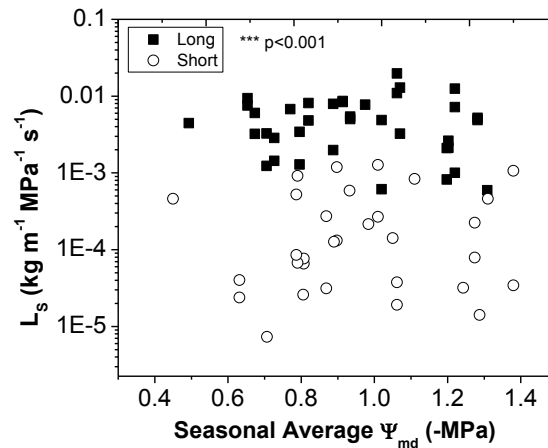


**Figure 6:** Stem-specific hydraulic conductivity,  $L_s$ , (maximum conductivity per stem cross-sectional area) of long and short shoots as a function of seasonal average midday stem water potential ( $\Psi_{md}$ ). \*\*\* indicates significantly different conductivities between long and short shoots at  $p < 0.001$ .

The cane-shoot junction resistivity showed a decreasing trend with respect to shoot length though with high variation. In general, longer shoots had lower junction resistivity than shorter shoots, and no long shoots had high junction resistivity (Fig. 7a). The short shoots had up to an order of magnitude higher junction resistivity compared to long shoots. When expressed as a fraction of the total resistivity of the cane-shoot combination (short cane section connected to the basal section of a shoot), the junction accounted for up to 95% of the total resistance in the hydraulic pathway (Fig. 7b). When expressed in this manner, there was no clear trend with shoot length. When selecting the 10 shortest (length < 1.0 m) and 10 longest (length > 1.5 m) shoots out of the samples analyzed, the average resistivity of the long and short cane-shoot junctions were calculated to be  $1.74 \times 10^{-4} \pm 3.71 \times 10^{-5}$  and  $3.94 \times 10^{-4} \pm 1.07 \times 10^{-4} \text{ m s MPa kg}^{-1}$ , respectively. Statistically, this difference was found to be non-significant ( $P < 0.1$ ) due to the very high variance in the short shoots.

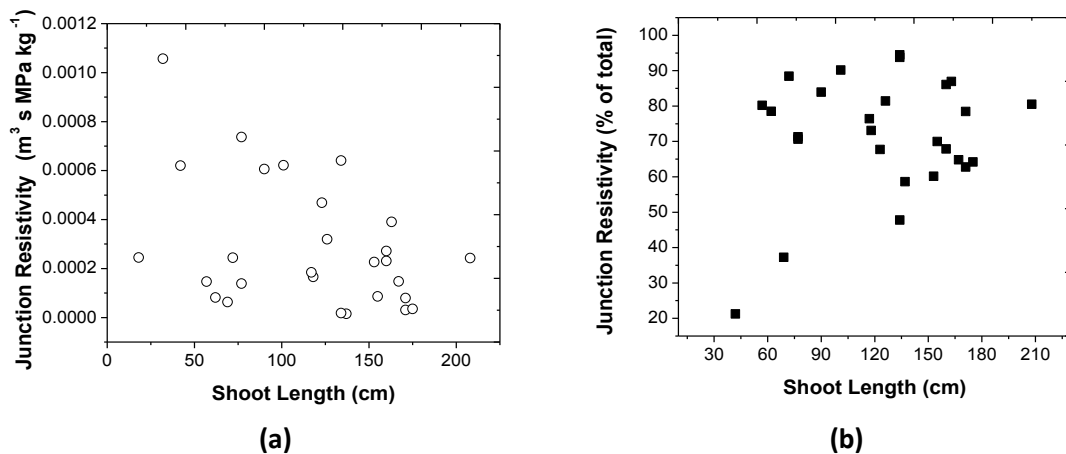


**Figure 7:** (a) Cane-shoot junction hydraulic resistivity as a function of shoot length; (b) Cane-shoot junction resistivity as a fraction of the total cane-shoot resistivity vs. shoot length (shoots sampled on 7/11/2013 and measured on 7/23/2013;  $n=30$ ).

Figure 8 shows the hydraulic conductivity,  $L_p$ , of the two shoot length categories both with and without the cane attached, to study the effect of the junction on conductivity. Significant

differences ( $P < 0.05$ ) were found when comparing the effect of the junction on the cane-shoot hydraulic conductivity; in both long and short shoots,  $L_p$  values were nearly 75% lower with the canes (or junctions) attached than without (shoot only).

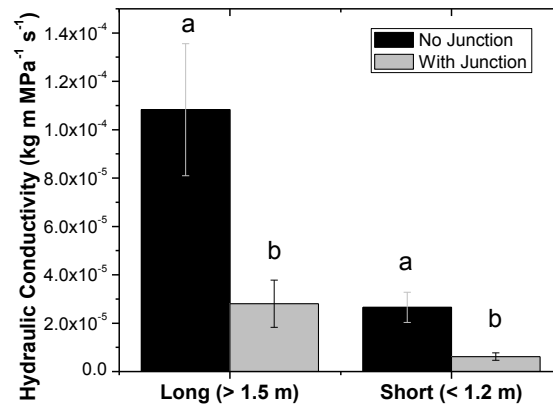


**Figure 8:** Average hydraulic conductivity,  $L_p$ , of shoots only (no junction) and cane-shoot combinations (with junction) of short and long shoots (2013 data; shoots sampled 7/11/2013 and measured on 7/23/2013). Different letters above column means indicate significantly different means ( $P < 0.05$ ) of the shoots only vs. those with junctions. (n=10)

### 3.3.5 Acoustic emissions estimation of xylem air-seeding

At mild water stress levels ( $\Psi_{md} > -0.8$  MPa), both long and short shoots had comparably low xylem air-seeding rates as indicated by their acoustic emissions (Fig. 9a). The two shoots' AE values appeared to separate at moderate water stress levels, when  $\Psi_{md} < -0.8$  MPa, suggesting an air-seeding threshold ( $\Psi_{as}$ ) at that water potential. Below  $\Psi_{as}$ , the air-seeding rate of short shoots increased exponentially. Long shoots still had few AE events even when  $\Psi_{md} < -1.2$  MPa. When  $\Psi_{md}$  values were binned into three classes representing low ( $\Psi_{md} > -0.6$  MPa), medium ( $-0.6 > \Psi_{md} > -1.3$  MPa), and high ( $\Psi_{md} < -1.3$  MPa) water stress, the short shoots were comparable in AEs to the long shoots at low water stress levels (Fig. 9b). However, at medium and high water stress levels, AEs were significantly higher in the short shoots compared to the long shoots ( $P < 0.05$ ). Short shoots had approximately double the AEs of long shoots at these moderate-to-high water stress levels.

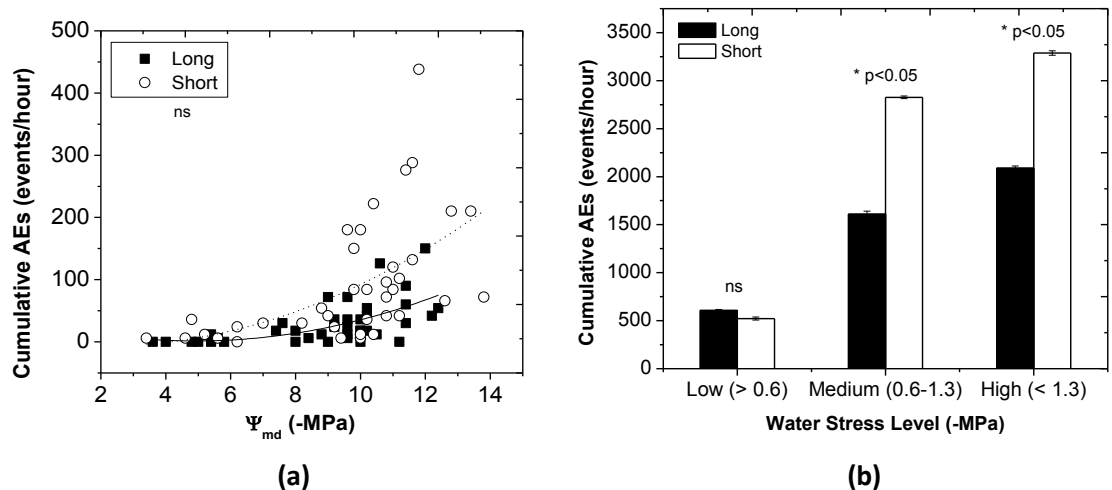


**Figure 9:** Shoot cavitation rates (indicated by cumulative acoustic emissions) vs. (a) midday stem water potential (2011) and (b) water stress level (expressed as a range of midday stem water potentials). \*, 'ns' indicate significant difference and no significant difference, respectively, between shoot length categories at  $P < 0.05$  (2012). Non-linear regression equations for (a): Cumulative AE(long shoot) =  $-12.94(\Psi_{md})^2 + 1.34(\Psi_{md}) + 33.32$ ; Cumulative AE (short shoot) =  $-6.76(\Psi_{md})^2 + 1.59(\Psi_{md}) + 0.62$ .

### 3.3.6 Xylem anatomical measurements

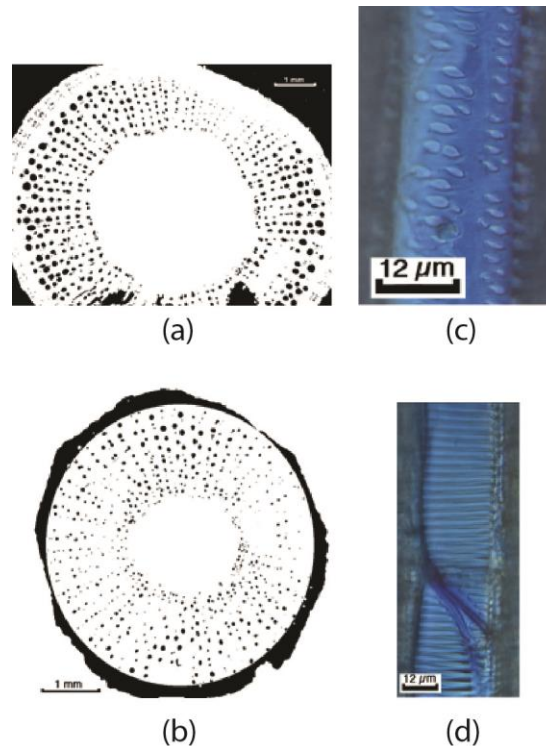


**Figure 10:** Cross-section of stem segments of long (a) and short (b) shoots showing xylem vessels (dark circular spots). Scale bar = 1 mm. Long shoots had more vessels and with larger diameter compared to short shoots. (b) Longitudinal sections of xylem vessels showing circular bordered pits (c) and scalariform pits (d). Scale bar = 12 μm.

Table 1 presents a summary of anatomical measurements of xylem vessels of long and short shoots (Fig. 10). Long shoots had larger vessel elements that resulted in significantly higher cross-sectional areas, both for individual vessels ( $P < 0.05$ ), and total vessel area ( $P < 0.001$ ) (Figs. 10a-b). The latter was two orders of magnitude higher in long shoots than in short shoots. In *Vitaceae*, two types of pitting structures were found: circular bordered pits (Fig. 10c), and scalariform pits (Fig. 10d). Inter-vessel pitting frequency was found to be higher in short shoots compared to long shoots. The largest circular pit aperture (diameter) was found in the vessels of long shoots; these shoots also had larger mean circular pit

apertures than those of short shoots. There was no significant relationship between the pitting frequency (number of pits per unit area or length) and  $\Psi_{md}$  (results not shown here), presumably since xylem vessel development was complete before water stress was significant. Circular pitting frequency was slightly higher in short shoots ( $P<0.1$ ), however, scalariform pitting was non-significantly higher in those shoots ( $P<0.5$ ).

**Table 1:** Xylem morphological characteristics of long and short shoots of ‘Riesling’ grapevines (2011).

Xylem Vessel Feature	Long Shoot	Short Shoot	Significance
Largest Vessel Diameter ( $\mu\text{m}$ )	193.4	87.0	--
Average Vessel Cross-sectional Area ( $\mu\text{m}^2$ )	$3.63 \pm 0.06$	$0.75 \pm 0.06$	**
Total Vessel Cross-sectional Area ( $\text{mm}^2$ )	$1.1 \pm 0.5$	$36.2 \pm 5.8 (\times 10^{-3})$	***
Scalariform Pitting Frequency (pits/mm)	$189 \pm 17$	$200 \pm 20$	ns
Circular Pitting Frequency (pits/ $\text{mm}^2$ )	$13.0 \pm 1.2$	$18.2 \pm 2.7$	*
Largest Circular Pit Aperture ( $\mu\text{m}$ )	$9.3 \pm 0.4$	$7.0 \pm 0.7$	**

Significance: ‘\*\*\*’  $P<0.01$ ; ‘\*\*’  $P<0.05$ ; ‘\*’  $P<0.1$ ; ‘ns’ non-significantly different.

### 3.3.7 Fruit measurements

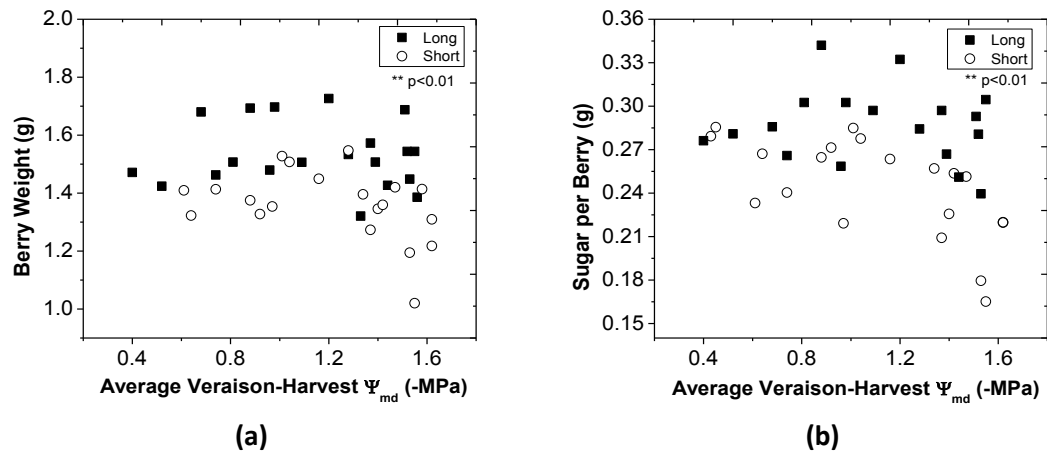


**Figure 11:** (a) Average berry weight and (b) average berry sugar content of ‘Riesling’ grapes harvested from long and short shoots at the end of the season, versus average midday stem water potential of shoots from veraison to harvest ( $n=22$ ). ‘\*\*\*’ indicates significant difference between shoot length categories at  $P<0.01$ .

Fruit size and composition parameters were measured in berries harvested from long and short shoots. Average berry weight was consistently and significantly ( $P<0.01$ ) higher in fruit from the long shoots compared to fruit from the short shoots (Fig. 11a). No relationship was found between berry weight and  $\Psi_{\text{md}}$  (average vine water status from véraison to harvest) except at high stress levels where the berry weight of short shoots appeared to drop by 20-30%. Similarly, the average sugar content of berries from long and short shoots showed no clear relationship to vine water status ( $\Psi_{\text{md}}$ ) except at high water stress levels when the sugar per berry in short shoots dropped by over 30% compared to the average value (Fig. 11b). Long shoots produced berries with significantly ( $P<0.01$ ) higher sugar content compared to short shoots. On average across all stress levels, fruit from short shoots had 0.4°Brix less than fruit from long shoots.

### **3.4 Discussion**

#### **3.4.1 Shoot Water Status and Physiological Performance**

The predawn water potential ( $\Psi_{\text{pd}}$ ) of both long and short shoots decreased progressively throughout the growing season (Fig. 2b), indicating that the rain shield was effective in excluding precipitation from the vineyard floor creating a soil moisture deficit. The consistent and statistically-significant difference in average  $\Psi_{\text{md}}$  of between 0.05-0.075 MPa observed between the two shoot length categories throughout the season indicated that short shoots were under slightly higher levels of water stress compared to long shoots despite the presumably similar basal water potential along the cane to which they were attached.

Assuming there were no marked differences in water potential along the ca. 1-m length of the cane, the measured differences in  $\Psi_{\text{md}}$  between long and short shoots could be due to

differences in either stomatal conductance hydraulic resistance of those shoots, or shoot-cane junctions. Lovisolo and Schubert (1998) found that there was a gradient of water potential along individual shoots increased moving from the base to the apex of the shoots (gradient range,  $d\Psi/dx = 0.015\text{-}0.09 \text{ MPa m}^{-1}$ ), and that water stress did not affect this trend. Over short periods where the hydraulics are relatively constant, the exact gradient will depend on the transpiration rate as well as length. Our finding that an individual shoot's length and rate of growth is positively correlated with its water potential ( $\Psi_{\text{md}}$ ) corroborate with other studies of whole plant performance including wheat (Molnar *et al.* 2004; Sutton and Dubbelde 1980), soybean (Brevedan and Egli 2003; Ohashi *et al.* 2006), corn (Denmead and Shaw 1960; Grant *et al.* 1989), grape (Flexas *et al.* 1999; Hardie and Considine 1976; Intrigliolo *et al.* 2012), apple (Mills *et al.* 1996; Powell 1976), pear (Chalmers *et al.* 1986), and peach (Girona *et al.* 2005).

The small difference in  $\Psi_{\text{md}}$  between long and short shoots could be attributed to higher resistances in the liquid pathway between the cane and the leaf, short shoots having higher resistance compared to long shoots. Shortly following véraison (JD229),  $\Psi_{\text{md}}$  stabilized to a minimum value, likely the result of slightly higher soil water levels as indicated by  $\Psi_{\text{pd}}$  (Fig. 2b) and low  $G_s$  (Fig. 2f). Shoot growth stopped by veraison, consistent with other studies (Cloete *et al.* 2006; Greer *et al.* 2010). The average leaf area of long shoots was also significantly higher than that of short shoots (Fig. 4a), concurring with the findings of Cloete *et al.* (2006). Differences in the average area per leaf between shoots of different vigor classes could not be explained by differences in light exposure (PPFD), leaf temperature, or leaf age, since these parameters were kept nearly identical during the measurements. When normalized by the maximum growth rate in each length category, short shoots were significantly more

sensitive to water stress than were long shoots, particularly at the onset of the stress (Fig. 3). The sensitivity of grapevine shoot growth to water stress has been characterized previously (Schultz et al 1988a; Lebon *et al.* 2006; Pellegrino *et al.* 2005); decreased shoot growth was attributed to declines in leaf and internode expansion, and reduced tendril extension (Lovisolo *et al.* 2010).

The total leaf area (TLA, cm<sup>2</sup>) per shoot was estimated by a strong correlation between TLA and primary shoot length (L, cm) developed from shoots taken from the adjacent row:

$$\text{TLA [cm}^2\text{]} = 7.71 \times L^{1.1665} \quad (R^2 = 0.94)$$

Using this relationship, the average TLAs in our ‘Riesling’ grapevine shoots ranged between 0.22-0.57 m<sup>2</sup> for the long shoots and between 0.07-0.13 m<sup>2</sup> for the short shoots from the beginning to the end of the growing season.

### 3.4.2 Shoot Gas Exchange

Stomatal conductance ( $G_s$ ) and net assimilation ( $P_n$ ) followed the general declining trends of soil and plant water potentials through the growing season. We observed declining stomatal conductance in response to progressive soil moisture deficits (Fig. 5a); this trend was rapid at the onset of the stress and then tapered off at higher stress levels as conductance approached zero. Photosynthesis had a more constant decrease across the range of water potentials (Fig. 5b). Under mild stress the greater decline in stomatal conductance compared to photosynthesis led to a clear increase in iWUE (Fig 2h). Mild to moderate water deficits have been observed to result in stomatal closure in grapevines (Chaves *et al.* 2003) whereas extreme levels of water stress can also inhibit photosynthesis (Flexas *et al.* 1998). The main factor contributing

to the down-regulation of photosynthesis under drought conditions appears to be stomatal limitations although non-stomatal limitations cannot be ruled out (Medrano *et al.* 2002). A comparison of normally-developed and under-developed shoots of Shiraz grapevines found that stomatal conductance, photosynthesis, and water use efficiency were reduced in under-developed shoots while internal CO<sub>2</sub> increased, concomitant with the decrease in photosynthesis (Cloete *et al.* 2008). However, in this study the gas exchange values and responses were essentially the same for both short and long shoots. Although shoot isohydry was one of our initial hypotheses to explain the observed differences in shoot vegetative growth (vigor), our findings did not support this hypothesis. Stomatal closure did not stabilize the mid-day water potentials although it certainly slowed the decline compared to remaining fully open.

### **3.4.3 Shoot hydraulic characteristics**

The hydraulic capacity and efficiency of water transport in plants is an important component of the availability of water to leaves, production of photosynthates, and growth rates (Tyree 2003; Tyree and Ewers 1991), and is a function of xylem vessel size, structure (Schultz and Matthews 1993), and the number and efficiency of aquaporins in the root and leaves. We show here that long shoots within an individual plant can have a stem-specific hydraulic conductivity ( $L_s$ ) several orders of magnitude greater than short shoots (Fig. 6). The higher water transport capacity of long shoots was correlated to the larger xylem vessel lumen diameters (Table 1) needed to support higher shoot transpiration from the larger average leaf area of those shoots (Fig. 4a). The latter is supported by a study that found a negative relationship between leaf growth rate and hydraulic resistance (Schultz and Matthews 1988b).

Differences in  $L_s$  between the two shoot length categories could be also attributed to the higher water transport efficiency of the vessels in the longer shoots due to fewer tyloses that would have occluded the vessels. Another hypothesis to explain this large difference is that  $L_s$  is expressed versus the stem cross-sectional area rather than the total xylem cross-sectional (X-S) area of each shoot. If long and short shoots had different proportions of non-conducting tissue in the stem, i.e. short shoots had much less xylem vessel area per unit stem X-S area compared to long shoots,  $L_s$  of short shoots would be disproportionately smaller than that of long shoots.

The measured difference (approximately 4x) in hydraulic conductivity ( $L_p$ ) of stem segments of long and short shoots (Fig. 8, without junctions) was surprising given that very similar values of leaf stomatal conductance and  $\Psi_{md}$  were observed (Figs. 2c, 2f, 5a). One explanation to reconcile this difference is to consider the total transpirational area or leaf area of the shoot that is supported by the xylem. The following equations (3.2-3.4) show the relationship between total leaf area per shoot ( $TLA$ ), transpiration per unit leaf area ( $E_l$ ), total transpiration of shoot ( $E_t$ ), stomatal conductance ( $G_s$ ), and  $\Psi_{md}$ :

$$E_l = G_s \times (C_l - C_{air}) \quad (3.2)$$

$$\Psi_{md} \cong \Psi_{cane} + E_t/L_p \quad (3.3)$$

$$E_t = E_l \times TLA \quad (3.4)$$

where  $C_{air}$  and  $C_l$  are the water vapor concentrations of ambient air (outside the leaf) and inside the leaf, respectively. Since  $G_s$  was measured to be similar between shoots, based on Eq. 3.2,  $E_l$  would be similar as well. Likewise, since both  $\Psi_{md}$  and  $\Psi_{cane}$  were similar, based on Eq. 3.3, the ratio of  $E_t/L_p$  would also be similar between long and short shoots. Finally, Eq. 3.4 shows that  $E_t$  would be higher based on differences in only  $TLA$ , since  $E_l$  was similar between

shoots. As indicated in Sec. 3.4.1, the total leaf area per shoot was estimated to be approximately four times higher in the long shoots compared to the short shoots, consistent with the difference in  $L_p$  measured of the stems.

The ability of a plant to efficiently transport water and nutrients from roots to shoots, depends largely on the resistances in the pathway between the two organs. Knowledge of these resistances is critical in understanding whole-plant responses to water stress (Aloni and Griffith 1991). Our study of the resistances of the cane-shoot junctions of grapevines found that junctions accounted for 60-90% (average ~72%) of the resistivity in the flow pathway between canes and shoots (Fig. 7b). We found a very general negative correlation between shoot-cane junction resistivity and shoot length (Fig. 7a). This large source of resistance, particularly in short shoots, which had three-fold higher junction resistance on average compared to long shoots (calculated from the inverse of  $L_p$  data shown in Fig. 8), combined with the lower  $L_s$  values found (Fig. 6), could have contributed to the more negative water potentials we observed in short shoots compared to long shoots.

Fig. 11 shows a hypothetical hydraulic model of a grapevine cane showing primary long and short shoot resistances, and the flow pathway of water from the cane up to the leaves of each shoot. The primary resistances in this pathway are the cane-shoot junction ( $R_{junc}$ ), xylem hydraulic resistance and bordered pit membrane resistance ( $R_{xylem+bp}$ ), and the resistance of the junction from the shoot to the leaf petiole ( $R_{leafjunc}$ ). Using an Ohm's Law analogy (based on Eq. 3.1), the driving force for transpiration,  $E$ , can be calculated as:

$$E = \frac{\Delta\Psi_w}{R_{total}} = \frac{\Psi_{cane} - \Psi_{atm}}{R_{junc} + R_{xylem+bp} + R_{leafjunc}} \quad (3.5)$$

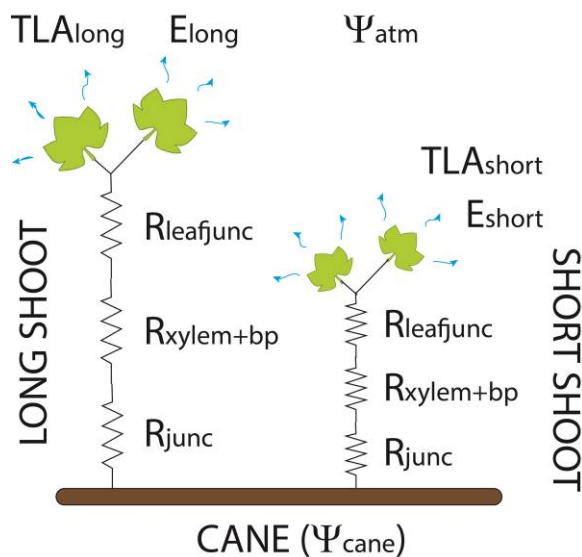


**Figure 11:** Schematic hydraulic model of grapevine cane showing long and short shoots and their hydraulic components.

This concept is useful to visualize the flow pathway and resistances within, as well as for modeling the behavior of the hydraulic system when one or more of its factors are changed. This study quantified the resistances of the cane-shoot junction ( $R_{junc}$ ) and shoot segment ( $R_{xylem+bp}$ ). Additional resistance in the flow pathway between the cane and leaf mesophyll lies in the leaf junction ( $R_{leafjunc}$ ), which was not measured in this study.

#### 3.4.4 Xylem morphology and air-seeding rates

Cavitation events, estimated as acoustic emissions (AE), of long and short shoots were found to be comparable at low stress levels (less negative  $\Psi_{md}$ ), at moderate to high stress levels, the trend became statistically-significant; short shoots produced AE events more often than long shoots (Fig. 9). This observation was somewhat unexpected given that, within a species, vulnerability to cavitation has been shown to be positively correlated with vessel diameter (Cochard and Tyree 1990; Davis *et al.* 1999; Lo Gullo *et al.* 1995; Lovisolo and

Schubert 1998; Sperry and Saliendra 1994; Tyree and Sperry 1989). However, MRI observations of grapevine (*Vitis vinifera* L.) embolism did not reveal any particular trend in vessel size (Holbrook *et al.* 2001). More recently, using high resolution computer tomography, one study found that smaller vessels (lumen diameter < 75  $\mu\text{m}$ ) cavitated more often than larger vessels (lumen diameter > 75  $\mu\text{m}$ ; Brodersen *et al.* 2013), in concurrence with our findings. It was also possible that short shoots had a greater number of vessel elements that could have resulted in a larger number of AEs compared to long shoots. We are unable to confirm this possibility since the number of vessel elements per shoot was not counted in this study (short shoots had fewer vessels per cross-sectional area but they could have been shorter in length, which we did not measure). Nonetheless, the differences in shoot vigor were established early in the season at very high water potentials where few AE events were found. The greater increase in AE events in short shoots as the water potentials declined may have led to an earlier termination of shoot growth in short shoots that has been noted in several related studies in our laboratory.

Differences in the morphology of xylem vessels have been observed to occur inter-season and even within a single season under the influence of water stress (Bauerle *et al.* 2011; Lovisolo and Schubert 1998). The water stress response is generally that of decreased vessel size or cross-sectional area. A recently published meta-analysis of 237 species spanning 40 angiosperm orders across a range of habitats revealed that smaller xylem conduits are a consequence of smaller plant sizes due to their drier habitats rather than solely due to their smaller stems (Olsen and Rosell 2013). Therefore, moist climatic regions will tend to have less water stress, larger plants with larger stems, and larger xylem vessels. Optimum conduit dimensions for a given species could be the result of natural selection to maximize hydraulic

conductance and transpiration while minimizing both conduit investment as well as the probability of air-seeding (Sperry *et al.* 2003). The higher frequency (number per unit area) of inter-vessel bordered pits observed in short shoots could have contributed to the higher AE rates as the probability of air-seeding is higher with more pits per vessel element. However, using a uniform stochastic model, pore frequency was shown to be a weak predictor of cavitation probability (Wheeler *et al.* 2005), so alternative theories for the higher air-seeding resistance in long shoots must be proposed.

### **3.4.5 Fruit growth and composition**

Grape berries harvested from shoots of different length classes showed differences in their size and composition (Fig. 11). Overall, short shoots tended to produce berries that were smaller (lower berry weight; Fig. 11a) and with less sugar content (Fig. 11b) than those from long shoots. This result was not surprising since short shoots had consistently smaller leaves (Fig. 4a) with less total leaf area per shoot (not specifically measured in this study but calculated; Sec. 3.4.1). The effect of progressive water stress on both average berry weight and sugar content did not show a significant trend except at very high water stress levels (more negative  $\Psi_{\text{md}}$  values) in the short shoots. This suggests that only where water transport capacity is severely limited, e.g. in short shoots, is the effect of water stress manifested. These results are consistent with other studies assessing the influence of vine water status on fruit growth and composition (Van Leeuwen *et al.* 2009; des Gachons *et al.* 2005). This result is also consistent with our observations in 2011 where berry weight was seen to be less sensitive to water stress compared to shoot growth rate or leaf gas exchange (Ch. 1, Fig. 4).

### 3.5 Conclusion

In this section, the physiological and reproductive differences of two shoot length categories from a single cane of a grapevine were examined. Differences in shoot length and growth rate were examined in relation to shoot water status that was found to differ slightly but significantly between long and short shoots. The differences in stem water potential were not large enough to explain the large difference in shoot growths noted in a single vine. The minor difference observed in water status was likely due to differences in shoot hydraulic architecture and performance under water stress rather than due to physiological attributes, e.g. stomatal behavior and shoot gas exchange. Higher cavitation rates were found in short shoots, but the embolisms did not lower stomatal conductance in those shoots. This indicates the possibility of high redundancy in the xylem for water transport.

This study is the first to examine the possible sources of variation in shoot growth within individual plants of a species. While our results do not explain all the sources of variation in shoot growth, other possibilities include differences in bud precocity, bud carbohydrate levels (determined by previous year's growing conditions), possible minor variations in light exposure, and variations in nutrition levels, leaving much to be ascertained in future research. Viticultural implications to the grape grower include shoot thinning only the shortest shoots pre-véraison (under 1 m in length by veraison) to allow for maximum light interception and water availability to the other (longer) shoots. Removing the short shoots would also decrease the percentage of under-ripe (low °Brix) fruit from short shoots that would lower the overall quality of the harvest.

### 3.6 References

- Aloni R. & Griffith M. (1991) Functional xylem anatomy in root-shoot junctions of 6 cereal species. *Planta*, **184**, 123-129.
- Anderegg W.R.L., Berry J.A., Smith D.D., Sperry J.S., Anderegg L.D.L. & Field C.B. (2012) The roles of hydraulic and carbon stress in a widespread climate-induced forest die-off. *Proceedings of the National Academy of Sciences of the United States of America*, **109**, 233-237.
- Bates D. (2005) Fitting linear mixed models in R. *R News*, pp. 27-30.
- Bauerle T.L., Centinari M. & Bauerle W.L. (2011) Shifts in xylem vessel diameter and embolisms in grafted apple trees of differing rootstock growth potential in response to drought. *Planta*, **234**, 1045-1054.
- Borger G.A. & Kozlowski T.T. (1972) Effects of water deficits on first periderm and xylem development in *Fraxinus pennsylvanica*. *Canadian Journal of Forest Research*, **2**, 144-151.
- Boyer J.S. (1968) Relationship of water potential to growth of leaves. *Plant Physiology*, **43**, 1056-1062.
- Boyer J.S. (1993) Temperature and growth-induced water potential. *Plant, Cell and Environment*, **16**, 1099-1106.
- Bresta P., Nikolopoulos D., Economou G., Vahamidis P., Lyra D., Karamanos A. & Karabourniotis G. (2011) Modification of water entry (xylem vessels) and water exit (stomata) orchestrates long term drought acclimation of wheat leaves. *Plant and Soil*, **347**, 179-193.
- Brevedan R.E. & Egli D.B. (2003) Short periods of water stress during seed filling, leaf senescence, and yield of soybean. *Crop Science*, **43**, 2083-2088.
- Brodersen C.R., McElrone A.J., Choat B., Lee E.F., Shackel K.A. & Matthews M.A. (2013) In vivo visualizations of drought-induced embolism spread in *Vitis vinifera*. *Plant Physiology*, **161**, 1820-1829.
- Brodribb T.J., Holbrook N.M., Edwards E.J. & Gutierrez M.V. (2003) Relations between stomatal closure, leaf turgor and xylem vulnerability in eight tropical dry forest trees. *Plant, Cell and Environment*, **26**, 443-450.

- Brodribb T.J., Holbrook N.M. & Gutierrez M.V. (2002) Hydraulic and photosynthetic co-ordination in seasonally dry tropical forest trees. *Plant, Cell and Environment*, **25**, 1435-1444.
- Bucci S.J., Scholz F.G., Goldstein G., Meinzer F.C. & Sternberg L.D.S.L. (2003) Dynamic changes in hydraulic conductivity in petioles of two savanna tree species: factors and mechanisms contributing to the refilling of embolized vessels. *Plant, Cell and Environment*, **26**, 1633-1645.
- Carlquist S.J. (1988) *Comparative wood anatomy: systematic, ecological, and evolutionary aspects of dicotyledon wood*. Springer-Verlag, Berlin; New York.
- Chalmers D.J., Burge G., Jerie P.H. & Mitchell P.D. (1986) The mechanism of regulation of 'Bartlett' pear fruit and vegetative growth by irrigation withholding and regulated deficit irrigation. *Journal of the American Society for Horticultural Science*, **111**, 904-907.
- Chaves M.M., Maroco J.P. & Pereira J.S. (2003) Understanding plant responses to drought - from genes to the whole plant. *Functional Plant Biology*, **30**, 239-264.
- Choat B., Jansen S., Brodribb T.J., Cochard H., Delzon S., Bhaskar R., Bucci S.J., Feild T.S., Gleason S.M., Hacke U.G., Jacobsen A.L., Lens F., Maherali H., Martinez-Vilalta J., Mayr S., Mencuccini M., Mitchell P.J., Nardini A., Pittermann J., Pratt R.B., Sperry J.S., Westoby M., Wright I.J. & Zanne A.E. (2012) Global convergence in the vulnerability of forests to drought. *Nature*, **491**, 752-755.
- Cloete H., Archer E. & Hunter J.J. (2006) Shoot heterogeneity effects on Shiraz/Richter 99 grapevines. I. Vegetative growth. *South African Journal of Enology and Viticulture*, **27**, 68-75.
- Cloete H., Archer E., Novello V. & Hunter J.J. (2008) Shoot heterogeneity effects on Shiraz/Richter 99 grapevines. III. Leaf chlorophyll content. *South African Journal of Enology and Viticulture*, **29**, 9-12.
- Cochard H., Coll L., Roux X.I., Ameglio T. & le Roux X. (2002) Unraveling the effects of plant hydraulics on stomatal closure during water stress in walnut. *Plant Physiology*, **128**, 282-290.
- Cochard H., Peiffer M., LeGall K. & Granier A. (1997) Developmental control of xylem hydraulic resistances and vulnerability to embolism in *Fraxinus excelsior* L.: Impacts on water relations. *Journal of Experimental Botany*, **48**, 655-663.

- Cochard H. & Tyree M.T. (1990) Xylem dysfunction in *Quercus*: vessel sizes, tyloses, cavitation and seasonal changes in embolism. *Tree Physiology*, **6**, 393-407.
- Cosgrove D.J. (1993) Water uptake by growing cells: an assessment of the controlling roles of wall relaxation, solute uptake, and hydraulic conductance. *International Journal of Plant Sciences*, **154**, 10-21.
- Costanza P., Tisseyre B., Hunter J. & Deloire A. (2004) Shoot development and non-destructive determination of grapevine (*Vitis vinifera* L.) leaf area. *South African Journal of Enology and Viticulture*, **25**, 43-47.
- Davis S.D., Sperry J.S. & Hacke U.G. (1999) The relationship between xylem conduit diameter and cavitation caused by freezing. *American Journal of Botany*, **86**, 1367-1372.
- Denmead O.T. & Shaw R.H. (1960) The effects of soil moisture stress at different stages of growth on the development and yield of corn. *Agronomy Journal*, **52**, 272-274.
- des Gachons C.P., Van Leeuwen C., Tominaga T., Soyer J.P., Gaudillere J.P. & Dubourdieu D. (2005) Influence of water and nitrogen deficit on fruit ripening and aroma potential of *Vitis vinifera* L. cv. Sauvignon blanc in field conditions. *Journal of the Science of Food and Agriculture*, **85**, 73-85.
- Flexas J., Escalona J.M. & Medrano H. (1998) Down-regulation of photosynthesis by drought under field conditions in grapevine leaves. *Australian Journal of Plant Physiology*, **25**, 893-900.
- Flexas J., Escalona J.M. & Medrano H. (1999) Water stress induces different levels of photosynthesis and electron transport rate regulation in grapevines. *Plant Cell and Environment*, **22**, 39-48.
- Fonti P., Heller O., Cherubini P., Rigling A. & Arend M. (2013) Wood anatomical responses of oak saplings exposed to air warming and soil drought. *Plant Biology*, **15**, 210-219.
- Franks P.J., Drake P.L. & Froend R.H. (2007) Anisohydric but isohydrodynamic: seasonally constant plant water potential gradient explained by a stomatal control mechanism incorporating variable plant hydraulic conductance. *Plant, Cell and Environment*, **30**, 19-30.

- Fregoni M. & Zioni E. (1972) Variations in the moisture content of grapevine buds during dormancy and possible connections with shoot vigour and variations in bud fertility. (in Italian). *Annali della Facolta di Agraria, Universita Cattolica del Sacro Cuore, Milano*, **12**, 337-364.
- Gibberd M.R., Walker R.R., Blackmore D.H. & Condon A.G. (2001) Transpiration efficiency and carbon-isotope discrimination of grapevines grown under well-watered conditions in either glasshouse or vineyard. *Australian Journal of Grape and Wine Research*, **7**, 110-117.
- Girona J., Gelly M., Mata M., Arbones A., Rufat J. & Marsal J. (2005) Peach tree response to single and combined deficit irrigation regimes in deep soils. *Agricultural Water Management*, **72**, 97-108.
- Grant R.F., Jackson B.S., Kiniry J.R. & Arkin G.F. (1989) Water deficit timing effects on yield components in maize. *Agronomy Journal*, **81**, 61-65.
- Greer D.H., Weston C. & Weedon M. (2010) Shoot architecture, growth and development dynamics of *Vitis vinifera* cv. Semillon vines grown in an irrigated vineyard with and without shade covering. *Functional Plant Biology*, **37**, 1061-1070.
- Hacke U.G., Sperry J.S., Wheeler J.K. & Castro L. (2006) Scaling of angiosperm xylem structure with safety and efficiency. *Tree Physiology*, **26**, 689-701.
- Hacke U.G. & Sperry J.S. (2001) Functional and ecological xylem anatomy. *Perspectives in Plant Ecology, Evolution and Systematics*, **4**, 97-115.
- Hardie W.J. & Considine J.A. (1976) Response of grapes to water-deficit stress in particular stages of development. *American Journal of Enology and Viticulture*, **27**, 55-61.
- Hochberg U., Degu A., Fait A. & Rachmilevitch S. (2013) Near isohydric grapevine cultivar displays higher photosynthetic efficiency and photorespiration rates under drought stress as compared with near anisohydric grapevine cultivar. *Physiologia Plantarum*, **147**, 443-452.
- Holbrook N.M., Ahrens E.T., Burns M.J. & Zwieniecki M.A. (2001) In vivo observation of cavitation and embolism repair using magnetic resonance imaging. *Plant Physiology*, **126**, 27-31.
- Hsiao T.C. (1973) Plant responses to water stress. *Annual Review of Plant Physiology and Plant Molecular Biology*, **24**, 519-570.

- Hubbard R.M., Ryan M.G., Stiller V. & Sperry J.S. (2001) Stomatal conductance and photosynthesis vary linearly with plant hydraulic conductance in ponderosa pine. *Plant, Cell and Environment*, **24**, 113-121.
- Intrigliolo D.S., Perez D., Risco D., Yeves A. & Castel J.R. (2012) Yield components and grape composition responses to seasonal water deficits in Tempranillo grapevines. *Irrigation Science*, **30**, 339-349.
- Jones H.G. (1992) *Plants and microclimate: a quantitative approach to environmental plant physiology*. Cambridge University Press, Cambridge [England]; New York, NY, USA.
- Jones H.G. & Sutherland R.A. (1991) Stomatal control of xylem embolism. *Plant, Cell and Environment*, **14**, 607-612.
- Kirkham M.B., Gerloff G.C. & Gardner W.R. (1972) Regulation of cell division and cell enlargement by turgor pressure. *Plant Physiology*, **49**, 961-962.
- Kramer P.J. & Boyer J.S. (1995) *Water relations of plants and soils*. Academic Press, San Diego.
- Lebon E., Pellegrino A., Louarn G. & Lecoœur J. (2006) Branch development controls leaf area dynamics in grapevine (*Vitis vinifera*) growing in drying soil. *Annals of Botany*, **98**, 175-185.
- Leeuwen C.v., Tregoeat O., Chone X., Bois B., Pernet D. & Gaudillere J.P. (2009) Vine water status is a key factor in grape ripening and vintage quality for red Bordeaux wine. How can it be assessed for vineyard management purposes? *Journal International des Sciences de la Vigne et du Vin*, **43**, 121-134.
- Li P., Chen J.L. & Wu P.T. (2011) Agronomic characteristics and grain yield of 30 spring wheat genotypes under drought stress and nonstress conditions. *Agronomy Journal*, **103**, 1619-1628.
- Lintunen A., Holtta T. & Kulmala M. (2013) Anatomical regulation of ice nucleation and cavitation helps trees to survive freezing and drought stress. *Scientific Reports*, **3**, srep02031.
- Lo Gullo M.A., Salleo S., Piaceri E.C. & Rosso R. (1995) Relations between vulnerability to xylem embolism and xylem conduit dimensions in young trees of *Quercus cerris*. *Plant, Cell and Environment*, **18**, 661-669.

- Lockhart J.A. (1965) Analysis of interactions of physical and chemical factors on plant growth. *Annual Review of Plant Physiology*, **16**, 37-52.
- Lovisolò C., Perrone I., Carra A., Ferrandino A., Flexas J., Medrano H. & Schubert A. (2010) Drought-induced changes in development and function of grapevine (*Vitis* spp.) organs and in their hydraulic and non-hydraulic interactions at the whole-plant level: a physiological and molecular update. *Functional Plant Biology*, **37**, 98-116.
- Lovisolò C. & Schubert A. (1998) Effects of water stress on vessel size and xylem hydraulic conductivity in *Vitis vinifera* L. *Journal of Experimental Botany*, **49**, 693-700.
- Martinez-Vilalta J., Prat E., Oliveras I. & Pinol J. (2002) Xylem hydraulic properties of roots and stems of nine Mediterranean woody species. *Oecologia*, **133**, 19-29.
- Medrano H., Escalona J.M., Bota J., Gulias J. & Flexas J. (2002) Regulation of photosynthesis of C<sub>3</sub> plants in response to progressive drought: stomatal conductance as a reference parameter. *Annals of Botany*, **89**, 895-905.
- Meyer W.S. & Ritchie J.T. (1980) Resistance to water flow in the sorghum plant. *Plant Physiology*, **65**, 33-39.
- Mills T.M., Behboudian M.H. & Clothier B.E. (1996) Water relations, growth, and the composition of 'Braeburn' apple fruit under deficit irrigation. *Journal of the American Society for Horticultural Science*, **121**, 286-291.
- Molnar I., Gaspar L., Sarvari E., Dulai S., Hoffmann B., Molnar-Lang M. & Galiba G. (2004) Physiological and morphological responses to water stress in *Aegilops biuncialis* and *Triticum aestivum* genotypes with differing tolerance to drought. *Functional Plant Biology*, **31**, 1149-1159.
- Ohashi Y., Nakayama N., Saneoka H. & Fujita K. (2006) Effects of drought stress on photosynthetic gas exchange, chlorophyll fluorescence and stem diameter of soybean plants. *Biologia Plantarum*, **50**, 138-141.
- Olson M.E. & Rosell J.A. (2013) Vessel diameter-stem diameter scaling across woody angiosperms and the ecological causes of xylem vessel diameter variation. *New Phytologist*, **197**, 1204-1213.

- Pellegrino A., Lebon E., Simonneau T. & Wery J. (2005) Towards a simple indicator of water stress in grapevine (*Vitis vinifera* L.) based on the differential sensitivities of vegetative growth components. *Australian Journal of Grape and Wine Research*, **11**, 306-315.
- Peterson J.R. & Smart R.E. (1975) Foliage removal effects on 'Shiraz' grapevines. *American Journal of Enology and Viticulture*, **26**, 119-124.
- Pou A., Medrano H., Tomas M., Martorell S., Ribas-Carbo M. & Flexas J. (2012) Anisohydric behaviour in grapevines results in better performance under moderate water stress and recovery than isohydric behaviour. *Plant and Soil*, **359**, 335-349.
- Powell D.B.B. (1976) Some effects of water stress on the growth and development of apple trees. *Journal of Horticultural Science*, **51**, 75-90.
- Salleo S., Logullo M.A. & Oliveri F. (1985) Hydraulic parameters measured in 1-year-old twigs of some Mediterranean species with diffuse porous wood - Changes in hydraulic conductivity and their possible functional significance. *Journal of Experimental Botany*, **36**, 1-11.
- Schiller L. (1933) *Drei Klassiker der Stromungslehre: Hagen, Poiseuille, Hagenbach*. Akad. Verlagsgesellschaft, Leipzig.
- Schultz H.R. (2003) Differences in hydraulic architecture account for near-isohydric and anisohydric behaviour of two field-grown *Vitis vinifera* L. cultivars during drought. *Plant, Cell and Environment*, **26**, 1393-1405.
- Schultz H.R. & Matthews M.A. (1988a) Vegetative growth distribution during water deficits in *Vitis vinifera* L. *Australian Journal of Plant Physiology*, **15**, 641-656.
- Schultz H.R. & Matthews M.A. (1988b) Resistance to water transport in shoots of *Vitis vinifera* L. *Plant Physiology*, **88**, 718-724.
- Schultz H.R. & Matthews M.A. (1993) Xylem development and hydraulic conductance in sun and shade shoots of grapevine (*Vitis vinifera* L.): evidence that low light uncouples water transport capacity from leaf area. *Planta*, **190**, 393-406.
- Smart R.E., Turkington C.R. & Evans J.C. (1974) Grapevine response to furrow and trickle irrigation. *American Journal of Enology and Viticulture*, **25**, 62-66.

- Soar C.J., Speirs J., Maffei S.M., Penrose A.B., McCarthy M.G. & Loveys B.R. (2006) Grape vine varieties Shiraz and Grenache differ in their stomatal response to VPD: apparent links with ABA physiology and gene expression in leaf tissue. *Australian Journal of Grape and Wine Research*, **12**, 2-12.
- Sparks J.P. & Black R.A. (1999) Regulation of water loss in populations of *Populus trichocarpa*: the role of stomatal control in preventing xylem cavitation. *Tree Physiology*, **19**, 453-459.
- Sperry J.S., Alder N.N. & Eastlack S.E. (1993) The effect of reduced hydraulic conductance on stomatal conductance and xylem cavitation. *Journal of Experimental Botany*, **44**, 1075-1082.
- Sperry J.S. & Hacke U.G. (2002) Desert shrub water relations with respect to soil characteristics and plant functional type. *Functional Ecology*, **16**, 367-378.
- Sperry J.S. & Saliendra N.Z. (1994) Intra- and inter-plant variation in xylem cavitation in *Betula occidentalis*. *Plant, Cell and Environment*, **17**, 1233-1241.
- Sperry J.S., Stiller V. & Hacke U.G. (2003) Xylem hydraulics and the soil-plant-atmosphere continuum: opportunities and unresolved issues. *Agronomy Journal*, **95**, 1362-1370.
- Stocker O. (1956). Die Abhängigkeit des transpiration von den umweltafaktoren. In: *Encyclopedia of Plant Physiology*. Vol. 3. ed. Ruhland W. Springer, Berlin, pp 436-488.
- Sutton B.G. & Dubbelde E.A. (1980) Effects of water deficit on yield of wheat and triticale. *Australian Journal of Experimental Agriculture and Animal Husbandry*, **20**, 594-598.
- Tardieu F. & Simonneau T. (1998) Variability among species of stomatal control under fluctuating soil water status and evaporative demand: modelling isohydric and anisohydric behaviours. *Journal of Experimental Botany*, **49**, 419-432.
- Tuberosa R., Salvi S., Giuliani S., Sanguineti M.C., Bellotti M., Conti S. & Landi P. (2007) Genome-wide approaches to investigate and improve maize response to drought. *Crop Science*, **47**, S120-S141.
- Turner N.C. (1988) Measurement of plant water status by the pressure chamber technique. *Irrigation Science*, **9**, 289-308.

- Twumasi P., Ieperen W.v., Woltering E.J., Emons A.M.C., Schel J.H.N., Snel J.F.H., Meeteren U.v. & Marwijk D.v. (2005) Effects of water stress during growth on xylem anatomy, xylem functioning and vase life in three *Zinnia elegans* cultivars. In: *Acta Horticulturae 669* (eds N. Marissen, W.G.v. Doorn, & U.v. Meeteren), pp. 303-311.
- Tyree M.T. (2003) Plant hydraulics: The ascent of water. *Nature*, **423**, 923-923.
- Tyree M.T. & Dixon M.A. (1983) Cavitation events in *Thuja occidentalis* L - Ultrasonic acoustic emissions from the sapwood can be measured. *Plant Physiology*, **72**, 1094-1099.
- Tyree M.T. & Ewers F.W. (1991) Tansley review No. 34. The hydraulic architecture of trees and other woody plants. *New Phytologist*, **119**, 345-360.
- Tyree M.T. & Sperry J.S. (1988) Do woody plants operate near the point of catastrophic xylem dysfunction caused by dynamic water stress? Answers from a model. *Plant Physiology*, **88**, 574-580.
- Tyree M.T. & Sperry J.S. (1989) Vulnerability of xylem to cavitation and embolism. *Annual Review of Plant Physiology and Plant Molecular Biology*, **40**, 19-38.
- Wheeler J.K., Sperry J.S., Hacke U.G. & Nguyen H. (2005) Inter-vessel pitting and cavitation in woody *Rosaceae* and other vesselled plants: a basis for a safety versus efficiency trade-off in xylem transport. *Plant, Cell and Environment*, **28**, 800-812.
- Woodruff D.R. & Meinzer F.C. (2011) Water stress, shoot growth and storage of non-structural carbohydrates along a tree height gradient in a tall conifer. *Plant Cell and Environment*, **34**, 1920-1930.
- Yordanov I., Velikova V. & Tsonev T. (2003) Plant responses to drought and stress tolerance. *Bulgarian Journal of Plant Physiology*, 187-206.
- Zimmermann M.H. (1983) *Xylem structure and the ascent of sap*. Springer-Verlag, Berlin; New York.
- Zimmermann M.H., Brown C.L. & Tyree M.T. (1971) *Trees: structure and function*. Springer-Verlag, New York.
- Zufferey V., Cochard H., Ameglio T., Spring J. & Viret O. (2011) Diurnal cycles of embolism formation and repair in petioles of grapevine (*Vitis vinifera* cv. Chasselas). *Journal of Experimental Botany*, **62**, 3885-3894.

## Appendix A: Water-stress induced xylem cavitations in oaks (*Quercus* sp.) and possible links to stomatal behavior

### Introduction

Acoustic emissions (AE), possibly representing cavitation events, in xylem vessels have been reported in the literature when plants are subjected to water stress resulting in high xylem tensions and consequent air-seeding into their lumens (see Sec. 1.5.3 for a review of the literature on AEs in plants). However, the interpretation of AE events from plants under water stress has been rather more controversial; while many researchers strongly believe AE events are associated with cavitations in xylem vessel elements (since they ‘hear’ more events when the stems are drying, and vice-versa), the discrepancy between the number of AE events heard and the number of xylem vessels counted on a given stem segment has not been reconciled. The latter has led to suggestions as to the source of these AE events (see ‘Discussion’ below for references): multiple AE events (oscillations) per actual vessel cavitation, and refilling or rehydration of parenchyma cells. Our

interest in initiating a study of AE patterns in water-stressed plants arose out of an observation on field-grown ‘Riesling’ grapevines (*Vitis vinifera* L.) under water stress of periodic oscillations of AE events (Fig. 1). This phenomenon was intriguing since it could be due to stomatal oscillations – periodicity in stomatal conductance ( $G_s$ )

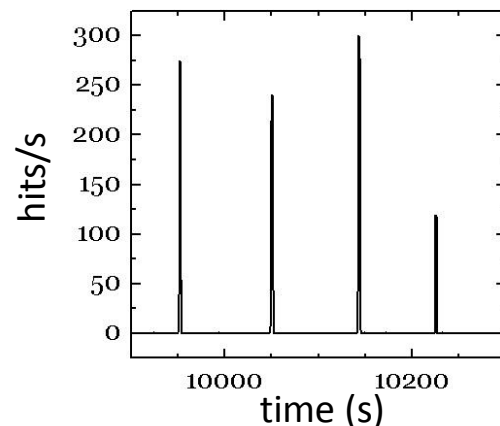


**Figure 1:** Periodicity in groups of acoustic events observed in a field-grown grapevine (*Vitis vinifera* L.) under water stress.

that might result in periodicity in cavitations as the water potential in the plant fluctuates in synchrony.

Cyclic variations or oscillations in stomatal aperture, transpiration, and photosynthesis are reported to occur due to perturbations of the surrounding environment (Yang *et al.* 2005), although they sometimes occur spontaneously in an undisturbed or steady-state environment (Cowan 1972). Oscillations in plants have been documented since the early 1930s (Boresch 1933), with a flurry of research activity in this area from the late 1950s and into the early 1970s (Stålfelt 1956; Ehrler *et al.* 1965; Cox 1968; Lang *et al.* 1969; Hopmans 1971; Farquhar and Cowan 1974). More recently, oscillations in stomatal conductance have been observed in a variety of fruit crops and other commercially important plants (Düring 2000; Hennessey and Field 1991; Cardon *et al.* 1994; Marengo *et al.* 2006; Dziki *et al.* 2007). This phenomenon is potentially important in the context of water balance and transport in leaves, to understand the fluxes of water, as well as the regulating factors that affect the water status of leaves. Barrs (1971) suggested that the phenomenon of stomatal oscillations could be useful to whole-plant physiologists who are interested in understanding the relationships between transpiration and photosynthesis, or transpiration and bioelectric potentials.

One approach to glean a better understanding of the sources and feedback responses associated with oscillations is dynamical mathematical modeling. Using this approach with physiologically-relevant assumptions, Cowan (1972) simulated continuous oscillations in stomatal conductance, leaf transpiration, and water flux in the plant. His model suggested a positive feedback response of the hydraulic system from changes in incident light levels and ambient CO<sub>2</sub> concentration via enhanced sensitivity of turgor of stomatal guard cells rather than via a global change in plant water potential. As per Cowan's model, sustained oscillations

in leaf stomatal conductance appear when the transpiration rate is positive; these oscillations increase with increasing transpiration. Cowan attributed these oscillations to transient differences in water potential between the subsidiary cells and guard cells. Another valuable prediction of Cowan's model vis-à-vis stomatal oscillations dealt with changing environmental conditions, e.g. changing vapor pressure deficit (VPD), that affected the potential transpiration rate, root temperature (affecting root resistance), and osmotic potential of the solution surrounding the roots (affecting the base water potential of the roots). Oscillations were observed with increasing values of transpiration, root resistance, and lower base (root) water potential, i.e. greater stress; the amplitude of oscillations were proportional to the step change of any of these parameters (Fig. 2).

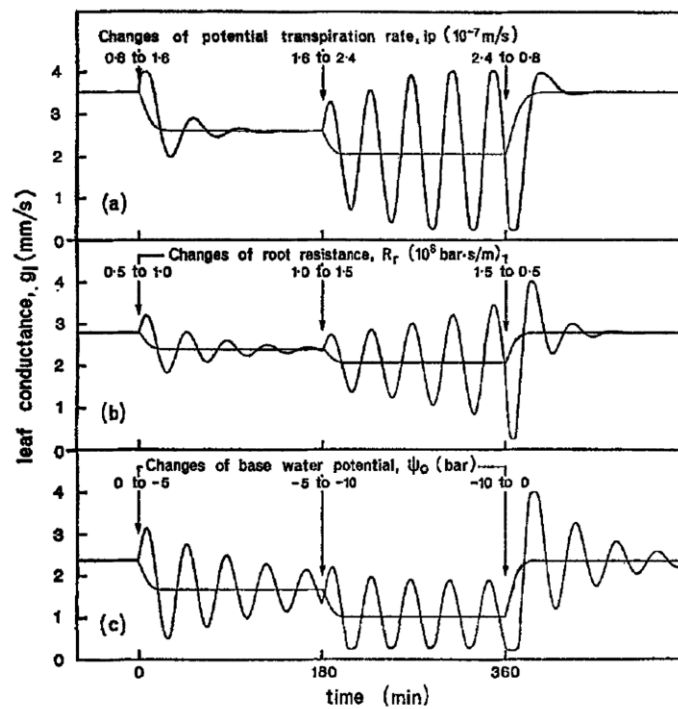


**Figure 2:** Changes in leaf conductance (oscillatory curves) as affected by transpiration rate (a), root resistance (b), and plant water potential (c). From Cowan (1972).

In the current study, we set out to establish whether stomatal oscillations indeed exist under steady-state conditions, as observed by Düring and Stoll (1996) in grapevine, and whether drought stress triggers or influences these oscillations. Additionally, we wanted to investigate whether oscillations were linked to xylem cavitation events, as proposed by one group (Marenco *et al.* 2006). We observed a periodicity of xylem acoustic events in field-grown grapevines under water stress (Fig. 1), leading us to hypothesize that the periodic events were related to stomatal oscillations since both were of generally similar period. Our study used young potted oaks (*Quercus macrocarpa* L.) in a growth chamber under controlled environment conditions. We hypothesized that plants experiencing drought stress, having low leaf water potentials, would induce xylem vessel cavitations, and the ensuing embolisms would disrupt the hydraulic continuity of the transpiration stream leading to higher plant hydraulic resistance. The increase in hydraulic resistance would result in negative feedback to the stomates and trigger their closure. We hypothesized that a closure of stomates in this manner could perhaps result in oscillations in leaf stomatal conductance.

## **Materials and Methods**

### **Location and plant material**

The experiment was undertaken during the winter of 2012-13 in a controlled-environment growth chamber located at Dimock Lab of Cornell University, Ithaca, NY. The chamber was maintained at a constant temperature (set) and relative humidity (uncontrolled) throughout each experiment (details below). Overhead fluorescent lighting at  $400 \mu\text{mol m}^{-2} \text{s}^{-1}$  was used for illumination for 16 h per day from 0600h-2200h. Supplemental lighting was provided to

the upper portion of the canopy using an external fluorescent bulb that raised the total incident light level to approximately  $1000 \mu\text{mol m}^{-2} \text{s}^{-1}$  to reach a saturating level of light for photosynthesis. Potted 1-year old oak trees (*Quercus macrocarpa* L.) were used for this experiment. These plants were grown in 3-gallon pots in a greenhouse (oaks). Only one plant was monitored in each experiment. A single experiment consisted of a well-watered plant (soil moisture at field capacity) that was kept under growth chamber conditions for a minimum of 24 h prior to commencing the experiment, then no longer irrigating the plant until all measurements were completed. In this manner, progressive drought stress was imposed on the plant via drying of the soil in the pot.

### **Drought stress experiments**

Experiment #1 (Oak): A potted oak was well-watered prior to commencing the experiment, then irrigation was withheld upon start of the experiment. The pots were uncovered and left to dry out over 16 days, the duration of the experiment. To study the recovery of the highly water-stressed plant, on Day 16, the pots were irrigated with approximately 1 L of water to replace approximately one-third of the total water lost over the 16 day period (ca. 3 L). The environmental conditions of the growth chamber were held constant at 32°C and between 15-20% RH. Continuous diurnal measurements of gas exchange and acoustic emissions were made, and one mature leaf per day was sampled for leaf water potential measurement.

Experiment #2 (Oak): The chamber conditions were the same as previously (T=32°C, RH 15-20%). Water was withheld from the tree on Day 0 (t=0 h) and only AE events were monitored for the first three days. On Day 4, continuous gas exchange measurements were initiated, and leaf water status was measured daily. On Day 7 when a high level of water stress

was reached, the lights and temperature control of the growth chamber were turned off. The new chamber conditions were: T=22°C, RH=30-35%. On Day 8, the plant was re-watered to replace approximately one-third of the water lost during the experiment. The experiment was stopped on Day 9.

### **Plant water status measurements**

Leaf water potential ( $\Psi_{\text{leaf}}$ ) measurements were made on one fully-expanded leaf adjacent to the leaf being used for gas exchange measurements. A leaf pressure chamber (3000 Series Plant Water Status Console, Soilmoisture Equipment Corp., Santa Barbara, CA) was used using the method of Scholander *et al.* (1965).  $\Psi_{\text{leaf}}$  was measured during the light period at the beginning of each day. The ‘balance pressure’ was noted as  $\Psi_{\text{leaf}}$  and did not include the osmotic component of xylem water potential as described by Boyer (1967).

### **Leaf gas exchange measurements**

Gas exchange was measured using a CIRAS-2 portable differential CO<sub>2</sub>/H<sub>2</sub>O infrared gas analyzer (PP Systems Inc., Amesbury, MA) with a 2.5 cm<sup>2</sup> leaf cuvette. Reference CO<sub>2</sub> concentration was set at 380 ppm. Water vapor concentration inside the cuvette was set as close as possible to ambient. Gas exchange parameters measured included leaf conductance ( $G_s$ ), net assimilation ( $P_n$ ), transpiration rate ( $E$ ), incident radiation ( $Q$ ), calculated leaf temperature ( $T$ ), and concentration of leaf internal CO<sub>2</sub> ( $C_i$ ). Gas exchange measurements were made continuously (once per minute) for 10 hours per day (or both day and night continuously for some experiments) on one mature, healthy, and well-exposed oak leaf on the upper section of the plant. Each experiment day, a different leaf on the same plant was selected for gas exchange measurement. In order to ensure that instrument noise was not being

misinterpreted as stomatal oscillations of the leaf, we ‘measured’ the gas exchange of a small piece of paper in place of a leaf. No oscillations in transpiration, stomatal conductance, or photosynthesis were observed with the paper in the chamber.

### **Ultrasonic acoustic emissions measurements**

Xylem cavitation was estimated using continuous measurements of ultrasonic acoustic emissions (Tyree and Dixon 1983) using a Pocket AE-2 portable dual-channel ultrasonic emissions system (18-bit, 20 MSPS A/D, 1.0 kHz-1.0 Mhz  $\pm$  1.5 dB; Physical Acoustics Corp., Princeton Junction, NJ). The system was equipped with one wideband (100-900 kHz) resonance sensor (Model ‘WSa’), and one narrowband (150 kHz) resonance sensor (Model ‘R15 $\alpha$ ’). The sensor surface area (circular) was  $\sim$  1.8 cm<sup>2</sup> and the contact area with the stem was approximately half this area,  $\sim$  0.9 cm<sup>2</sup>. The pre-amplifier and thresholds were both set at 40 dB to minimize interference from human conversation or the growth chamber climate control system. Maximum event duration, peak definition time, hit definition time, and hit lockout times were set at 100 ms, 200  $\mu$ s, 800  $\mu$ s, and 1 ms, respectively. These settings were determined based on our characterization tests (described previously in Chapter 3), using the manufacturer’s recommendations as a starting point. Data analysis was performed using AEwin Replay software (Physical Acoustics Corp., Princeton Junction, NJ) on a Windows-based PC. Recorded data include hit time, counts, amplitude, and absolute energy. On the measurement stem on which gas exchange data was continuously recorded, ca. 3 cm<sup>2</sup> bark was removed from a basal section of the stem so as to expose the surface of the xylem. A thin film of silicone grease was applied on the acoustic sensor and then attached to the exposed region of the stem using metal laboratory clamp. AE data was collected continuously over the

duration of each experiment except briefly (~ 1 min per day) when a leaf was excised for water potential measurement, since leaf excision produced large acoustic events.

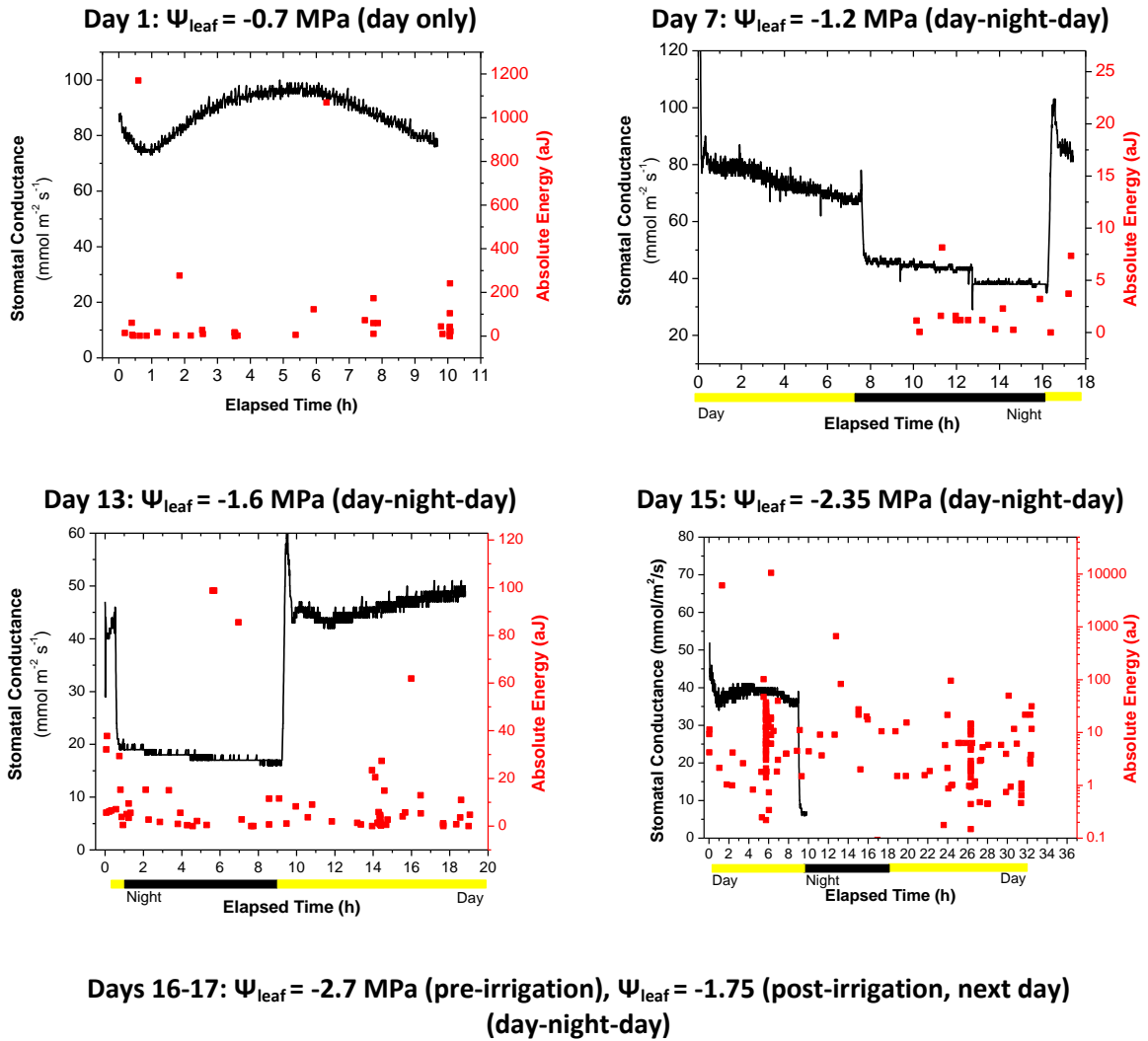
## Results and Discussion

### Experiment #1 (Oak)

In the interest of brevity, only select data from the experiment is presented here; this concise dataset shows the most interesting and relevant trends of the experiment. Each graph is presented with the day number, and  $\Psi_{\text{leaf}}$  as measured at the start of each day before continuous stomatal conductance and acoustic emissions measurements were started.

In the first experiment (Fig. 3), a new single potted oak tree was subjected to progressive water stress over a period of over two weeks in which the leaf water potential ( $\Psi_{\text{leaf}}$ ) decreased from -0.7 MPa to -2.7 MPa. Intermittent irrigation was applied such that the water stress was relieved for a short period to investigate whether stomatal conductance would also recover, and whether stomatal oscillations could be triggered via the re-hydration route rather than solely during dehydration. On the first day, the plant was well-watered and  $\Psi_{\text{leaf}}$  was -0.7 MPa. An oscillation in  $G_s$  was observed with amplitude and period of approximately 20 mmol H<sub>2</sub>O m<sup>-2</sup> s<sup>-1</sup> and 11 h, respectively. This was the only day during the entire series of experiments where there was any indication of the presence of stomatal oscillations. During this period, a number of acoustic events were observed that had relatively low energy, under 300 aJ. By Day 7,  $\Psi_{\text{leaf}}$  had reached -1.2 MPa indicating that the plant water status was decreasing in response to the imposed soil moisture deficit. This was also the first complete diurnal (day and night) measurement of  $G_s$  and AEs.  $G_s$  began to drop steadily from 80 to around 70 mmol H<sub>2</sub>O m<sup>-2</sup> s<sup>-1</sup>. Interestingly,  $G_s$  did not drop to zero at night when the lights were turned off, possibly

owing to the high VPD in the chamber;  $G_s$  remained around 40-45  $\text{mmol H}_2\text{O m}^{-2} \text{s}^{-2}$ , approximately 50% of the day-time value.



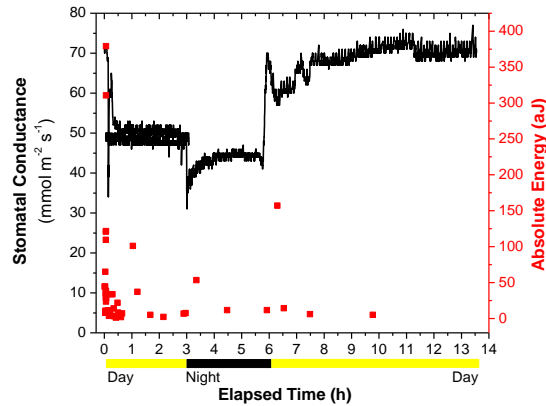


**Figure 3:** Stomatal conductance in *Quercus* over two weeks at given levels of irrigation application (% ET) and leaf water potential ( $\Psi_{\text{leaf}}$ ) as measured at the beginning of each period. Arrows in each graph indicate when irrigation was applied. Irrigation applied on D16 at the start of the day period.

Night transpiration has been reported previously (Muchow *et al.* 1980; Benyon 1999), and can reach up to 50% of maximum day transpiration in grapevines (Rogiers and Clarke 2013; Fuentes *et al.* 2013; Rogiers *et al.* 2009). This has been attributed to partial stomatal closure and results in reduced water use efficiency in horticultural crops (Caird *et al.* 2007). In this experiment, non-zero night  $G_s$  was observed consistently throughout the experiment independent of the level of water stress ( $\Psi_{\text{leaf}}$ ), and was as high as 50% of the day  $G_s$  value.

By D13,  $\Psi_{\text{leaf}}$  had dropped to -1.6 MPa, and by D16 below -2.7 MPa after which irrigation was applied. During this period, day  $G_s$  values remained around 40-50  $\text{mmol H}_2\text{O m}^{-2} \text{s}^{-1}$  until irrigated on D16. Even at these levels of  $\Psi_{\text{leaf}}$ , there were no signs of stomatal oscillations or other gas exchange parameters measured. However, the number and energy of AE events increased from D7 onwards when  $\Psi_{\text{leaf}}$  values dropped below -1.2 MPa, indicating perhaps that this was the cavitation threshold for the particular species and plant. From then on, AE events were consistently observed; these increased markedly when  $\Psi_{\text{leaf}}$  dropped below -1.6 MPa (D13), and were observed during the day and at night. Night AE events are not surprising given that transpiration is non-zero, so some level of tension is maintained in xylem vessels at

night. Nocturnal transpiration has been proposed to contribute to hydraulic lift and the redistribution of water in roots at night (Donovan *et al.* 2001, 2003; Domec *et al.* 2004). Furthermore, we cannot exclude the possibility that AE events were originating from other sources such as non-conducting fibers (not present in conifers), ray tracheids, xylem parenchyma cells flanking the vessel elements as they rehydrated, or intercellular cavities in the xylem (Rosner *et al.* 2006; Wolkerstorfer *et al.* 2012). The large burst of AE events (stacked) observed on D15 could represent a population of relatively high vulnerability vessels cavitating;  $\Psi_{\text{leaf}}$  was fairly low at this time, below -2.3 MPa.  $G_s$  measurements temporarily stopped at the end of the first day period. On the final day, D16, irrigation was applied at the start of the day to relieve the water stress;  $G_s$  increased shortly after irrigation to  $\sim 70 \text{ mmol H}_2\text{O m}^{-2} \text{ s}^{-1}$  while AE events dropped off significantly to almost zero. This finding – that re-watering a water-stressed plant decreases AE events – corroborates with a study of rehydration of dried cedar (*Thuja* sp.) stems (Tyree and Dixon 1983), and another of irrigating water-stressed potted wheat (Jia *et al.* 2006). The number of AE events on D17 at  $\Psi_{\text{leaf}} = -1.75 \text{ MPa}$  during rehydration was negligible compared to a similar  $\Psi_{\text{leaf}}$  on D13 during dehydration. This hysteresis could be explained by the possibility that during dehydration, as xylem tensions increased, larger diameter xylem vessels cavitared before smaller diameter vessels (Salleo and Lo Gullo 1986; Lo Gullo and Salleo 1993), and these larger embolized vessels had not yet refilled upon rehydration, so did not produce any AE events. Given the likely positive correlation between vessel lumen volume and AE energy (AE energy = lumen volume  $\times$  xylem pressure; Mayr and Rosner 2011), it is interesting to note that, if indeed larger lumen vessels cavitate before smaller lumen vessels, the larger lumens should produce a larger AE energy signal upon cavitation (Mayr and Rosner 2011; Tyree and Sperry 1989). This is

something we only observed fairly late in the experiment, on D15 and early D16, when  $\Psi_{\text{leaf}}$  dropped below -2.4 MPa.

## Experiment #2 (Oak)

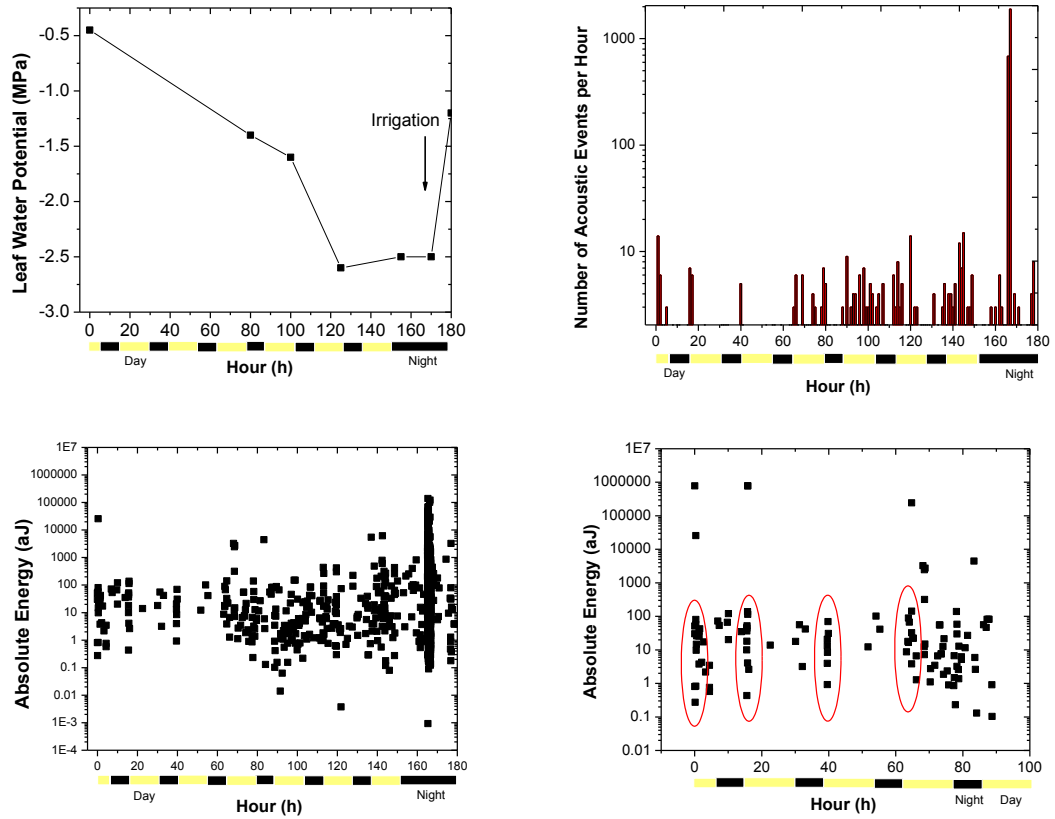


**Figure 4:** Clockwise from top left: Leaf water potential ( $\Psi_{\text{leaf}}$ ), acoustic emissions (AE) rate, absolute energy of AE events showing bursts of AE events early in the day (ellipses), and absolute energy of AE events during entire experiment on *Quercus* over 10 days under progressive water stress.

In the second experiment (Fig. 4), a new potted oak that was initially well-watered was subjected to progressive water stress; the pot was not watered for the entire duration of the experiment resulting in a rapid decline in  $\Psi_{\text{leaf}}$  to -2.7 MPa, a stress level that was reached in the previous experiment albeit over a much shorter period (and on a different plant). AE events were observed from the beginning of the experiment even when the plant was not water-stressed, possibly owing to the high rates of transpiration due the large gradient in water potential (high chamber VPD). At even low or moderate water stress levels, there were a high

number of ‘stacked’ AE events early on each day (red ellipses in Fig. 4, bottom right), indicating perhaps re-cavitation of small vessels that were filled overnight, or a dehydration of parenchyma cells when transpiration initiated during the day. When the water stress level was high,  $\Psi_{\text{leaf}} \sim -2.6$  MPa, AE events were observed even at night, which could indicate either continued cavitation of xylem from night transpiration, refilling of embolized vessels, or rehydration of xylem fibers. The large burst of AE events observed at low  $\Psi_{\text{leaf}}$  (-2.5 MPa) might have been the population of vessels that were relatively robust against cavitation (low vulnerability vessels) that finally succumbed to the high tensions in their lumens. Interestingly, this large burst of AE events around  $t=78$  h was followed by a rapid drop in  $G_s$  to below  $5 \text{ mmol H}_2\text{O m}^{-2} \text{ s}^{-1}$  ( $G_s$  data not shown here); this should not be surprising since a large proportion of embolized vessels would result in lower xylem hydraulic conductance and, consequently, lower  $G_s$  (Jones and Sutherland 1991). Upon re-watering, a gradual recovery in  $G_s$  was observed albeit with a delay of several hours or a day. One plausible explanation for the delay in  $G_s$  recovery is the accumulation of abscisic acid (ABA) in the leaf symplast of the plant (Wilkinson and Davies 2002; Bauerle *et al.* 2004). Stomatal closure is known to occur when the soil begins drying and without a change in turgor (Hartung *et al.* 2002),  $\Psi_{\text{leaf}}$ , or  $\Psi_{\text{stem}}$  (Lovisol *et al.* 2002), pointing to the key role of ABA as a chemical signal involved in stomatal closure during drought.

## Conclusions

Drought stress resulted in marked decreases in leaf water potential, leaf stomatal conductance, and increases in acoustic events, often interpreted as cavitations. The main observations from this study were: (i) there appear to be two or more different populations of vessels having different vulnerabilities to cavitation, or  $\Psi_{\text{cav}}$ ; (ii) during periods of high water

stress, bursts of AE events occur early in the day followed by a quieter or quiescent period; (iii) night transpiration can be a significant source of water loss from the plant, up to 50% of the total daily amount; and, (iv) while  $G_s$  responds promptly to progressive water stress (as indicated by decreasing  $\Psi_{\text{leaf}}$ ), recovery from water stress is a slow process physiologically as indicated by the slow increase in  $G_s$  upon rewatering. During the entire experiment, there was no indication of stomatal oscillations or periodicity (time auto-correlation) of AE events, the latter which were previously observed in field-grown grapevines experiencing drought stress (Fig. 3), which led to this study. It is quite likely that the reason for the lack of observed oscillations or periodicity was a lack of changing environmental conditions. The growth chamber conditions in this study were maintained relatively constant during the experiment with no changes in temperature or relative humidity. The only environmental parameter that was modified was the light level between day and night; clearly, this was inadequate at triggering a response in  $G_s$  but often led to a high frequency of AE events soon after the lights went on.

Future studies in this area should perturb the system by rapidly changing one of the environmental parameters, e.g. VPD, and observing  $G_s$  and AE simultaneously. Cowan (1978) described the basic assumption of the mechanism used to describe the phenomenon of stomatal oscillations as being the properties of the loop in which the rate of transpiration affects stomatal aperture and, hence, conductance ( $G_s$ ), which in turn affect transpiration. So, inducing such oscillatory behavior might be best achieved by perturbing the hydraulic feedback loop by manipulating the environmental gain, e.g. relative humidity or VPD (Farquhar and Cowan 1974). However, the caveat of altering “simple” environmental gain parameters such as humidity, temperature, or  $\text{CO}_2$  is that these parameters may not, in fact, be

adequate in triggering oscillations. Rather, more dynamic properties such as  $\partial w/\partial E$ ,  $\partial T/\partial E$ , and  $\partial c/\partial A$  (where  $w$ =humidity,  $E$ =transpiration,  $c$ =CO<sub>2</sub> concentration,  $A$ =net assimilation,  $T$ =temperature) could be playing a role (Cowan 1978). Clearly, this is a complex system which needs to be better understood and perhaps initially modeled, as did Cowan (1972) rather wisely.

## References

- Barrs H.D. (1971) Cyclic variations in stomatal aperture, transpiration and leaf water potential under constant environmental conditions. *Annu. Rev. Plant Physiol.*, **22**, 223-236.
- Benyon R.G. (1999) Nighttime water use in an irrigated Eucalyptus grandis plantation. *Tree Physiology*, **19**, 853-859.
- Boresch K. (1933) Zur graphischen Registrierung der Transpiration von Blättern. *Zeitschr Wiss Biol Abt E Planta*, **20**, 448-469.
- Boyer J.S. (1967) Leaf water potentials measured with a pressure chamber. *Plant Physiology*, **42**, 133-137.
- Caird M.A., Richards J.H. & Donovan L.A. (2007) Nighttime stomatal conductance and transpiration in C-3 and C-4 plants. *Plant Physiology*, **143**, 4-10.
- Cardon Z.G., Mott K.A. & Berry J.A. (1994) Dynamics of patchy stomatal movements, and their contribution to steady-state and oscillating stomatal conductance calculated using gas-exchange techniques. *Plant, Cell and Environment*, **17**, 995-1007.
- Cowan I. (1978) Stomatal behaviour and environment. *Advances in botanical research*, **4**, 117-228.
- Cowan I.R. (1972) Oscillations in stomatal conductance and plant functioning associated with stomatal conductance: observations and a model. *Planta*, **106**, 185-219.
- Cox E.F. (1968) Cyclic changes in transpiration of sunflower leaves in a steady environment. *Journal of Experimental Botany*, **19**, 167-175.

- Domec J.C., Warren J.M., Meinzer F.C., Brooks J.R. & Coulombe R. (2004) Native root xylem embolism and stomatal closure in stands of Douglas-fir and ponderosa pine: mitigation by hydraulic redistribution. *Oecologia*, **141**, 7-16.
- Donovan L.A., Linton M.J. & Richards J.H. (2001) Predawn plant water potential does not necessarily equilibrate with soil water potential under well-watered conditions. *Oecologia*, **129**, 328-335.
- Donovan L.A., Richards J.H. & Linton M.J. (2003) Magnitude and mechanisms of disequilibrium between predawn plant and soil water potentials. *Ecology*, **84**, 463-470.
- During H. (2000) Induction of stomatal oscillations in grape leaves: Determination by gas exchange measurement. *Vitis*, **39**, 45-46.
- During H. & Stoll M. (1996) Stomatal patchiness of grapevine leaves II Uncoordinated and coordinated stomatal movements. *Vitis*, **35**, 69-71.
- Dzikiti S., Steppe K., Lemeur R. & Milford J.R. (2007) Whole-tree level water balance and its implications on stomatal oscillations in orange trees [*Citrus sinensis* (L.) Osbeck] under natural climatic conditions. *Journal of Experimental Botany*, **58**, 1893-1901.
- Ehrler W.L., Nakayama F.S. & Vanbavel C.H. (1965) Cyclic changes in water balance and transpiration of cotton leaves in a steady environment. *Physiologia Plantarum*, **18**, 766-775.
- Farquhar G.D. & Cowan I.R. (1974) Oscillations in stomatal conductance. The influence of environmental gain. *Plant Physiology*, **54**, 769-772.
- Fuentes S., Bei R.d., Tyerman S. & de Bei R. (2013) Night-time plant water loss: the unseen process for local and global water footprint and water balance estimations in grapevines. *Wine and Viticulture Journal*, **28**, 50-52.
- Hennessey T.L. & Field C.B. (1991) Circadian rhythms in photosynthesis Oscillations in carbon assimilation and stomatal conductance under constant conditions. *Plant Physiology*, **96**, 831-836.
- Hopmans P.A.M. (1971) Rhythms in stomatal opening of bean leaves. *Mededelingen van de Landbouwhogeschool te Wageningen*, **71**, 86.
- Jia X., Zhang L., Ma R., Wang Z., Zhang Q., Yao Y., Jia X.L., Zhang L.H., Ma R.K., Wang

- Z.L., Zhang Q.G. & Yao Y.R. (2006) Ultrasonic acoustic emissions from leaf xylem of potted wheat subject to a soil drought and rewatering cycle. *Agricultural Sciences in China*, **5**, 346-355.
- Jones H.G. & Sutherland R.A. (1991) Stomatal control of xylem embolism. *Plant, Cell and Environment*, **14**, 607-612.
- Lang A.R.G., Klepper B. & Gummig M.J. (1969) Leaf water balance during oscillation of stomatal aperture. *Plant Physiology*, **44**, 826-830.
- Lo Gullo M.A. & Salleo S. (1993) Different vulnerabilities of *Quercus ilex* L. to freeze-induced and summer drought-induced xylem embolism: an ecological interpretation. *Plant, Cell and Environment*, **16**, 511-519.
- Lovisollo C., Hartung W. & Schubert A. (2002) Whole-plant hydraulic conductance and root-to-shoot flow of abscisic acid are independently affected by water stress in grapevines. *Functional Plant Biology*, **29**, 1349-1356.
- Marenco R.A., Siebke K., Farquhar G.D. & Ball M.C. (2006) Hydraulically based stomatal oscillations and stomatal patchiness in. *Functional Plant Biology*, **33**, 1103-1113.
- Mayr S. & Rosner S. (2011) Cavitation in dehydrating xylem of *Picea abies*: energy properties of ultrasonic emissions reflect tracheid dimensions. *Tree Physiology*, **31**, 59-67.
- Muchow R.C., Ludlow M.M., Fisher M.J. & Myers R.J.K. (1980) Stomatal behaviour of kenaf and sorghum in a semiarid tropical environment. I. During the night. *Australian Journal of Plant Physiology*, **7**, 609-619.
- Rogiers S.Y. & Clarke S.J. (2013) Nocturnal and daytime stomatal conductance respond to root-zone temperature in 'Shiraz' grapevines. *Annals of Botany*, **111**, 433-444.
- Rogiers S.Y., Greer D.H., Hutton R.J. & Landsberg J.J. (2009) Does night-time transpiration contribute to anisohydric behaviour in a *Vitis vinifera* cultivar? *Journal of Experimental Botany*, **60**, 3751-3763.
- Rosner S., Klein A., Wimmer R. & Karlsson B. (2006) Extraction of features from ultrasound acoustic emissions: a tool to assess the hydraulic vulnerability of Norway spruce trunkwood? *New Phytologist*, **171**, 105-116.
- Salleo S. & Gullo M.A.I. (1986) Xylem cavitation in nodes and internodes of whole *Chorisia*

*insignis* H. B. et K. plants subjected to water stress: relations between xylem conduit size and cavitation. *Annals of Botany*, **58**, 431-441.

Scholander P.F., Hammel H.T., Bradstreet E.D. & Hemmings E.A. (1965) Sap pressure in vascular plants - Negative hydrostatic pressure can be measured in plants. *Science*, **148**, 339-346.

Stålfelt M.G. (1956) Die stomatäre transpiration und die physiologie der spaltöffnungen. In: *Encyclopedia of Plant Physiology* pp. 351-426. Springer Verlag, Berlin.

Tyree M.T. & Sperry J.S. (1989) Vulnerability of xylem to cavitation and embolism. *Annual Review of Plant Physiology and Plant Molecular Biology*, **40**, 19-38.

Wolkerstorfer S.V., Rosner S. & Hietz P. (2012) An improved method and data analysis for ultrasound acoustic emissions and xylem vulnerability in conifer wood. *Physiologia Plantarum*, **146**, 184-191.

Yang H., Zhang J. & Zhang X. (2005) Regulation mechanisms of stomatal oscillation. *Journal of Integrative Plant Biology*, **47**, 1159-1172.

## Appendix B: Microtensimeter fabrication process flow

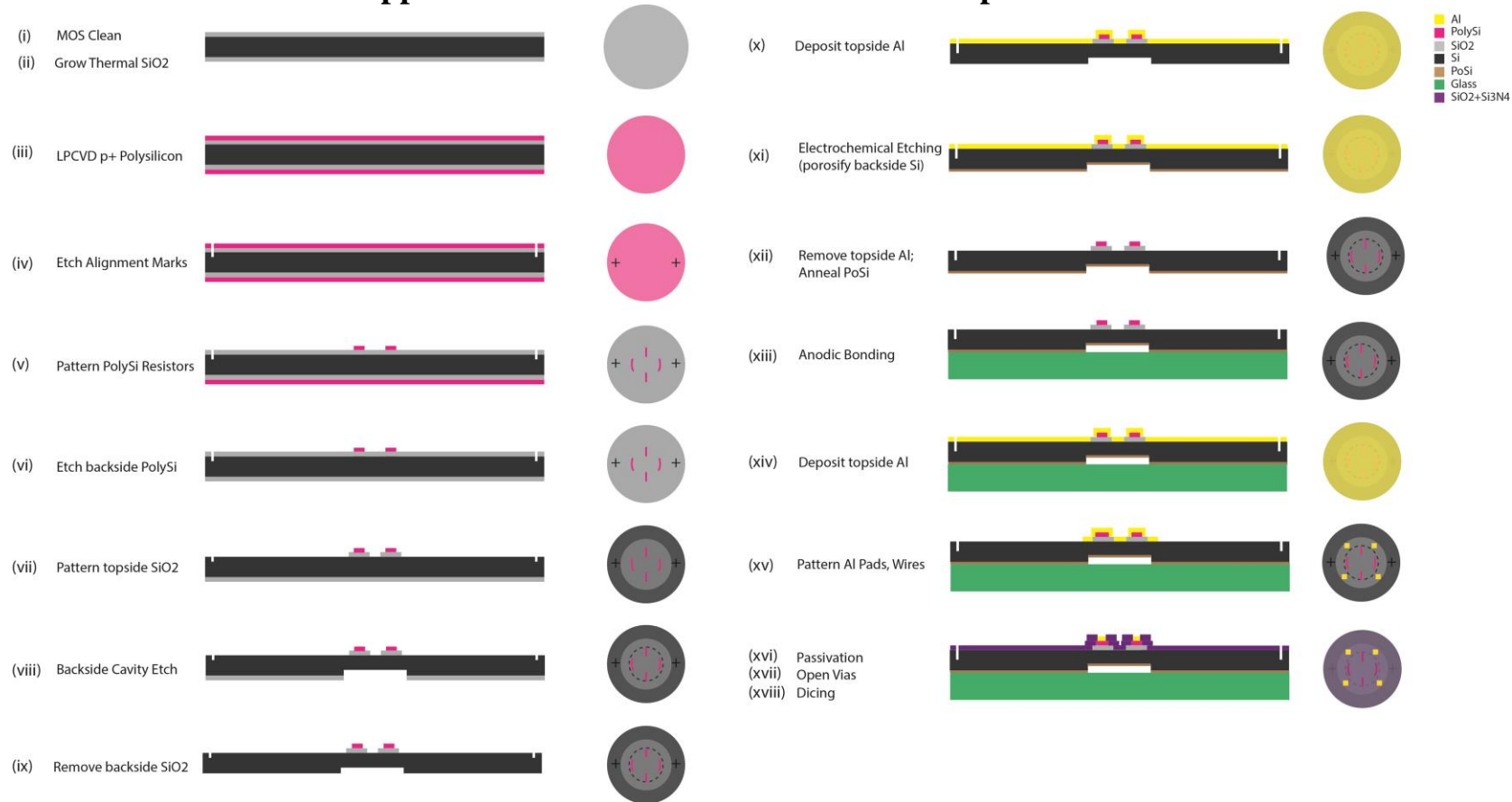


**Figure B-1:** Microtensimeter fabrication process flow (full). Wafer cross-sectional view (left side), top view (right side).

## Appendix C: Photolithographic masks for microtensiometer fabrication

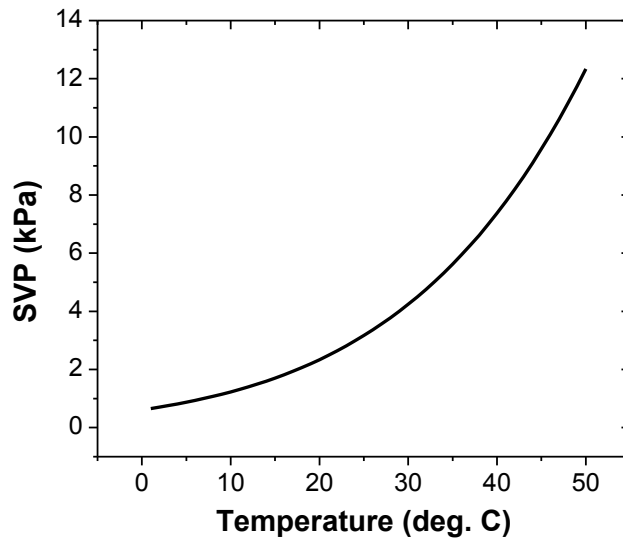
Mask Name	Side of Wafer	Description
Mask1-Alignment	Top	Wafer front-side alignment marks used to align all subsequent mask layers.
Mask1-Alignment_Closeup	Top	Detail of alignment marks on one side of wafer.
Mask2-Oxide	Top	Thermally-grown silicon dioxide pattern for electrical isolation.
Mask3-Resistor	Top	Pattern for the polysilicon piezoresistors on the front-side of the wafer.
Mask4-Cavity	Back	Pattern on back-side to form both the cavity (to fill with water) and the diaphragm.
Mask5-Metal	Top	Metal wires connecting the piezoresistors with the contact pads.
Mask6-Vias	Top	Pattern to open holes (vias) over the metal pads through the passivation layers.

## Appendix D: Calculation of Vapor Pressure Deficit (VPD)

**Step 1:** Calculate the saturation vapor pressure (SVP, [Pa]) at a given temperature, T [°C], using the following relationship:

$$SVP [Pa] = 610.7 \times 10^{7.5T/(237.3+T)}$$

The saturation vapor pressure curve is shown below for various temperatures.



**Step 2:** The vapor pressure deficit (VPD) is the difference between the saturated vapor pressure and that at a given relative humidity (RH, %), and can be calculated as:

$$VPD [Pa] = \left(\frac{100 - RH}{100}\right) \times SVP = \left(1 - \frac{RH}{100}\right) \times SVP$$

**Examples:**

<b>Temperature [°C]</b>	<b>RH [%]</b>	<b>SVP (kPa)</b>	<b>VPD (kPa)</b>
20	60	2.34	0.94
20	40	2.34	1.40
25	60	3.17	1.27
25	40	3.17	1.90
30	60	4.24	1.70
30	40	4.24	2.54
35	30	5.62	3.93

**References:**

Murray FW (1967) On the computation of saturation vapor pressure. *J. Appl. Meteorol.*, **6**, 203-204.

Monteith JL, Unsworth MH (1990) *Principles of environmental physics*. Arnold.